Enabling Ethanol Use as a Renewable Transportation Fuel: A Micro- and Macro-scale Perspective

by

Ripudaman Singh

A dissertation submitted in partial fulfillment
of the requirements for the degree of
Doctor of Philosophy
(Mechanical Engineering)
in the University of Michigan
2019

Doctoral Committee:

Professor Margaret S. Wooldridge, Chair
Professor Andre Boehman
Associate Professor Mirko Gamba
Professor Gregory Keoleian
Assistant Professor Andrew Mansfield, Eastern Michigan University

Ripudaman Singh

singhrd@umich.edu

ORCID iD: 0000-0002-7159-0242

Dedication

“To my grandparents who taught me to surpass the boundaries”

Acknowledgments

Just as great things cannot be achieved in isolation, this dissertation work was possible only with the support, guidance and love from a community of people.

First, I would like to thank Professor Margaret S. Wooldridge for giving me the opportunity to be a part of her research group. She is the best advisor I could have asked for, it is only her nurturing and belief in me that I have been able to complete this work. She gave me the freedom to explore opportunities and guided me on way to achieving the goals I wanted to. The rich intellectual environment in her group has helped me grow as a researcher.

I would also like to thank Professor Andre Boehman, Associate Professor Mirko Gamba, Professor Gregory Keoleian and Assistant Professor Andrew Mansfield for serving on my committee. Their invaluable feedback and recommendations played a significant role in shaping this dissertation. My sincere thanks to Dr. Francis Kemausuor and the Energy Center at Kwame Nkrumah University of Science and Technology (KNUST), Kumasi, Ghana for being such great hosts during my work at Ghana.

I would like to express my sincere gratitude to my research sponsors including the Department of Energy, Robert BOSCH LLC, Ford Motor Co., UM Rackham graduate school and the Department of Mechanical Engineering, University of Michigan. Without the monetary and intellectual support from sponsors, this work would have not been possible.

I am thankful for the valuable help and support of the staff and technicians in the Mechanical Engineering department. Jim Elkins for helping put the two engine set-ups in the test facility; Bill Kirkpatrick for helping ensure the auxiliary systems to the test cell were always

functional; Kent Pruss for machining all those complex parts; Melissa Mcgeorge for expediting the ordering and shipping of all the packages required for the test facility.

Thanks to my friends, my past lab-mates, and my present lab-mates, who made being in the lab fun and exciting. Dr. Mohammad Fatourie and Dr. Dimitris Assanis for guiding me throughout my Ph.D. work. Dr. Cesar Barraza Botet, Luis Gutierrez, Mario Medina, Rachel Schwind, Miles Burnett for their friendship, having insightful discussions on topics ranging from future of the automotive industry to losing body fat.

I am thankful to all the friends who are like a family here in Ann Arbor.

Most importantly, I am grateful for my family's constant love and support. My grandparents who inculcated the spirit of working hard and staying honest. My parents, Gurmeet Singh and Devinder Kaur, who have let me explore whatever I have wanted to in life, even though at times I could tell that they had little idea what I was working on. My sister, Ardaman Kaur and brother, Harshpreet Singh who motivated and supported me to pursue a degree in the U.S. I am grateful for the trust my family has put in me.

Table of Contents

List of Tables

List of Figures

List of Appendices

Abstract

The transportation sector remains the most challenging area to reduce greenhouse gas emissions from the combustion of fossil fuels. A successful transition away from fossil fuels is possible through the use of ethanol as an alternative fuel. Ethanol has considerable promise to reduce the carbon intensity of passenger vehicles, but a better understanding of the promise and limitations of ethanol as a renewable energy carrier is required, particularly using non-food feedstocks. Blending ethanol with gasoline has been demonstrated at a significant scale in the United States and Brazil. Currently, ethanol is blended with gasoline in the U.S. as an octane booster to a maximum blend level (E10 – 10% by volume); which is indistinguishable from gasoline to the engine application and the fueling infrastructure. However, optimum blend levels have not been determined from an engine application perspective. Also, current production of ethanol from primary food crops presents challenges like competition with food sources; thus, alternative feedstocks for ethanol production are required. This dissertation takes a novel approach which presents micro and macro-scale perspectives to enable ethanol as a transportation fuel.

First at the micro or device scale, physical experiments were used to determine the optimum blend level of ethanol and gasoline for production spark ignition engines. Engine operating strategies which provide the most benefit, in terms of improving efficiency and lowering emissions, with the use of these blends were identified. Mid-level blends (30%) of ethanol by volume with gasoline show the most benefit in terms of several engine performance metrics. An improvement of 2% in thermodynamic efficiency on an absolute basis, and more

than 90% reduction in particulate emissions was observed by combining use of such a blend with a triple-injection per cycle fueling strategy.

Second at the macro scale of the transportation fuel production and distribution level, analytical methods were applied to determine the feasibility of producing cellulosic ethanol based on high-fidelity geographically-resolved data on agricultural waste for the regional districts of Ghana. Biorefinery locations and fuel blending infrastructure recommendations are made, by minimizing transportation costs involved in the biomass residue feedstock collection and distribution of the ethanol produced by the biorefinery. Previous studies have shown significant potential of biofuel production in Ghana, but there were no previous studies that focused on development of geographic infrastructure for 2nd generation transportation biofuels (i.e. based on non-food feedstocks). This study was the first attempt in this direction. Both the process used and the outcomes of this study provide valuable input for the development of sustainable biofuels infrastructure in Ghana.

This work demonstrates considerable benefit of ethanol blending for modern engine architecture, with identification of strategies which leverage the thermo-physical fuel properties of ethanol and translate across engine hardware architectures. The thesis outcomes also offer an unprecedented attempt towards development of a geographic infrastructure for producing and distributing 2nd generation transportation biofuels in Ghana based on minimizing the costs of collecting crop residue and distributing ethanol from biorefineries. The application-scale and system scale perspectives enable transitions to lower carbon emissions from the transportation sector using sound engineering principles and provide foundations for future work at both the micro- and macro-scale and for integration of the methods.

Chapter 1

Introduction

Providing energy solutions which are sustainable is a critical challenge for global energy systems. For an energy solution to be 'sustainable' it needs to address the three challenges: economic, social and environmental sustainability. Energy solutions need to deliver on the legitimate aspiration towards further economic and social progress, and at the same time strengthening environmental protection.

Historically, the easy availability of fossil fuels since the industrial era has pushed research and technologies in the direction of fossil-based energy production devices. But it was realized that the greenhouse gas (GHG) emissions from use of fossil fuels, to meet ever-increasing energy demands, pose a serious threat to the environment. The recent report by the Intergovernmental Panel on Climate Change (IPCC) [1] conveys that owing to these GHG emissions human-induced global warming reached approximately 1^{o}C above pre-industrial levels in 2017. One of the key messages that came out very strongly from the IPCC report was that the consequences of 1°C of global warming are already being observed through more extreme weather, rising sea levels and diminishing Arctic sea ice, among other changes. The report highlights a number of climate change impacts that could be avoided by limiting global warming to 1.5^{o}C; but this would require rapid, far reaching and unprecedented changes in all aspects of society.

The challenge historically has been due to the conflict between the more expensive but lower CO_2 emissions of renewable technologies and the high CO_2 emissions of inexpensive fossil fuel technologies. Environmental concerns are motivating energy production devices to be more efficient, less polluting and based on renewable resources. But the cheap, easy availability, higher energy density and geopolitical significance of fossil fuel energy sources make it hard to move away from them, especially in developing nations.

The transportation sector is a significant contributor to global energy consumption and greenhouse gas emissions. The transportation sector produced 7.0 GtCO2eq of direct GHG emissions (including non-CO2 gases) in 2010 and hence was responsible for approximately 14% of total energy-related GHG emissions [2]. Without aggressive and sustained mitigation policies, transportation emissions could increase at a faster rate than emissions from the other energy end-use sectors and reach around 12 Gt CO2eq/yr by 2050. In 2016, the transportation sector in the U.S. accounted for the largest portion (28%) of total U.S. GHG emissions [3].

To address the concerns of increasing GHG emissions from the transportation sector, the energy policies for vehicles specify aggressive improvements in fuel economy and vehicle emissions. One method to achieve this goal is to blend renewable biofuels like ethanol with fossil fuels. This method has been adopted in the U.S. as a national policy via- the Renewable Fuels Standard (RFS) program [4]. The RFS program requires a certain volume of renewable fuel to replace or reduce the quantity of petroleum-based transportation fuel used. The RFS program was authorized under the Energy Policy Act of 2005 and expanded under the Energy Independence and Security Act (EISA). As per the 2007 enactment of EISA, the total target volume for renewable fuel is set at 36 billion gallons for the year 2022.

The Environmental Protection Agency (EPA), the party responsible for implementation of the RFS program by setting renewable volume commitments for the obligated parties, has indicated its intent to increase the volume of renewable fuel blending in conventional gasoline fuel sold in the U.S. At present, the biofuel ethanol seems to be the only renewable fuel which can realistically meet the target volume standards. Almost all gasoline currently available at gas stations is already a blend of 10% (by volume) ethanol in gasoline, also known as gasohol or E10. The success of ethanol on a commercial scale in the U.S. and around the globe is unparalleled by any other renewable biofuel. However, currently ethanol is blended with gasoline in the U.S. and other nations (except Brazil) as an octane booster to a maximum blend level (E10 – 10% by volume); which is indistinguishable from gasoline to the engine application and the fueling infrastructure. The use of blend limits for ethanol in transportation sector are not based on energy efficiency.

Ethanol has considerable promise to reduce the carbon intensity of passenger vehicles; but a successful transition away from fossil fuels requires better understanding of the promise and limitations of ethanol as an energy carrier. In order to assess the promise and limitations, each process involved in ethanol production and use (from farm to consumption) should be carefully analyzed. **Figure 1.1** shows the different processes involved in an ethanol cycle.

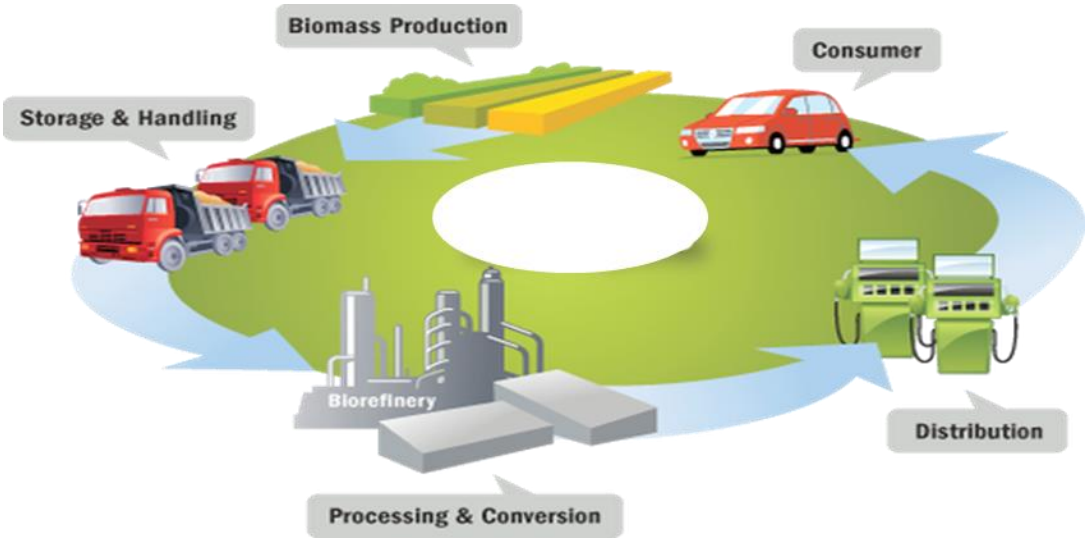

Figure 1.1. Processes involved in biofuel life cycle [5]

Each of the processes brings in its own challenges, like

- What feedstock to use?
- How to transport the feedstock?
- How to process the feedstock?
- Where to locate the biorefinery?
- Where to locate the distribution center?
- What are the optimal biofuel blend levels for the automotive fleet?
- What is the final selling price of ethanol?

and many more. Additionally, consideration of economic and social effects is critically needed for particular needs and aspirations of individual communities. The results for these assessments are expected to vary geographically based on locational, social, cultural or developmental differences. Hence, the assessment of the impact of biofuels requires research that transcends traditional disciplinary boundaries.

1.1 Focus of Thesis Work:

This thesis introduces micro- and macro-scale perspectives towards enabling the use of ethanol as a renewable transportation fuel. First, the work enhances the understanding of the thermosphysical and chemical mechanisms important to improve engine performance of ethanol and gasoline fuel blends. Second, the study evaluates an extensive matrix of fueling strategies with ethanol and gasoline fuel blends, which has not been explored in any of previous work and is of great interest to assess if advancements in fuel injection technology can help meet future emissions regulations. Third, the study assesses the potential of geographically distributed ethanol production from second generation bio-residue feedstocks in Ghana, Africa. Fourth, the study introduces methods to optimize the location of ethanol production and distribution from cellulosic materials, with specific application and recommendations for Ghana. Some previous studies have shown significant potential of biofuel production in Ghana, but there are no studies to date that focus on development of a geographic infrastructure for 2nd generation transportation biofuels. This study was a first attempt in this direction based on input from a large variety of important national statistical data, such as the bioresidue available regionally in the country and the existing vehicle fleet in Ghana. The process and outcomes of the work are valuable input for developing a sustainable biofuels infrastructure in Ghana.

For the micro-scale approach physical experiments were conducted using two state-of-the-art production gasoline turbocharged direct injection (GTDI) engines. The engines were installed and instrumented at the automotive laboratory at the University of Michigan. The first engine, a Ford 1.0L 3-cylinder GTDI engine, was modified to operate as a single-cylinder engine. The set-up focused on fundamental studies by exploring the effects of the properties of a range of ethanol and gasoline fuel blends. Experiments on the second engine, a production

Daimler M274 2.0L 4-cylinder GTDI engine (i.e. a multi-cylinder engine), validated the results and further identified the best fueling strategies to maximize the gains achievable with the use of ethanol blending.

During the single-cylinder engine experiments, fuels with different levels of ethanol blending ranging from E0 (pure gasoline) to E100 (pure ethanol) were tested under different power-demand conditions and fuel injection strategies. GT-Power simulations were used to evaluate the contributions of the fuels' thermophysical properties on the thermodynamic efficiency of engine. The work is described in **Chapter 2**. The work has been published [6] in the Society of Automotive Engineers (SAE) International Powertrains, Fuels and Lubricants meeting.

The experiments conducted on the multi-cylinder engine setup validated the results from single-cylinder engine studies on entirely different in-production engine architecture. This demonstrated the thermophysical properties of ethanol dominate the engine performance and hence the recommendations are not dependent on engine specifics. The work on the multi-cylinder engine expanded the study of multiple injection strategies, compared with the injection strategies considered in the single cylinder engine study. Multiple injection strategies have a potential to reduce the PN emissions form GDI engines, for which stringent regulations are being introduced. However, few studies have explored the benefits of application of multiple injections[7][8][9] and none of the previous work has reported a strategy which helps achieve benefits to the scale reported in this study with a combined application of ethanol blending and multiple injection strategies. The results of the multi-cylinder work included data at over 1000 operating conditions. The study demonstrated the effects of multiple injections in conjunction

with the use of ethanol fuel blends in improving the engine performance. **Chapter 3** describes the multi-cylinder engine study and the results.

Identifying the optimal blend of ethanol with gasoline to maximize thermal efficiency is valuable but not enough to advocate for ethanol use in the transportation sector. **Chapter 4** presents a brief timeline of ethanol fuel use in the U.S. The chapter presents how different social, economic and environmental drivers have guided the policies for ethanol fuel use in the country. Two major concerns hindering the implementation of a large-scale ethanol program are discussed: the long-term sustainability of production of ethanol from food crops and the inadequate distribution infrastructure. Keeping these concerns in mind the subsequent work presented in **Chapter 5** considers a case study set in Ghana, Africa. The study was supported through the Rackham Global Engagement Program (Univ. of Michigan), in collaboration with the Energy Center at the Kwame Nkrumah University of Science and Technology in Kumasi, Ghana.

In particular, the goal of the Ghana case-study presented in **Chapter 5** was to make recommendations for an ethanol production and distribution infrastructure based on geographical availability of agricultural residue and minimizing transportation costs. The national annual cellulosic ethanol production potential in Ghana is estimated to be greater than 2000 million liters per year (ML/yr) [10]. The Strategic National Energy Plan developed by Ghana's Energy Commission targets 10% of petroleum fuels to be displaced by renewable biofuels by 2020 [11]. However, there are currently no recommendations for creating a bio-refining and fuel distribution infrastructure for Ghana. To address the missing link of cellulosic ethanol infrastructure, the objective of the study in Ghana was to propose an ethanol production and distribution network by identifying best candidate locations for biorefineries, which minimize the

cost of the transport required to bring feedstock to and supply ethanol from these biorefineries. The outcomes include not only the candidate sites for the refineries, but also the crops most well suited for ethanol production were identified; the sensitivity of the results to major key assumptions was also carried out. The results of this study show the feasibility of using crop residue in Ghana to provide a significant amount of biofuel to the nation. The work has been presented to the Energy Commission in Ghana, and it was well-received. The study results are presented in **Chapter 5** and the work has also been published in the journal *Renewable and Sustainable Energy Reviews* [12].

This study demonstrates the favorability of mid-level ethanol blends with gasoline to maximize engine thermal efficiency; and provides valuable recommendations for ethanol supply and demand infrastructure development in Ghana, Africa**.** The overall conclusions of the study and recommendations for future work are provided in **Chapter 6.**

References

1. Global Warming of 1.5°C, an IPCC special report on the impacts of global warming of 1.5°C above pre-industrial levels and related global greenhouse gas emission pathways, in the context of strengthening the global response to the threat of climate change, sustainable development, and efforts to eradicate poverty.

2. The Intergovernmental Panel on Climate Change (2018). IPCC Working Group-3 Assessment Report, available from (https://www.ipcc.ch/pdf/assessment-report/ar5/wg3/ipcc_wg3_ar5_chapter8.pdf); [accessed 11/23/2018].

3. United States Environmental Protection Agency. Fast Facts on Greenhouse Gas Emissions, available from (https://www.epa.gov/greenvehicles/fast-facts-transportation-greenhouse-gas-emissions); [accessed 10/15/2018]

4. United States Environmental Protection Agency. The Renewable Fuels Standard Program, available from (https://www.epa.gov/renewable-fuel-standard-program); [accessed 10/15/2018].

5. Biofuels Life Cycle, available from (https://www.jbei.org/research/applications/biofuels-life-cycle/); [accessed 11/22/2018]

6. Singh, R., Burch, T., Lavoie, G., Wooldridge, M., and Fatouraie, M. (2017). Effects of Fuel Injection Events of Ethanol and Gasoline Blends on Boosted Direct-Injection Engine Performance. *SAE Technical Paper No. 2017-01-2238*.

7. Schmidt, L., Seabrook, J., Stokes, J., Zuhdi, M. F. A., Begg, S., Heikal, M., and King, J. (2011). Multiple injection strategies for improved combustion stability under stratified part load conditions in a spray guided gasoline direct injection (SGDI) engine. *SAE Technical Paper No. 2011-01-1228*.

8. Su, J., Xu, M., Yin, P., Gao, Y., and Hung, D. (2015). Particle number emissions reduction using multiple injection strategies in a boosted spark-ignition direct-injection (SIDI) gasoline engine. *SAE International Journal of Engines, 8(1), 20-29 (SAE paper 2014-01-2845)*.

9. Whitaker, P., Kapus, P., Ogris M., & Hollerer, P. (2011). Measures to reduce particulate emissions from gasoline DI engines. *SAE International Journal of Engines (SAE Paper 2011-01-1219*)

10. Kemausuor, F., Kamp, A., Thomsen, S. T., Bensah, E. C., and Østergård, H. (2014). Assessment of biomass residue availability and bioenergy yields in Ghana. *Resources, Conservation and Recycling*, *86*, 28-37.

11. Energy Commission, Ghana. Strategic National Energy Plan 2006-2020, available from (http://energycom.gov.gh/files/snep/PETROLEUM%20final%20PD.pdf); [accessed 05/22/2017]

12. Singh, R., Kemausuor, F., and Wooldridge, M. (2018). Locational analysis of cellulosic ethanol production and distribution infrastructure for the transportation sector in Ghana. *Renewable and Sustainable Energy Reviews*, *98*, 393-406.

Chapter 2

Effects of Fuel Injection Events of Ethanol and Gasoline Blends on Boosted Direct Injection Engine Performance

This chapter was published as Singh, R., Burch, T., Lavoie, G., Wooldridge, M., & Fatouraie, M. (2017). Effects of Fuel Injection Events of Ethanol and Gasoline Blends on Boosted Direct-Injection Engine Performance. *SAE Technical Paper No. 2017-01-2238*. (doi: *https://doi-org.proxy.lib.umich.edu/10.4271/2017-01-2238*)

2.1 Abstract

Numerous studies have demonstrated the benefits of ethanol in increasing the thermal efficiency of gasoline-fueled spark ignition engines via the higher enthalpy of vaporization and higher knock resistance of ethanol compared with gasoline. This study expands on previous work by considering a split fuel injection strategy with a boosted direct injection spark ignition engine fueled with E0 (100% by volume reference grade gasoline; with research octane number = 91 and motor octane number = 83), E100 (100% by volume anhydrous ethanol), and various splash-blends of the two fuels. Experiments were performed using a production 3-cylinder Ford Ecoboost engine where two cylinders were de-activated to create a single-cylinder engine with a displacement of 0.33 L. The engine was operated over a range of loads with boosted intake manifold absolute pressure (MAP) from 1 bar to 1.5 bar. The fuel injection timing of single fuel injection events was varied at MAP = 1 bar using different blend ratios (E0, E30, E50, E85 and

E100) to identify the range of injection timing corresponding to maximum thermal efficiency for each fuel blend.

The results indicated knock limited operation for E0 at MAP higher than 1 bar (boosted), whereas none of the ethanol blends was knock-limited even at the highest MAP tested. A split fuel injection strategy with 50% of the fuel mass in each of two injection events was investigated for the range of MAP conditions studied. The different fuel blends showed little sensitivity to the split injection strategy, which indicated fuel air mixing did not significantly affect combustion at the conditions studied. The highest gross indicated thermal efficiencies (GITE) of 38.4% were achieved with E85 and E100 at 1.1 and 1.2 bar MAP for an absolute improvement of 4% compared with baseline gasoline for the same intake pressures. The improvement in GITE scaled with the fraction of ethanol in the fuel blend. GT-Power simulations were used to evaluate the contributions of the enthalpy of vaporization and cooling effects on GITE. Comparison of the simulation results with the experimental data indicates the benefit of increasing GITE with increasing ethanol in the fuel blend is due to enthalpy of vaporization accounting (e.g. of liquid versus gas-phase fuel) and cooling effects on thermodynamic properties such as the ratio of specific heats.

2.2 Introduction

Federal energy policies for vehicles specify aggressive improvements in fuel economy and vehicle emissions. One method to achieve these goals is to blend renewable biofuels like ethanol with fossil fuels. Although ethanol blending can reduce oil dependence and greenhouse gas emissions, vehicle miles travelled per volume of fuel is typically lower when using blends of ethanol and gasoline compared with unblended gasoline due to the lower heating value of ethanol. However, ethanol blending improves knock behavior, which enables an increase in

compression ratio and can thus improve the thermal efficiency of the engine [13], [14], [15], [16]. At present, most gasoline sold commercially in United States contains 10% ethanol (E10), and as of 2011, the U.S. Environmental Protection Agency began allowing the use of E15 (gasoline fuel with ethanol content between 10-15%) in model year 2001 and newer gasoline vehicles.

Numerous studies have demonstrated the benefits of ethanol to increase the thermal efficiency of gasoline spark ignition engines (e.g., [13], [14], [15], [16] and references therein). Stein et al. [13] provides an excellent review of the effects of ethanol on engine performance in terms of fuel efficiency and exhaust emissions. Stein et al. [13] also documents the differences in key thermophysical properties of gasoline and ethanol that play a role on engine performance. Several studies [13], [14], [15], [16] have specifically focused on the knock benefits of ethanol blends. The studies demonstrated the benefits of ethanol blends to improve thermal efficiency by increasing compression ratio e.g., [17], [18] and/or by expanding the range of high load and boosted conditions where the engine could operate at optimum maximum brake torque (MBT) spark timing, e.g., [15], [19]. Without the addition of ethanol, spark timing is typically retarded from MBT timing to avoid knock, resulting in retarded combustion phasing and lower thermal efficiency. Leone et al. [15] reported in their landmark study of gasoline and ethanol blends a remarkable improvement of 13% points in brake thermal efficiency (BTE) at low speed (1000 RPM) mid-load (11 bar brake mean effective pressure (BMEP)) conditions by increasing the ethanol content of the blend to 30% (E30) from the base fuel of their study, E10. This was possible as the splash-blended E30 had a higher resistance to knock with a research octane number of RON = 101 compared with the E10, which had RON = 91. The higher-octane rating allowed operation using E30 at a higher load without spark retard or enrichment. Nakata et al.

[19] showed ethanol allowed MBT operation without knock over a wider load range, and thermal efficiency improved from 31.7% for unblended gasoline (RON = 92) to 37.9% for E100. In the study by Whitaker et al. [20], an efficiency improvement of 7.8% for high load operation was found with E85 compared with regular U.S. grade gasoline (RON = 91).

The beneficial effects of ethanol can be less pronounced if the engine is not knock-limited. Jo et al. [16] through their experimental and simulation study of gasoline and ethanol blends reported the efficiency of the engine was fuel independent as long as the engine was not knock limited, and adding ethanol allowed the engine to operate at MBT timing over a much higher load range. Similarly, Stein et al. [13] stated "The increase in knock-limited BMEP can be limited by the peak pressure capability of the engine structure or the boost capability of the boosting system," in which case the benefits of ethanol may be restricted to a smaller operating range. In Jung et al. [21], equivalent part-load conditions of a turbocharged direct injection spark ignition (DISI) engine were compared between E85 and E0 (RON = 90.7). The authors reported E85 exhibited fundamental benefits in BTE of about 4% (on a relative basis) compared with E0. The improvement in BTE was reported at conditions where neither fuel was knock limited. Thus, the benefit from ethanol was not due to the improved knock resistance of E85.

The majority of the previous work comparing ethanol with gasoline at turbocharged direct injection conditions used single fuel injection events. An exception was the study by Whitaker et al. [20], who used multiple fuel injection events as a means to accelerate catalyst heating during cold start conditions. Multiple injection events can alter the end gas conditions thereby controlling knock, and strategies using multiple fuel injection events have been successfully demonstrated in gasoline-fueled DISI engines studies to extend knock limits (e.g., Yang and Anderson [22]). Leveraging charge cooling effects to increase volumetric efficiency

and power output in a DI engine is also dependent upon the injection strategy [22], and there are fewer studies of the effects of multiple injection events on ethanol and gasoline blends.

The fuel properties for E0 and E100 used for blends in this study are listed in **Table 2.1**. The Reid vapor pressure, distillation curves, RON, motor octane number (MON), octane sensitivity (S, where S = RON - MON), enthalpy of vaporization and specific heating value all vary as a function of ethanol content in the gasoline blend [13], and affect the end gas composition and state. Furthermore, differences in spray break-up and the amount of liquid injected in each event will affect the local mixture conditions and the local thermal conditions, affecting the local reactivity and knocking propensity of the end gas, and therefore multiple injection events may potentially expand the thermal efficiency benefits of ethanol. The objective of this work was to evaluate the effects of different fueling strategies of ethanol, gasoline and blends of both fuels on combustion performance in a turbocharged single cylinder DISI engine over a range of boosted intake air conditions using single-injection and binary-injection events.

Table 2.1. Fuel properties based on supplier specifications, unless stated otherwise.

Property	Units	Reference grade gasoline (E0)	Anhydrous ethanol (E100)
Reid Vapor Pressure	kPa	62.5*	5.95**
Lower Heating Value (gravimetric fuel basis)	MJ/ kg-fuel	42.9*	26.9 [23]
Lower Heating Value (gravimetric stoichiometric fuel and air mixture basis)	MJ/ kg-stoich mixture	2.9	3.0
Stoichiometric Air/Fuel Ratio	Mass basis	14.6	9.0
H/C Ratio	Mole basis	1.89*	3.0
O	Mass fraction [%]	<0.05	0.5
Research Octane Number	-	91*	~108 [24]
Motor Octane Number	-	83*	~91 [24]
Octane Sensitivity (S)		8*	17
Enthalpy of Vaporization (gravimetric fuel basis)	kJ/ kg-fuel	373 [23]	840 [23]

Property	Units	Reference grade gasoline (E0)	Anhydrous ethanol (E100)
Enthalpy of Vaporization (gravimetric fuel and air mixture basis)	kJ/ kg-stoich mixture	25.5	93.3
Initial Boiling Point	°C	34*	78**

**Halterman (http://www. Halterman.com)*
***Sigma Aldrich (http://www.sigmaaldrich.com)*

2.3 Experimental Set-up

The study was conducted using a production 2013 Ford Ecoboost 3-cylinder 1.0 L turbocharged DISI engine modified to operate as a single cylinder engine. Cylinders 1 and 3 were deactivated by grinding the respective cam lobes of the intake and exhaust valves off the camshafts and by removing the piston and con-rod assemblies. The crankshaft was rebalanced using dummy weights. **Table 2.2** lists the engine specifications.

Table 2.2. Test engine specifications

Spark plug	Centrally mounted
Valvetrain	twin independent variable cam timing with dual overhead camshaft and 4 valves per cylinder
Displaced Volume	333 cm^3
Cylinders	1
Stroke	82 mm
Bore	71.9 mm
Compression Ratio	10:1
Fuel injector and location	Bosch 6- hole HDEV5 injector Centrally mounted

The valve timing was fixed for all experiments. The head was modified to allow a sensor to be mounted for in-cylinder pressure measurements using a piezoelectric transducer (Kistler 6052C) and charge amplifier (Kistler 5010B). The intake and exhaust manifold pressures were

measured using an absolute pressure sensor in the intake plenum (Measurement Specialties US331-000005-030PA) and a gauge pressure sensor (Measurement Specialties US331-000005-030PG) in the exhaust plenum. A crank angle encoder (BEI, H20EB-37-F12-SS-360) was used with 1440 signals per revolution, and the timing of top dead center (TDC) was measured with a TDC marker sensor. The signals were used for engine speed control and monitoring, fuel injection timing, and spark timing. The pressure and crank angle encoder data were acquired using a data acquisition system (National Instruments Compact cDAQ). The data were acquired at 60 kHz for 10 seconds with the engine speed fixed at 1000 RPM, which corresponded to approximately 82-85 combustion cycles at each experimental condition. Knocking is more prevalent at low speed and high load conditions (as these conditions yield high end-gas temperature and pressure and sufficient time for end-gas autoignition) consequently a relatively low engine speed of 1000 RPM was selected for the study.

Figure 2.1 is a schematic of the engine and dynamometer facility used in the study. An engine control module (from Electro Mechanical Associates) was used to control spark and fuel timing with a fuel driver unit (Bosch P06). All experiments used stoichiometric conditions and stoichiometry was controlled by varying the fuel injector driver pulse width duration while setting a constant fuel rail pressure of 100 bar. The fuel/air equivalence ratio was measured using a lambda meter (ETAS LA4) with a broadband lambda sensor (Bosch LSU 4.9) based on the O_2 measurement in the exhaust. The lambda meter settings were changed for each fuel blend using the appropriate O/C and H/C ratios. No engine-out gas emissions data were collected as part of this study. A filter type smoke meter (AVL 415) was used as a threshold test to evaluate the soot emissions in the exhaust. The smoke meter reports filter smoke number (FSN) as an indication of soot or particulate matter concentration with a minimum detection limit of 0.02

mg/m^3. Thus, any non-zero FSN values measured using the smoke meter indicated the soot concentration was higher than 0.02 mg/m^3, and were considered unacceptably high particulate emissions.

The experimental operating conditions are provided in **Table 2.3**. The MAP was varied from 1 bar to 1.5 bar using filtered, boosted air. The air flow rate was measured using a flow meter (Alicat, model #MCR-500SLPM-TFT) and the fuel flow rate was measured using a piston type flow meter (Max Machinery, model #213-611-000). The baseline reference grade gasoline (E0) fuel used in this study was Haltermann HF0072; an 87-octane index ((RON+MON)/2) research grade, unoxygenated gasoline. The E0 was splash blended by volume with anhydrous E100 (Sigma Aldrich, E100 anhydrous, purity $\geq$ 99.5%, $H_2O \leq 0.005\%$) to produce each fuel mixture. The fuel system was purged between each set of fuel blend experiments. The fuels considered in this study were E0, E30, E50, E85 and E100. E85 was chosen due to its commercial significance. E30 and E50 were selected as mid-level blends. Mid-level blends have been proposed (e.g. [13]) as more realistic targets for the future transportation fueling infrastructure. In addition, the properties of ethanol and gasoline do not blend linearly, and a blend ratio of ~30% ethanol with gasoline has a vapor pressure that is higher than either 100% gasoline or 100% ethanol [13].

Table 2.3. Experimental Operating Conditions

Variable	**Range/Value**
Manifold Absolute Pressure	1 – 1.5 bar
Fuels	E0, E30, E50, E85, E100
Engine Speed	1000 RPM
Lambda (λ)	1 (Stoichiometric)
Fuel Injection pressure	100 bar
Fuel Injection Strategy	Number of Injections: 1) Single Injection 2) Binary injection (fuel mass ratio of 1:1) Start of Injection Timing: Ranged from 300° bTDC to 50° bTDC for MAP = 1 bar

Variable	Range/Value
Intake Valve Opening	5° aTDC (gas exchange)
Intake Valve Closing	232° aTDC
Exhaust Valve Opening	228° bTDC
Exhaust Valve Closing	0° aTDC
Coolant Temperature	90 °C
Engine Operating Limits	Average Maximum In-Cylinder Pressure ≤ 90 bar Knock Limit: KI20≤ 0.1 FSN = 0

2.4 Experimental Approach

The fuel injection parameters were varied systematically to determine the effects of the different fuels on engine performance. The approach started with single fuel injection events to determine the baseline operating conditions of the fuels. The start of injection (SOI) was varied from 300° to 50° bTDC (firing) in intervals of 50° or until a decrease in gross indicated mean effective pressure (GIMEP) or gross indicated thermal efficiency (GITE) was observed for each fuel at MAP = 1 bar. Advanced fuel injection timing was limited by increased smoke emissions using the FSN criterion described above. The increase in particulate emissions may be due to fuel impingement on the piston for the earlier injection timings where the piston is closer to TDC. Late fuel injection timing was limited by FSN and/or reduced GIMEP. **Figure 2.2** shows the range of SOI values considered in the study for single fuel injection events.

For each injection timing the spark timing was varied to achieve MBT. At boosted intake air conditions, knocking was a concern and prevented MBT operation for E0. Knocking conditions were identified using the in-cylinder pressure data. A knock intensity factor KI20 was defined and calculated using high pass filtered pressure crank angle data, based on the work by König and Sheppard [25] as

$$KI20 = {}_{i=1}\sum^{Nsamp} (P_i - P_{mean})^2/N_{samp}$$

where P_{mean} is the zero level of the high pass filtered data, N_{samp} is the number of pressure samples P_i within a 20° crank angle range. As shown in **Table 2.3**, a KI20 threshold of 0.1 was defined, corresponding to a pressure rise of 1 bar above P_{mean}. If KI20 values were above this limit, spark timing was not advanced any further.

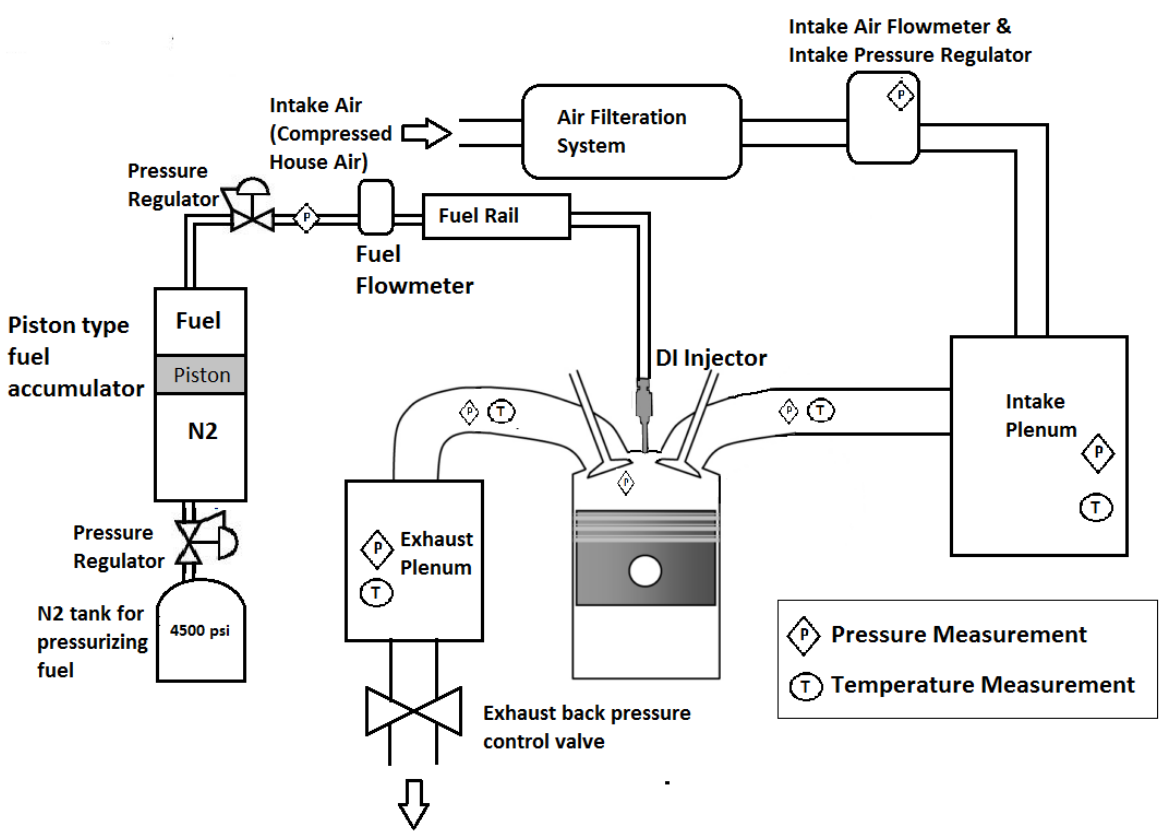

Figure 2.1. Schematic of the single-cylinder Ford Fox Ecoboost engine facility and the supporting systems.

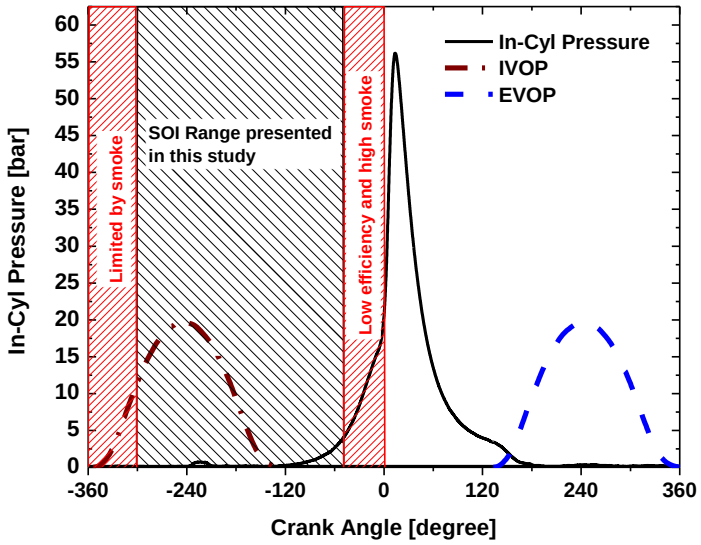

Figure 2.2. Engine timing set-up showing the range of injection timings studied for single fuel injection events with respect to the valve events (intake valve opening profile = IVOP, exhaust valve opening profile = EVOP) at MAP = 1 bar.

2.5 Experimental Results

2.5.1 Single Fuel Injection Events- Effects of Injection Timing at intake manifold absolute pressure (MAP) = 1 bar:

The results for GIMEP at MBT spark timing for the different fuels and fuel injection timings are presented in **Figure 2.3**, for MAP = 1 bar. The error bars in all figures are the standard deviations of the recorded combustion cycles, unless stated otherwise (the methodology used for determining error bars is included in the Appendix). **Figure 2.4** presents the results for the gross indicated thermal efficiency (GITE) corresponding to the data of **Figure 2.3**. In both figures the timing of the intake valve opening profile (IVOP) is provided for reference. None of the conditions studied for MAP = 1 bar were constrained by knocking. For E0, the earlier injection timings of 300°, 250° and 200° bTDC yielded the highest GIMEP and GITE values, and retarding the fuel injection timing decreased the GIMEP and GITE. Fuel injection events

earlier than 260° bTDC and later than 50° bTDC resulted in unacceptable FSN values for E0. For the E30 blend, unacceptable FSN values were observed for SOI earlier than 240° bTDC and later than 50° bTDC. For E50, smoke numbers were unacceptable for SOI earlier than 210° bTDC and later than 50° bTDC. Based on these trends for the blends with lower ethanol concentrations, the SOI timing study for E50 focused on a small range of SOI conditions that were not smoke limited and would identify the range of SOI conditions leading to maximum GIMEP and GITE.

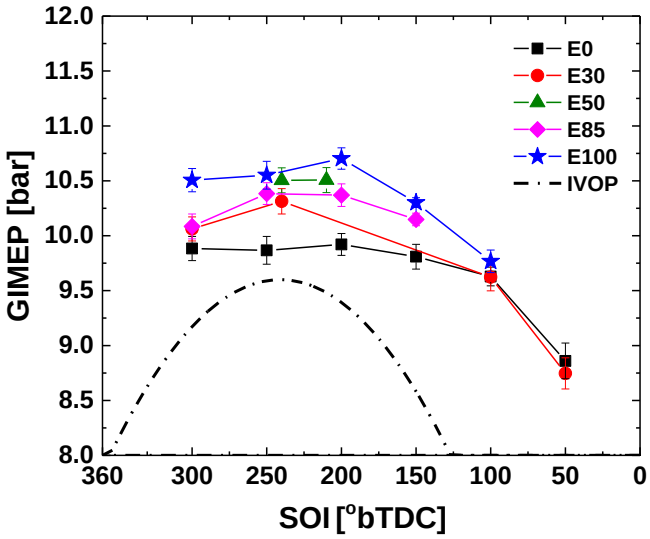

Figure 2.3. Comparison of GIMEP for single fuel injection events at MAP = 1 bar. The error bars represent the standard deviation of the data. The dashed line represents the intake valve opening profile.

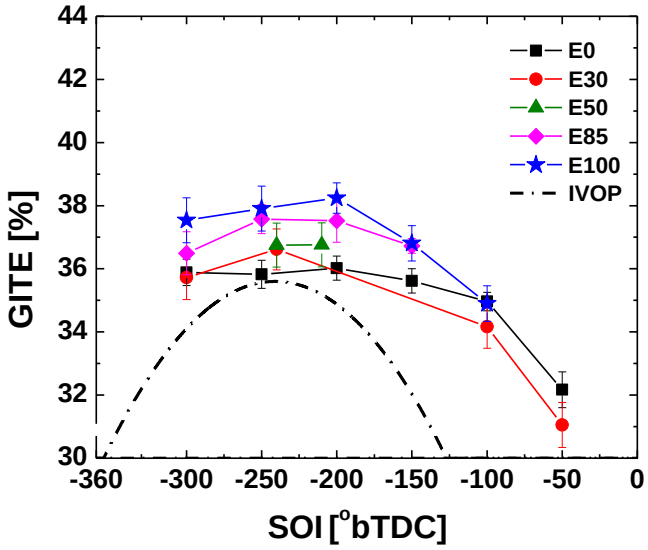

Figure 2.4. Comparison of GITE for single fuel injection events at MAP = 1 bar corresponding to data presented in **Figure 2.3**

FSN values were below the detectable limit for E85 and E100 at all fuel injection timings. As the ethanol content in the blend increased, the injection duration also increased, as more fuel was needed to maintain stoichiometric conditions. As SOI was advanced to earlier timing, the increased smoke emissions were likely due to fuel impingement on the piston. The longer injection durations of the higher ethanol content fuels could lead to more fuel wetting of the piston at earlier SOIs relative to E0. However, the results for E85 and E100 indicate either the intrinsic chemical kinetic properties of more ethanol in the mixture suppressed soot formation or the fuel spray properties changed enough to reduce fuel impingement and the associated smoke emissions, relative to E50, E30 and E0. Specifically, regarding the ethanol spray characteristics, while volatility is important, other features of the fuel blends also affect the spray. For example, Serras-Pereira et al. [26] observed for ethanol, butanol, iso-octane and gasoline, the fuel properties impacted spray characteristics like spray collapse, spray area, etc. Changes in the physical spray characteristics and operating conditions, such as coolant temperature, combustion chamber geometry, engine speed, etc. will affect the fuel impingement

on the combustion chamber walls and the piston which is directly associated with soot formation (e.g. see Fatouraie et al. [27]). Regarding the chemical effects of ethanol on sooting, Westbrook et al. [28] found the formation of soot precursor species were reduced with increasing fraction of oxygen content in the fuel (by mass) in their studies of the chemical kinetics of oxygenated hydrocarbons. The results of the current work support the widely observed trends of reducing engine-out soot emissions with increasing oxygen fraction in the fuel mass.

Regarding the lower GIMEPs and GITE observed for the later SOIs, Kakuho et al. reported [29] as the fuel injection timing is retarded in the latter half of the compression stroke, it is more difficult to transport the injected fuel towards the spark plug at the top of the combustion chamber because of the sharp attenuation of the tumble flow. There is also significant charge stratification due to less time for fuel vaporization and mixing which can result in poor combustion efficiencies.

Comparing the results for the different fuels, systematically the fuels with higher ethanol content yielded higher GIMEPs and GITEs. This trend is, in part, due to the higher specific energy per unit stoichiometric charge of E100 compared with E0 (see **Table 2.1**); however, volumetric efficiency plays a role as well, as discussed below. Based on the results for each fuel, the ranges for the values of SOI for single injection events corresponding to the maximum GIMEP and GITE were identified and are provided in **Table 2.4**. The maximum GIMEP and GITE for E0 showed little sensitivity to SOI as long as SOI was during IVO for MAP = 1 bar. In comparison, the ethanol blends indicated maximum GIMEP and GITE was in the range of SOI = 175 to 275° bTDC, or during the latter half of the IVO event for MAP = 1 bar.

Table 2.4. Results for range of SOI timing leading to maximum GIMEP for single fuel injection events, and SOI timing used for the binary fuel injection study.

Fuel	Range of SOI of single fuel injection event for maximum GIMEP and GITE [° bTDC]	Limiting condition for single injection event	SOI of two fuel injection events[a]	
			SOI1 [° bTDC]	SOI2 [° bTDC]
E0	325-175	Advance limited by smoke	300	260
E30	275-175		280	240
E50	275-175		250	210
E85	275-175	Maximum GIMEP/ GITE	n/a	n/a
E100	275-175		250	200

[a] *50% fuel mass in each event*

Figure 2.5 presents the volumetric efficiency for the results of **Figures 2.3** and **2.4** with the IVOP provided for reference. As seen in **Figure 2.5**, injecting earlier in the cycle when the intake valve is open increases the volumetric efficiency in a DISI engine due to the charge cooling effect of fuel evaporation. The data also show E100 was more sensitive to advancing SOI compared with E0. This sensitivity is attributed to the higher enthalpy of vaporization of ethanol. Further advancing SOI during IVO, i.e. beyond approximately 250°bTDC and earlier than the maximum open position of intake valves decreased the volumetric efficiency of the ethanol blends, due to the reduced benefits of charge cooling. The SOI for maximum volumetric efficiency for E100 was 200° bTDC which corresponds with the SOI of maximum GIMEP and GITE for E100. Furthermore, the weak sensitivity of the volumetric efficiency of E0 to SOI supports the trends observed of the weak sensitivity of GIMEP and GITE of E0 to SOI.

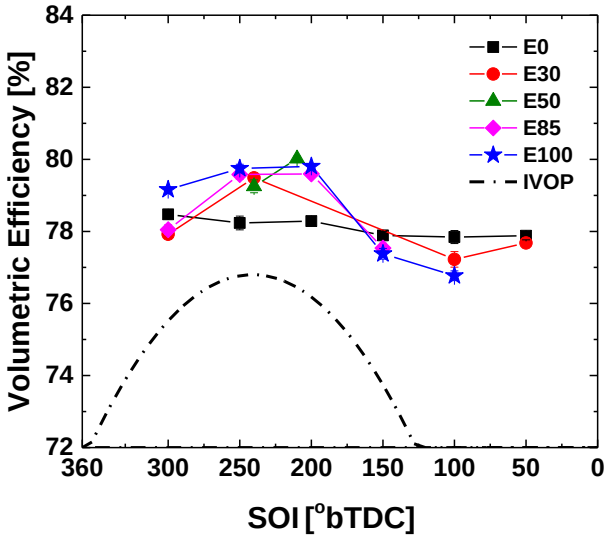

Figure 2.5. Comparison of volumetric efficiency for different fuel blends and single injection events at MAP = 1 bar. Error bars are included in the figure and are generally on the same scale as the size of the symbol.

2.5.2 Single Fuel Injection Events- Effects of intake manifold absolute pressure (MAP):

For the next set of experiments, single fuel injection events were used, and the effects of boosting the intake manifold air (MAP >1 bar) were determined. The SOI for each fuel was set in range of the optimum timing determined for the 1 bar MAP results, specifically SOI = 260° for E0; SOI = 240° for E30; SOI = 210° for E50; SOI = 200° for E85; SOI = 200° for E100. Additionally, for E100 at 1.4 and 1.5 bar MAP, the maximum injection duration time became hardware limited, and consequently the injection was split with the injection events spaced as close as possible to each other (< 7° between the end of the first injection event and the start of the second event) and the maximum possible fuel amount was injected in the first event (93% at 1.4 bar and 87% at 1.5 bar). The MAP was increased from 1 bar to an absolute pressure of 1.5 bar in increments of 0.1 bar. For E0 at all boosted conditions, i.e. MAP of 1.1 bar and higher, the performance was limited by knock. Consequently, spark timing could not be advanced to

MBT for boosted intake pressures with E0. Knocking was not observed for any of the ethanol blends tested in the study for any of the boosted conditions. At MAP = 1.5 bar, the engine was limited by the maximum in-cylinder pressure of 90 bar, and hence no further boosting was considered.

Figure 2.6 shows the GIMEP and coefficient of variation (CoV) of the GIMEP for the fuels as a function of the air intake pressure. As with the results for MAP = 1 bar, the higher the ethanol content in the blend, the higher the GIMEP at each boost pressure. The large increase in GIMEP between E0 and E30 is the effect of retarding spark for E0. The offset in GIMEP relative to E0 increased slightly for the ethanol blends with increasing MAP, which is attributed to the later heat release with E0 as discussed below. The CoV results in **Figure 2.6** show all conditions were stable with CoV values less than ~1.5% (where 3% was considered the maximum stability limit), and increased ethanol content in the blend reduced CoV at all intake pressures. Similar observations of improved engine stability with increasing ethanol content in the fuel blend have been reported by other researchers like Zhuang et al. [30], who attributed the improvement to the higher flame speed of ethanol.

Figure 2.7 shows the CA50 (crank angle position where 50% of the total heat is released) for all the ethanol blends is around the MBT point of 10° aTDC, whereas for E0 the CA50 was retarded by ~10° for the highest MAP conditions. The CA50 for E0 was more retarded with increasing MAP, which explains the trend of increasing offset of GIMEP between E0 and the ethanol blends observed in **Figure 2.6**. The spark timings associated with the data of **Figure 2.7** are presented in **Table 2.5**. The spark timing for the ethanol blends remained very consistent between 8^{o} to 10^{o} bTDC for all operating conditions. The spark timing for E0 was retarded

significantly - by 11° - from the 1 bar to the 1.5 bar MAP operating conditions which is consistent with the change in phasing of the CA50 for E0.

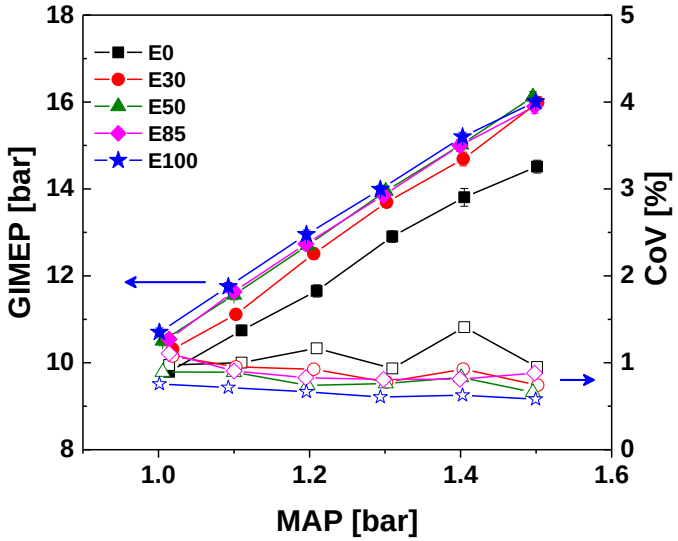

Figure 2.6. Comparison of GIMEP (solid symbols) and CoV of GIMEP (open symbols) as a function of MAP for single fuel injection events at the fixed SOI timing provided in **Table 2.3**. Error bars representing the standard deviation of the data are included in the figure but are typically smaller than the size of the symbols.

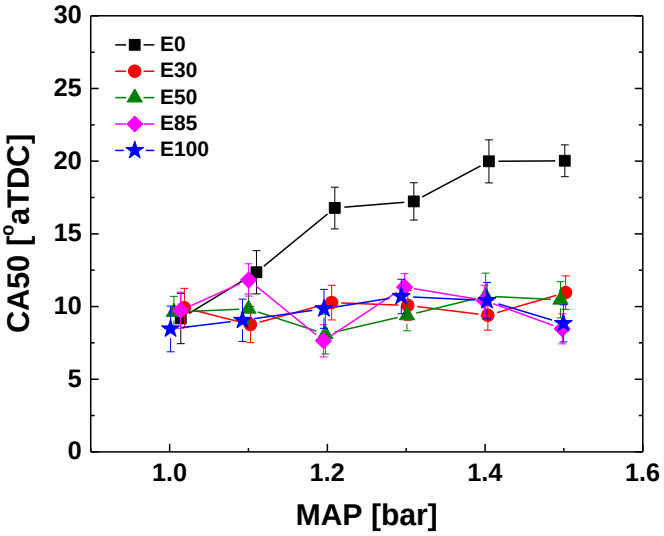

Figure 2.7. CA50 phasing corresponding to the data presented in **Figure 2.6.**

Table 2.5. Spark/Ignition timing corresponding to data presented in **Figure 2.6**

MAP [bar] / Fuel	Spark Timing [° bTDC]					
	1	**1.1**	**1.2**	**1.3**	**1.4**	**1.5**
E0	11	7	4	3	1	0
E30	10	10	9	9	9	8
E50	10	9	10	9	9	9
E85	10	8	10	8	8	9
E100	10	10	10	9	10	8

Table 2.6 presents the amount of fuel injected per cycle for each of the fuels at the various intake air pressures. The lower energy content of the ethanol requires more mass per cycle compared with E0 as seen in **Table 2.6**, and the boosted intake air conditions led to an additional increase in fuel mass per cycle of a factor of 1.6 for E100 at 1.5 bar MAP compared with E100 at 1 bar MAP. E0 required the same factor increase in fuel mass between the 1 bar and 1.5 bar MAP operating conditions.

Table 2.6. Fuel injection quantity as a function of the intake air pressure

MAP [bar] / Fuel	Fuel Injection Quantity [mg/cycle]					
	1	**1.1**	**1.2**	**1.3**	**1.4**	**1.5**
E0	21.3	23.8	26.2	28.7	30.9	34.5
E30	24.6	26.8	29.5	32.5	35.3	38.6
E50	27.3	29.7	32.8	36.3	39.0	41.8
E85	31.4	34.3	37.9	41.4	44.8	48.2
E100	34.5	37.9	41.6	45.8	49.9	55.0

Figure 2.8 compares the 0-10% burn duration of the fuel blends. While the results for the ethanol blends were generally similar (i.e., within the standard deviations of the data) at all

MAPs, E0 had longer burn durations at higher MAP due to the increased need to retard spark from MBT.

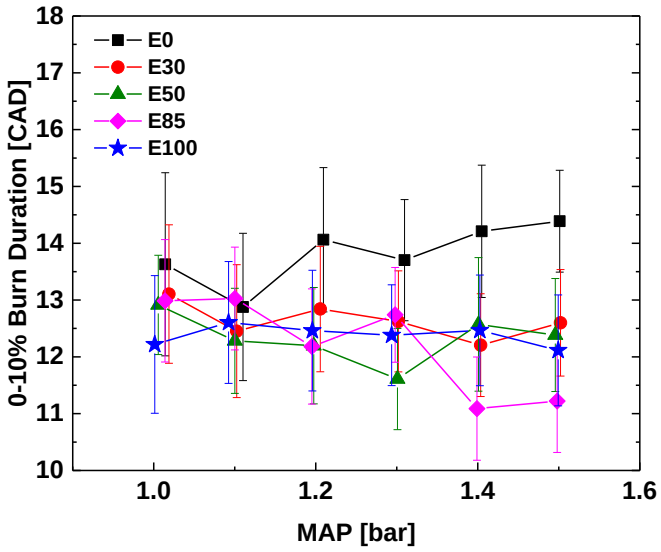

Figure 2.8. 0-10% burn duration results corresponding to the data presented in **Figure 2.6.**

Figure 2.9 compares the GITE for the fuels as a function of MAP. Again, since operation with E0 was limited by knock at the boosted intake air pressure conditions, the GITE was systematically lower for E0 compared with the ethanol blends. The efficiency for E0 also decreased as MAP increased as the spark timing was retarded further from MBT. The decrease in the E0 GITE was larger from 1 to 1.2 bar, after which the GITE values were approximately constant. These trends are attributed to the magnitude of the change in spark timing (**Table 2.5**) and the associated decrease in CA50 (**Figure 2.7**) required to avoid knock for E0. Larger changes in spark timing were required at 1.1 and 1.2 bar MAP compared with higher values of MAP. The GITE of the E85 and E100 fuels were nearly identical, and the maximum values observed were ~38% for 1.1 1.2 bar MAP for E85 and E100. Higher MAPs decreased the GITE of the ethanol blends slightly.

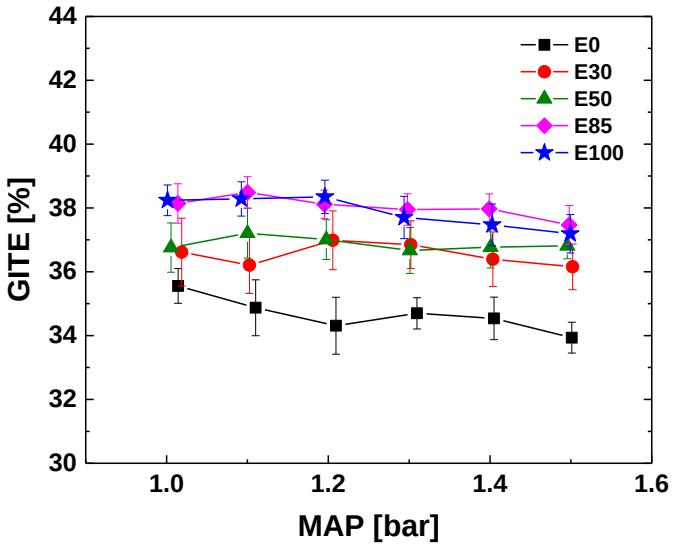

Figure 2.9. GITE results corresponding to the data presented in **Figure 2.6.**

The results for gross indicated specific fuel consumption (GISFC) were very sensitive to the ethanol content in the fuels as seen in **Figure 2.10**. GISFC increased with increased ethanol content, due to the lower heating value of ethanol compared with gasoline. Thus, the GISFC values were higher for the ethanol blends even though the thermal efficiency values for the ethanol blends were higher. The results capture the challenge of ethanol blends, where unless the anti-knock qualities of the ethanol are exercised, e.g. by increasing the compression ratio of the engine to further improve the thermal efficiency and thereby lower the GISFC, the effects of the lower heating value dominate the GISFC.

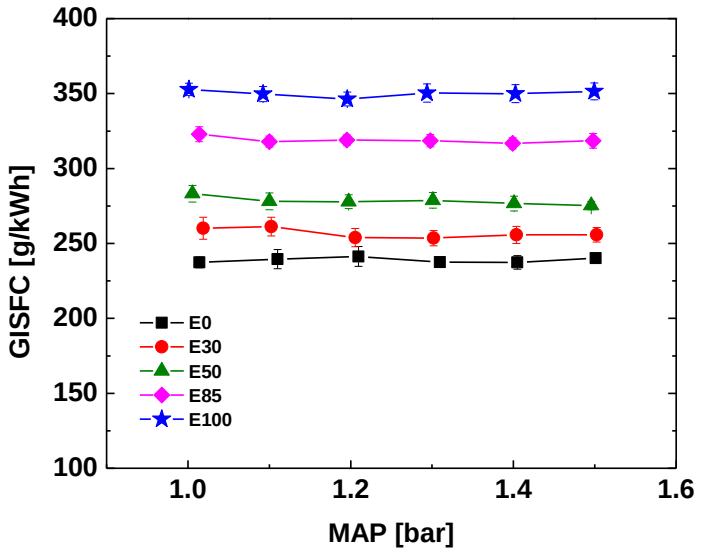

Figure 2.10. GISFC results corresponding to the data presented in **Figure 2.6.**

2.5.3 Binary Fuel Injection Events- Effect of intake manifold absolute pressure (MAP):

The effects of a binary fuel injection strategy, with equal fuel mass injected in each of the two injection events (SOI1 and SOI2) in each engine cycle, were studied for the fuel blends. In previous studies of split injection strategies, the second injection event has been timed to occur later in the compression stroke to lower the end-gas temperature and thereby extend knock limits. However, only the boosted E0 conditions were knock-limited in this study. In addition, the results of the single injection events at MAP = 1 bar indicated volumetric efficiency improved when fuel injection occurred earlier during IVO. Therefore, a split injection strategy with both injection events occurring during IVO was used in this study. The timing of the second injection event, SOI2, was kept in the range that led to maximum GIMEP, as listed in **Table 2.4**. The timing of the first injection event, SOI1, was selected to be 40° earlier than SOI2 for all fuels except E100. This constraint was selected because further advancing SOI1 beyond 300° bTDC resulted in particulate emissions for E0. For E100, the first injection event was

advanced by 50° to accommodate the longer injection duration required for pure ethanol fuel. The SOI timing for each of the fuel injection events in the binary fueling study is listed in **Table 2.4**. Spark timing was kept the same for each fuel as identified in the single injection event study. For all split injection conditions, smoke levels were below the detectible limit.

Figure 2.11 compares the results for GIMEP, GITE and CoV of GIMEP for the single and split fuel injection operating conditions. The data show the split injection strategy resulted in comparable GIMEP, CoV, and GITE for all blends and MAPs. No significant benefit was observed to the binary fueling strategy in comparison with the single injection strategy based on these metrics. The results indicate there were no further gains in volumetric efficiency with the earlier SOI of the first injection event for either the E0 or the ethanol fuel blends.

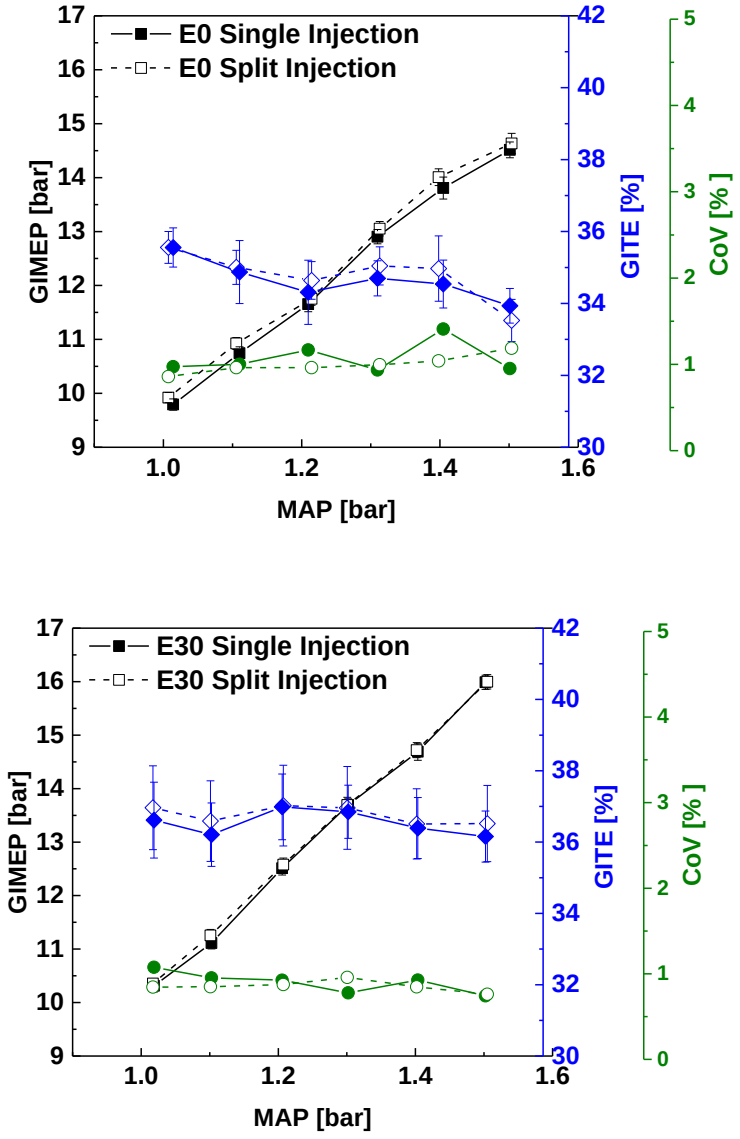

Figure 2.11. Comparison of GIMEP, CoV of GIMEP and GITE for single and binary fuel injection strategy

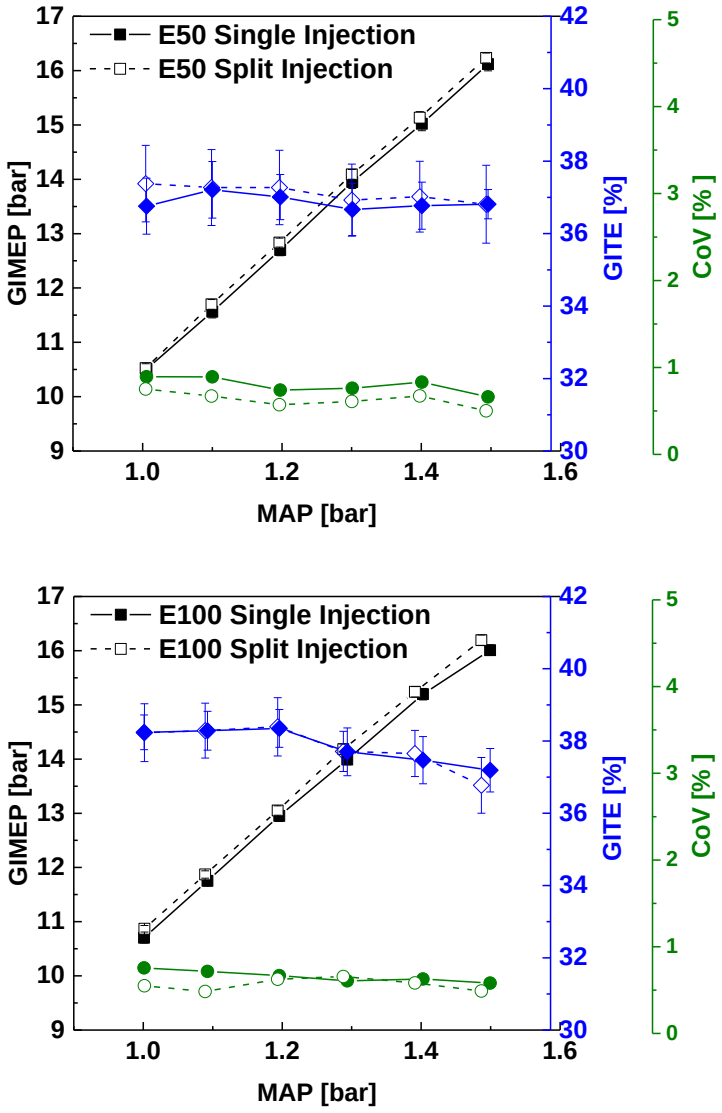

Figure 2.11 (continued). Comparison of GIMEP, CoV of GIMEP and GITE for single and binary fuel injection strategy

2.5.4 GT-Power Model Set-Up & Model Results

To further investigate and understand the observed ~7% relative increase in gross efficiency of ethanol over gasoline, at MAP = 1 bar, a GT-Power model of fuel evaporation was configured as the single cylinder Ford Ecoboost engine used in the experiments. With the aid of the model it was possible to enhance understanding of the evaporation and chemical effects of

the alternative fuels observed in experiments. Constant pressure plenums were used for intake and exhaust with valve timings taken from the experiment. The 10-90 crank angle burn duration of the Weibe function burn curve was set to 25° with a CA50 value of 10° aTDC to approximately match the un-retarded MBT values of the experiment. A sequential injector model was used with experimental air-to-fuel ratio and start of injection values. With typical injection rates, the injection durations ranged from 30° to 50°. To control the source of heat for fuel evaporation, either from the walls or from the gas, the fraction of fuel evaporating directly during injection was set to zero, but upon injection each portion of the injected fuel evaporated with a 50% lifetime of 1^{o}. The standard Woschni heat transfer model was used with nominal multiplier of 1.0. Beyond these specifications no attempt was made specifically to validate the model in detail, rather the focus was on understanding the trends arising from the evaporation effects.

Figure 2.12 shows the model results of the investigation of evaporation effects and how they relate to efficiency gains with ethanol and ethanol blends. The symbols represent the experimental data over the range of MAP from 1 to 1.5 bar (and are the same data presented in **Figure 2.9**). For E0, knock-free operation was observed only at 1 bar intake pressure and that is the only E0 result shown in **Figure 2.12**. Excluding the other E0 data removes the effect of spark retard from the comparison. The model results shown are for the case of MAP = 1.0 bar. Calculations for MAP = 1.5 bar were also completed and resulted in similar behavior, but with efficiencies all shifted upward by ~ 0.5%, most likely due to decreasing relative heat transfer at higher densities but are not shown for clarity.

The model compares well with the experimental data. In **Figure 2.12**, the curves indicate the GT-Power simulations which employed a DI injector setup with SOI = 240° bTDC and the option to take the enthalpy of vaporization (HoV) from either

1) the walls (with no change in intake temperature) – dashed red line in **Figure 2.12** or
2) the intake charge (with significant cooling) – solid red line in **Figure 2.12**

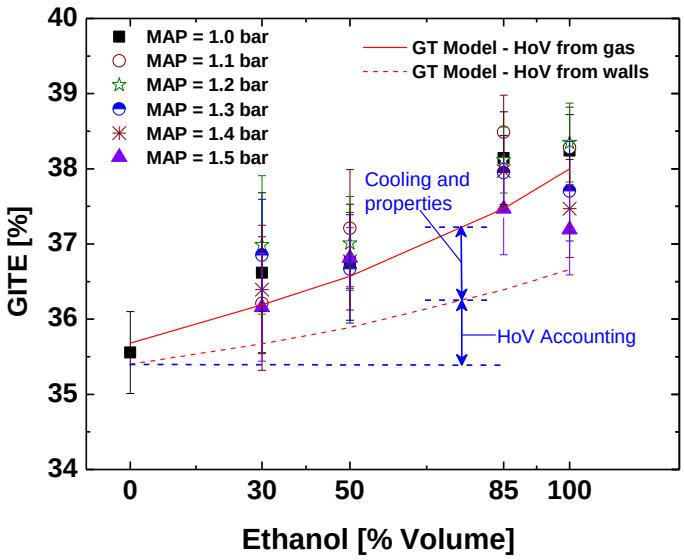

Figure 2.12. GT-Power simulations of gross efficiency as a function of ethanol content. Symbols with error bars are engine experimental data for various MAPs as indicated. The error bars are the standard deviation of the data. CA50 for all results was ~ 10°ATC.

Two main effects of ethanol are seen in the figure. The first is simple HoV accounting and is apparent for the case with all enthalpy of vaporization coming from the walls. Since the incoming fuel energy is computed for the liquid fuel, and the heat released is from the vapor state there is a net benefit for the ethanol fuel [21] which has a higher enthalpy of vaporization compared with gasoline. For pure ethanol, this results in an increase of about 3.5% in efficiency on a relative basis. The other effect arises from charge cooling and burned gas temperature reduction which will improve gas properties (specifically by increasing the ratio of the specific

heats or gamma), as well as reduce the amount of dissociation. The thermal property effects result in an additional increase of 3.5% for pure ethanol with a total relative gain of 7%.

The absolute agreement in efficiency may be fortuitous given the simplicity of the model; nevertheless, trend wise the model agrees with the data well, and the results indicate almost all of the HoV appears to come from the gas. However, for the highest ethanol content and at the highest intake pressure, there is a significant decrease in efficiency gain from those predicted by model, perhaps due to the longer injection event and more impingement on the chamber walls.

2.6 Discussion

A key outcome of the study was that the operating conditions were never knock-limited for the ethanol fuel blends. Only E0 at boosted conditions was constrained by knocking. Consequently, the benefits of the split fuel injection strategy were minimal in comparison with the single fuel injection event strategy; however, the benefits of adding ethanol to the fuel were significant at all operating conditions. The results for GITE of the single injection events for MAP = 1 bar are presented as a contour map as a function of SOI and ethanol content in the blend in **Figure 2.13**. The results showed significant thermal efficiency benefits to ethanol even at the lowest blend levels considered, i.e. E30.

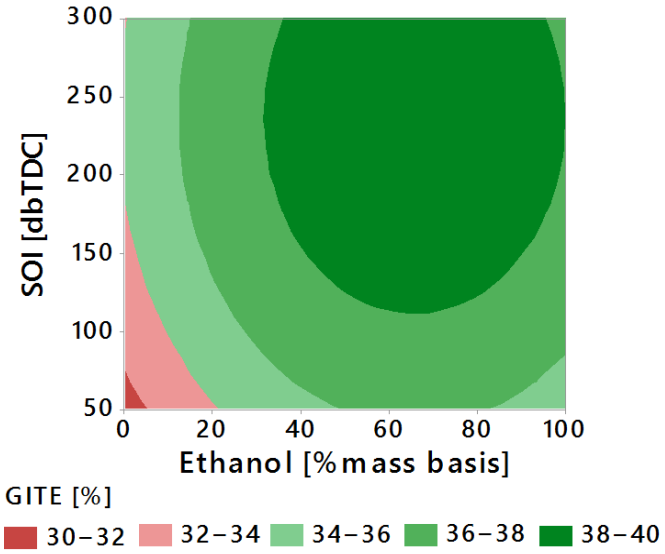

Figure 2.13. Contour plot of GITE generated from the experimental results for single fuel injection events at MAP = 1 bar. The ethanol content is provided on a mass basis.

The benefits of ethanol at part-load conditions, where engine operation was not knock-limited, have been observed in other studies [19], [21], [31], [32]. In the study Jung et al. [21], the authors observed a thermal efficiency gain of 4% for E85 relative to gasoline at equivalent part load conditions. The results from the current study are within the same range for the different MAP conditions and **Figure 2.14** presents the gain in efficiency relative to the E0 baseline for MAP = 1 bar as a function of mass fraction of ethanol in the blend. The efficiency gain scales with the mass fraction of ethanol in the fuel which is consistent with the expected sources of the gain in thermal efficiency, namely the enthalpy of vaporization and thermal properties effects.

In Jung et al. [21], the authors reported the efficiency gains were primarily due to the differences in the net heating value (NHV) and lower heat transfer losses of E85 relative to E0. The lower heat losses were attributed to lower in-cylinder temperatures associated with the higher charge cooling of effects of ethanol compared with E0. The NHVs per mass of air for

ethanol (E100) and gasoline (E0) are nearly identical (3.00 MJ/kg$_{air@stoich}$ and 2.98 MJ/kg$_{air@stoich}$, respectively [13], [21]), but the NHVs per mass of mixture at stoichiometric values differ by 3.6% with NHV = 2.69 MJ/kg$_{stoich\ mix}$ for E100 and NHV = 2.79 MJ/kg$_{stoich\ mix}$ for E0. But as noted by Jung et al. [21] these values do not take into consideration the enthalpy of vaporization of the fuel, and they estimated the offset in NHV due to HoV accounted for approximately half of the relative benefit they observed in brake thermal efficiency.

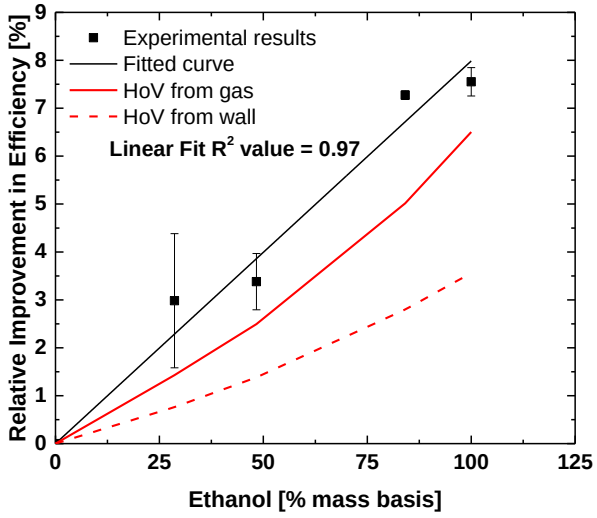

Figure 2.14. Gain in efficiency relative to E0 as a function of mass fraction of ethanol in the fuel blend for MAP= 1 bar.

The HoV of the fuel also affects charge cooling, and the HoV of the fuel per mass of stoichiometric mixture varies non-linearly with the volumetric concentration of ethanol in the fuel blend as shown in Stein et al. [13], where HoV of E0 is ~24 kJ/kg$_{stoich\ mix}$ and HoV of E100 is ~93 kJ/kg$_{stoich\ mix}$. But the HoV has a more linear correlation with mass fraction than with mole fraction. The NHV is not affected by changing SOI; however, the amount of charge cooling can be affected by SOI by shifting the source of heat transfer for fuel vaporization. For example, if SOI occurs at a time in the cycle with significant piston or wall impingement, where

surfaces provide the heat for fuel vaporization, compared with SOI timing where the air charge is the primary source for fuel vaporization, there will be reduced charge cooling benefits. The results of the current work support that a primary source of the thermal efficiency benefit of the ethanol blends originated from charge cooling, where an optimal SOI for volumetric efficiency was observed within the IVO timing (see **Figure 2.5**). Based on the experimental trends observed, if SOI was too advanced within IVO timing, surface wetting likely occurred, increasing particulate emissions and decreasing charge cooling. If the SOI timing was too late, i.e. after the intake valve had closed, the volumetric efficiency significantly decreased. The limited range of optimal fuel injection timing constrained the potential of split fuel injection to positively affect the fuel/air charge via HoV effects.

2.7 Conclusions

In the current work, the effects of two fuel injection strategies for various blends of ethanol and gasoline were evaluated at low speed and high load conditions. The load varied by sweeping the intake manifold absolute pressure (MAP) from 1 bar to 1.5 bar. Conclusions of the study include the following.

1. As expected, ethanol yielded a major improvement in terms of expanding the range of MBT operation of the engine for the engine speed and loads studied. For all boosted conditions, the spark timing for E0 had to be retarded, which prevented MBT operation; whereas for all the ethanol blends, MBT timing was maintained at all operating conditions. The highest GITE of 38.4% was achieved with E85 and E100 at 1.1 and 1.2 bar MAP for an absolute improvement of 4% and a relative improvement of 7.5% compared with baseline gasoline for the same MAP.

2. The ethanol blends were not knock-limited at any of the operating conditions studied. Thus, the benefits of changing the amount of ethanol in the fuel at a specific load condition were to improve the thermal efficiency and reduce the engine-out particulate emissions relative to E0.
3. SOI timing between 275-175° bTDC yielded the highest volumetric efficiencies for all ethanol fuel blends at MAP = 1 bar. This optimal SOI range was attributed to a tradeoff between increasing soot emissions at earlier SOIs and reducing the benefits of charge cooling at later SOIs relative to IVO timing.
4. A linear dependence on relative gain in GITE was observed as a function of mass fraction of the ethanol content in the fuel blend. This scaling supports the conclusion that effects of HoV were a significant factor in controlling the thermal efficiency gains. This was confirmed by a GT-Power model simulation which showed that the efficiency gains with ethanol are partly due to HoV accounting, and partly due to beneficial effects of charge cooling.
5. The GIMEP and GITE of the different fuel blends showed little sensitivity to the split injection strategy, implemented in this study, relative to using a single fuel injection event, which was attributed to the limited range of SOI where the HoV of ethanol could positively impact the fuel air charge, i.e. during IVO.

More data at intermediate ethanol blend levels would be valuable to build fidelity into the contour map presented in this work. However, a conclusion based on this study is that there are diminishing returns to increasing the ethanol content beyond a threshold value in the blend if knock does not constrain engine operation. This is the same conclusion articulated by Stein et al.

[13] in their comprehensive review of the effects of ethanol on engine performance, where peak in-cylinder pressure limits were met prior to knocking onset with ethanol blends.

2.8 Acknowledgements

The work presented here was funded in part by the Office of Energy Efficiency and Renewable Energy (EERE), U.S. Department of Energy (DOE), under Award Number DE-EE0006831. The authors would like to thank Robert Bosch, LLC and Ford Motor Company for their technical support.

2.9 Abbreviations:

aTDC - after top dead center
bTDC - before top dead center
BMEP - brake mean effective pressure
BTE - brake thermal efficiency
CA50 - crank angle position where 50% of the total heat is released
CoV - coefficient of variation
DISI - direct injection spark ignition
EVO - exhaust valve opening
EVOP - exhaust valve opening profile
FSN - filter smoke number
GIMEP - gross indicated mean effective pressure
GITE - gross indicated thermal efficiency
GISFC - gross indicated specific fuel consumption
HoV - enthalpy of vaporization
IVO - intake valve opening
IVOP - intake valve opening profile
KI20 - knock intensity factor
NHV - net heating value
MAP - manifold absolute pressure
MBT - maximum brake torque
MON - motor octane number
N - number of pressure data samples
P - pressure

RON - research octane number
S - octane sensitivity
SOI - start of injection
TDC - top dead center

References

13. Stein, R. A., Anderson, J. E., and Wallington, T. J. (2013). An overview of the effects of ethanol-gasoline blends on SI engine performance, fuel efficiency, and emissions. *SAE International Journal of Engines, 6(1), 470-487 (SAE Paper 2013-01-1635).*

14. Jung, H. H., Leone, T. G., Shelby, M. H., Anderson, J. E., and Collings, T. (2013). Fuel Economy and CO_2 Emissions of Ethanol-Gasoline Blends in a Turbocharged DI Engine. *SAE International Journal of Engines, 6(1), 422-434 (SAE Paper 2013-01-1321).*

15. Leone, T. G., Olin, E. D., Anderson, J. E., Jung, H. H., Shelby, M. H., and Stein, R. A. (2014). Effects of fuel octane rating and ethanol content on knock, fuel economy, and CO2 for a turbocharged DI engine. *SAE International Journal of Fuels and Lubricants, 7(1), 9-28 (SAE Paper 2014-01-1228).*

16. Jo, Y. S., Lewis, R., Bromberg, L., and Heywood, J. B. (2014). Performance Maps of Turbocharged SI Engines with Gasoline-Ethanol Blends: Torque, Efficiency, Compression Ratio, Knock Limits, and Octane, *SAE Technical Paper No. 2014-01-1206.*

17. Caton, P. A., Hamilton, L. J., and Cowart, J. S. (2007). An experimental and modeling investigation into the comparative knock and performance characteristics of E85, gasohol [E10] and regular unleaded gasoline [87 (r+ m)/2], *SAE Technical Paper No. 2007-01-0473.*

18. Thewes, M., Müther, M., Brassat, A., Pischinger, S., and Sehr, A. (2012). Analysis of the Effect of Bio-Fuels on the Combustion in a Downsized DI SI Engine. *SAE International Journal of Fuels and Lubricants, 5(1), 274-288 (SAE Paper 2011-01-1991).*

19. Nakata, K., Utsumi, S., Ota, A., Kawatake, K., Kawai, T., and Tsunooka, T. (2006). The effect of ethanol fuel on a spark ignition engine. *SAE Technical Paper No. 2006-01-3380*.

20. Whitaker, P., Shen, Y., Spanner, C., Fuchs, H., Agarwal, A., and Byrd, K. (2010). Development of the combustion system for a flexible fuel turbocharged direct injection engine. *SAE International Journal of Engines*, *3*(1), 326-354 *(SAE Paper 2010-01-0585).*

21. Jung, H. H., Shelby, M. H., Newman, C. E., and Stein, R. A. (2013). Effect of Ethanol on Part Load Thermal Efficiency and CO_2 Emissions of SI Engines. *SAE International Journal of Engines, 6(1), 456-469 (SAE Paper 2013-01-1634).*

22. Yang, J., and Anderson, R. W. (1998). Fuel injection strategies to increase full-load torque output of a direct-injection SI engine, *SAE Technical Paper No. 980495*.

23. Daniel, R., Wang, C., Xu, H., and Tian, G. (2012). Split-injection strategies under full-load

using DMF, a new biofuel candidate, compared to ethanol in a GDI engine. *SAE Technical Paper No. 2012-01-0403*.

24. Anderson, J. E., Leone, T. G., Shelby, M. H., Wallington, T. J., Bizub, J. J., Foster, M., and Polovina, D. (2012). Octane numbers of ethanol-gasoline blends: Measurements and novel estimation method from molar composition. *SAE Technical Paper No. 2012-01-1274*.

25. König, G. and Sheppard, C. (1990). End Gas Autoignition and Knock in a Spark Ignition Engine," *SAE Technical Paper No. 902135*.

26. Serras-Pereira, J., Aleiferis, P.G., Richardson, D., Wallace, S. (2008). Characteristics of Ethanol, Butanol, Iso-Octane and Gasoline Sprays and Combustion from a Multi-Hole Injector in a DISI Engine, *SAE Int. J. Fuels Lubr. 1(1):893-909 (SAE Paper 2008-01-1591)*.

27. Fatouraie, M., Wooldridge, M. S., Petersen, B. R., and Wooldridge, S. T. (2015). Effects of Ethanol on In-Cylinder and Exhaust Gas Particulate Emissions of a Gasoline Direct Injection Spark Ignition Engine. *Energy and Fuels*, *29*(5), 3399-3412.

28. Westbrook, C. K., Pitz, W. J., and Curran, H. J. (2006). Chemical kinetic modeling study of the effects of oxygenated hydrocarbons on soot emissions from diesel engines. *The journal of physical chemistry A*, *110*(21), 6912-6922.

29. Kakuho, A., Yamaguchi, K., Hashizume, Y., Urushihara, T., Itoh, T., and Tomita, E. (2004). A study of air-fuel mixture formation in direct-injection SI engines. *SAE Technical Paper No. 2004-01-1946*.

30. Zhuang, Y., Hong, G., and Wang, J. (2012). Preliminary investigation to combustion in a SI engine with direct ethanol injection and port gasoline injection (EDI+ GPI). In *The 18th Australasian Fluid Mechancis Conference*. Australasian Fluid Mechanics Society.

31. Szybist, J., Foster, M., Moore, W., Confer, K., Youngquist, A., Wagner, R. (2010). Investigation of Knock Limited Compression Ratio of Ethanol Gasoline Blends. *SAE Technical Paper No 2010-01-0619*.

32. Marriott, C. D., Wiles, M. A., Gwidt, J. M., and Parrish, S. E. (2009). Development of a naturally aspirated spark ignition direct-injection flex-fuel engine. *SAE International Journal of Engines, 1(1), 267-295 (SAE Paper 2008-01-0319)*.

Chapter 3

Influence of Fuel Injection Strategies on Efficiency and Particulate Emissions of Gasoline and Ethanol Blends in a Turbocharges Multi-cylinder Direct Injection Engine

3.1 Abstract

The effects of a broad range of fuel injection strategies on thermal efficiency and engine-out emissions (CO, THC, NOx and particulate number) were studied for gasoline and ethanol fuel blends. A state-of-the-art production multi-cylinder turbocharged gasoline direct-injection engine equipped with piezoelectric injectors was used to study fuels and fueling strategies not previously considered in the literature. A large parametric space was considered including up to four fuel injection events with variable injection timing and variable fuel mass in each injection event. Fuel blends of E30 (30% by volume ethanol) and E85 (85% by volume ethanol) were compared with baseline E0 (reference grade gasoline). The engine was operated over a range of loads with intake manifold absolute pressure (MAP) from 800 mbar to 1200 mbar. A combined application of ethanol blends with a multiple injection strategy yielded considerable improvement in engine emissions while maintaining or slightly improving engine brake thermal efficiency. The weighted injection spread parameter defined in this study, combined with the weighted center of injection timing defined in the previous literature, were found well suited to

characterize multiple injection strategies, including the effects of the number of injections, fuel mass in each injection and the dwell time between injections.

3.2 Introduction

The benefits of blending ethanol with gasoline to improve the thermal efficiency of direct injection spark ignition engines have been established in numerous studies [33], [34], [35], [36], [37]. Previous work has also shown gasoline direct injection (GDI) engines tend to have higher particulate mass (PM) and particulate number (PN) emissions compared with port fuel injection (PFI) engines [38]. Stringent particulate emission standards like EURO 6 with a limit of 6×10^{11} PN/km may be challenging for GDI engines to meet without the use of after-treatment [39].

Ethanol provides a means to reduce PN and PM emissions from GDI engines while simultaneously providing efficiency benefits [40], [41]. Moreover, advances in fuel injection technologies provide a wider range and more precise control over parameters like fuel rail pressure, fuel injection timing and injection duration [42]. While many studies have considered the effects of different injection strategies on diesel compression ignition engines, e.g. [43], [44], [45], [46], there are fewer studies using GDI engine architectures. Prior GDI work includes studies of the effects of split injection, i.e. two injection events [33], [47], [48], but fast piezo-electric injectors allow up to five injections per cycle. The potential of multiple injections remains largely unexplored. Su et al. [49] used a triple injection strategy to demonstrate 80% reduction in particulate emissions with a turbocharged GDI engine. Schmidt et al. [50] showed multiple injections could be used to improve combustion stability at part load conditions in a GDI engine. The current work fills a gap in the literature on the combined effects of ethanol and multiple injection events on the performance of a production flex-fuel turbocharged direct injection engine. The objective of the study was to identify the efficiency and particulate

emissions benefits achievable using a broad range of fuel injection strategies of ethanol fuel blends. The results show the sensitivity of different ethanol/gasoline fuel blends to more advanced injection strategies.

3.3 Experimental Set-up

Figure 3.1 is a schematic of the experimental facility and the supporting systems. The experimental setup consists of a production Mercedes 2.0 L four-cylinder, in-line turbocharged GDI engine (155 kW Daimler M274), equipped with Bosch piezo-electric fuel injectors. The engine specifications are listed in **Table 3.1**.

Table 3.1. Test engine specifications.

Engine Configuration	Inline 4
Displacement (cc)	1991
Valvetrain	Twin independent variable cam timing with dual overhead camshaft and 4 valves per cylinder
Stroke (mm)	92
Bore (mm)	83
Compression Ratio	9.8:1
Spark Plug	Center mounted
Air Supply	Turbocharger with charge air cooling
Injection	DI-center mounted Bosch piezoelectric injectors

Pressure measurements are made in each of the cylinders using spark-plug pressure transducers (Kistler 6115BFD34Q04) and charge amplifiers (Kistler 5010). The engine can be operated at the manufacturer calibration settings through the Bosch engine control unit (ECU) or using manual control via the ETAS tool INCA, which provides access to override the pre-programmed ECU settings. In addition to the standard measurements recorded from the engine ECU, intake air pressure, exhaust pressure (both pre-and post-turbo), exhaust temperature, oil

and coolant temperatures, engine oil pressure and fuel rail pressure are recorded. The fuel/air equivalence ratio measurement is made using a lambda meter (ETAS LA4) with a broadband lambda sensor (Bosch LSU 4.9). The engine was operated at fixed speed, valve timing, coolant temperature, oil temperature and intake air temperature. The fixed operating conditions and the operating limits in terms of maximum allowable in-cylinder pressure, knock limits and component (turbocharger) protection constraints are listed in the **Table 3.2.**

Table 3.2. Fixed experimental operating conditions.

Variable	**Range/Value**
Engine Speed	1750 RPM
Lambda/φ	1 (stoichiometric)
Fuel Injection Pressure	200 bar
Intake Valve Opening	15 crank angle degree after top dead center (^{o}aTDC, gas exchange)
Intake Valve Closing	178 °aTDC (gas exchange)
Exhaust Valve Opening	177 crank angle degree before top dead center (^{o}bTDC, gas exchange)
Exhaust Valve Closing	14 °bTDC (gas exchange)
Coolant In / Out Temperature	80 °C / 82 °C
Intake Air Temperature (Post-Intercooler)	30 °C
Engine Operating Limits	Average Maximum In-Cylinder Pressure ≤ 100 bar Knock Limit ≤ 1 bar[a] Pre-Turbo Exhaust Temp ≤ 900 ^{o}C

[a] Knocking conditions were determined based on the absolute maximum of the in-cylinder pressure oscillations

The engine is not equipped with any exhaust after treatment systems, and engine-out PN emissions measurements are made by sampling from the engine exhaust runner using insulated stainless-steel tubing (1.3 cm diameter). Particle number and size distribution in the exhaust are measured with a Cambustion DMS500 system, which uses mobility of nanoparticles in an electric field to produce particle number spectra of nanoparticles between 5 nm and 1000 nm in size. The time response of the system is 200 ms. Exhaust gas is sampled through a choked

orifice and diluted with 150 °C dry air in two stages. The first stage has a 6:1 dilution ratio (volume basis) to prevent hydrocarbon and water condensation and particle agglomeration. The second stage dilution uses a 12:1 ratio. Additional details and working principles of the PN instrument are provided in Hagena et al. [51]. For the PN study presented here, the total PN concentration and PN size distribution were recorded for 90 seconds after the engine reached steady-state at the target operating conditions.

Gaseous emission measurements of CO, CO_2, total hydrocarbons (THC), NOx and O_2 are made using a fast-response analytical system (HORIBA MEXA 7100DEGR). The sample is transported to the analyzer using heated lines to avoid condensation. The analyzer settings were changed for each ethanol-gasoline fuel blend using the appropriate O/C and H/C ratios.

Three fuels were considered in this study: E0, E30 and E85. The fuel flow rate was measured using a piston type flow meter (Max Machinery, #213-611-000). The baseline gasoline (E0) fuel used in the study was research grade, unoxygenated gasoline (Gage Product 40665-55F). The E0 was splash blended by volume with anhydrous ethanol (Sigma Aldrich, E100 anhydrous, purity $\geq$ 99.5%, $H_2O \leq 0.005\%$) to produce the ethanol-gasoline fuel blends: E30 (30% by volume ethanol) and E85 (85% by volume ethanol). The fuel properties are provided in **Table A2.1** of the **Appendix 2**.

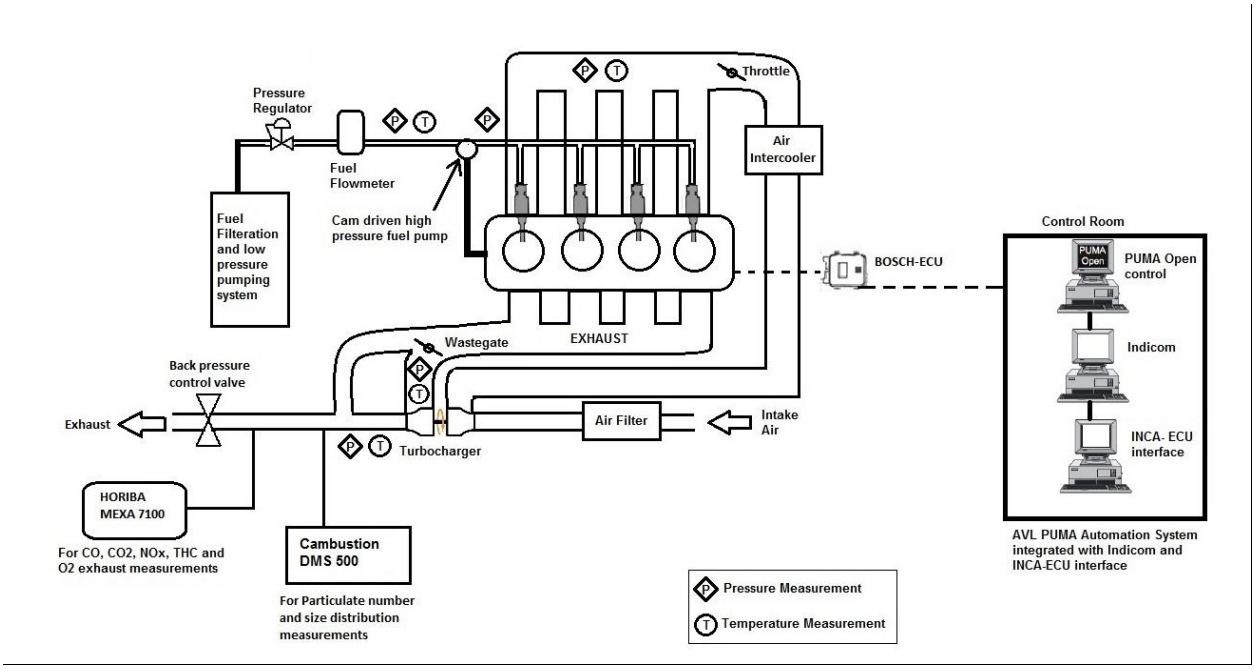

Figure 3.1. Experimental schematic of the GTDI engine facility and supporting systems

3.4 Experimental Approach

The fuel injection parameters were varied systematically to determine the effects of different fuels and injection strategies on engine performance. The approach started with single fuel injection events as the baseline operating conditions for each fuel. For the single injection experiments, the start of injection (SOI) timing was varied from 300° to 180° before top dead center (bTDC of the firing cycle) in intervals of 20° and the intake manifold absolute pressures (MAP) varied from 800 to 1200 mbar.

For the multiple injection experiments, a progression of experiments was used to investigate the large parametric space of the number of events, fuel injection timing and fuel mass. First, the effects of multiple injection events were studied by increasing the number of injections per cycle to double, triple and quadruple. For these experiments, the total fuel mass was divided equally between the total number of injection events per cycle. The timing of the

first injection event, SOI1, and the pause or dwell time between each injection event were varied. For the second series of multiple injection experiments the fuel mass was varied between the events of a triple injection strategy with fixed injection timing. For the last series of experiments, a triple injection strategy was also used where both the fuel mass and the timing of the third injection event were varied, while the timing of the first and second injection events were held constant.

The values considered in the first multiple injection experimental matrix are presented in **Table 3.3,** and the range of the SOI timings for each injection is presented in **Figure 3.2.** The test matrix for the second and third series of multiple injection experiments was created based upon the results from the first series of experiments. The same are presented in the following sections. The final set of results present the effects of triple injection strategies on particulate emissions.

Table 3.3. Input parameters and range of values considered in the initial experimental matrix for multiple fuel injection events

Parameter	**Value**
Manifold Absolute Pressure (MAP, mbar)	800, 900, 1000, 1200
Fuels	E0, E30, E85
# of Injection Events	1, 2, 3, 4
Fuel Mass Distribution	Equal fuel mass injected in each event, i.e. 100% (1 injection), 50% (2 injections), 33% (3 injections), 25% (4 injections)
Timing of the First Injection Event, SOI1 (^{o}bTDC)	300, 280, 260, 240, 220, 200, 180
Pause Time between Each Injection Event (^{o})	21, 31.5, 42, 52.5, 63

For each injection strategy tested, the spark timing was varied to achieve maximum brake torque (MBT). At boosted intake air conditions, knocking became significant and prevented MBT operation for E0. For the boosted E0 conditions, the spark timing was advanced no further

to where the peak in-cylinder pressure oscillations reached the knocking criteria provided in **Table 3.2**.

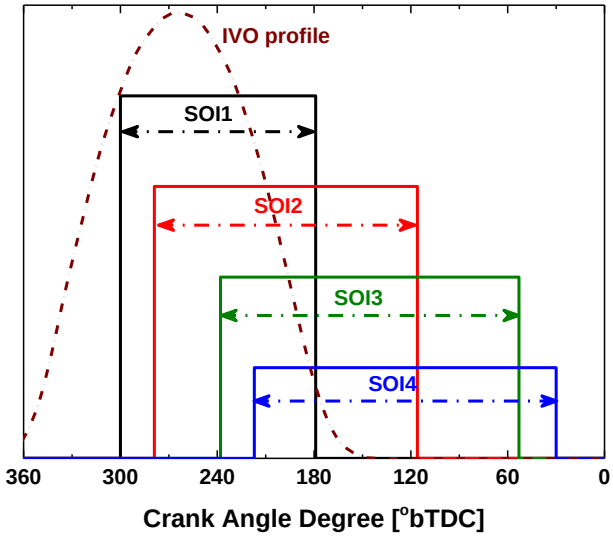

Figure 3.2. The range of SOI timings [°bTDC] studied for the different injection events. The timing of the intake valve opening (IVO) is provided for reference.

Weighted Center of Injection Timing

In order to facilitate the comparison between the different strategies using multiple injection events, the weighted center of injection (WCOI) timing was used. WCOI was defined in the GDI fuel injection study by Imaoka et al. [52] as the center timing for all fuel injection durations in a multiple injection event, based on the mass-weighted average for the injection strategy:

$$WCOI = \frac{(\sum_{i=1}^{N} COI_i * ID_i)}{(\sum_{i=1}^{N} ID_i)}$$

Here, COI_i is the center of the injection timing of the i^{th} injection event and ID_i is the injection duration of the i^{th} injection. The expression in parentheses is therefore the mass fraction of fuel injected in i^{th} injection event.

Brake Thermal Efficiency (BTE) Calculation

For all experiments, the BTE was calculated using the following formula:

$$BTE = \frac{BP}{(FFR * LHV_{fuel})}$$

Here, BP is the Brake Power (kW), calculated using the torque and speed measurements from the AVL AC induction dynamometer; FFR is the Fuel Flow Rate (kg/s), measured by a piston type fuel flow meter (Max Machinery, #213-611-000); and LHV_{fuel} is the Lower Heating Value of the fuel blend (kJ/kg) calculated as a mass-weighted average of the LHVs of pure gasoline (E0) and pure ethanol (E100) (listed in Table 2.1).

3.5 Experimental Results

3.5.1 Single Fuel Injection Events- Effects of Injection Timing and Intake Pressure

The baseline trends and performance of the fuels for single injection events was established as a function of SOI. Results for brake thermal efficiency (BTE) and coefficient of variance (CoV) of the indicated mean effective pressures (IMEP) are presented in **Figure 3.3** for 800 mbar MAP. For MAP > 800 mbar, E0 was limited by knock. All fuels behaved similarly in terms of sensitivity to SOI timing for single injection events. BTE decreased slightly and CoV increased with later injection timing, and performance for the fuels was comparable until very late SOIs (after 200 ^{o}bTDC) when combustion stability increased dramatically.

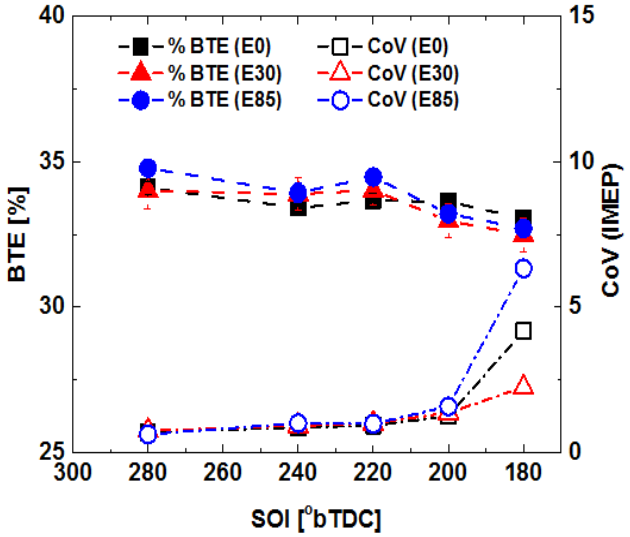

Figure 3.3. Comparison of BTE and CoV for different fuel blends tested with single fuel injection events and MAP = 800 bar.

The results for CO and THC emissions corresponding to the single injection data shown in **Figure 3.3** are presented in **Figure 3.4**. The CO emissions for E0 and E30 were comparable, whereas CO emissions for E85 were ~30-35% lower for earlier SOIs. The THC emissions for both E30 and E85 fuel were ~20% lower than for E0 fuel for earlier SOI timing. The NOx emissions (not shown here) were also lower with increasing ethanol content in fuel.

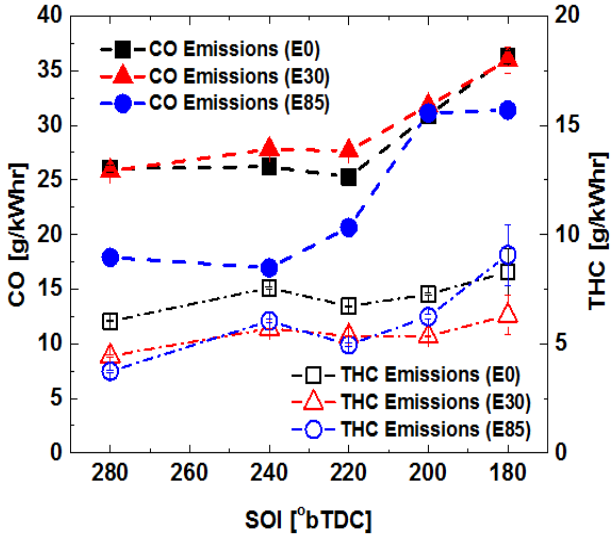

Figure 3.4. CO and THC emissions comparison for the conditions and results presented in **Figure 3.3.**

Figure 3.5 presents the results for the BTE and CA50 for the range of intake MAPs tested. BTE improved for E30 and E85 with increasing MAP whereas BTE decreased for E0 due to knock constraints. E0 could not be operated at MBT timing above MAP of 800 mbar. An absolute BTE improvement of 3% was observed for E85 compared with gasoline within the range of MAP tested. The engine could not be operated above MAP of 1200 mbar for E0 due to the constraint on the maximum pre-turbo exhaust temperature. For E30 and E85 fuel blends, no knock or high exhaust temperatures were observed; however, engine operation was limited by the maximum in-cylinder pressure for MAP > 1200 mbar. Refer to **Table 3.2** for engine operating limits.

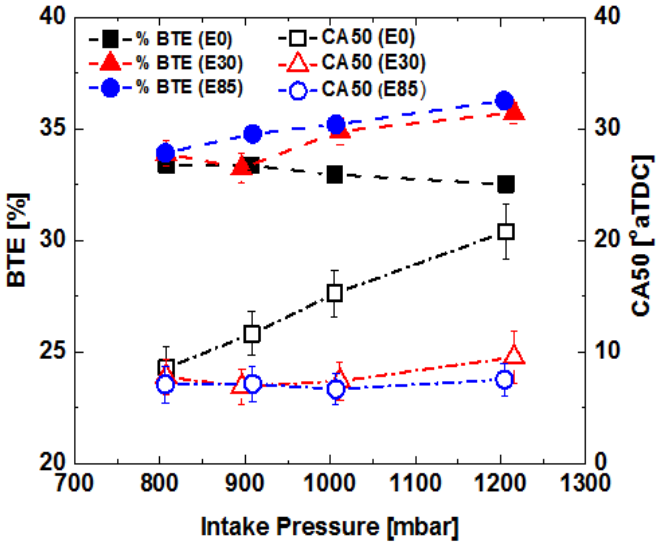

Figure 3.5. Comparison of BTE and CA50 for different fuel blends tested with single fuel injection events with varying intake MAP.

Figure 3.6 shows the results for brake specific fuel consumption (BSFC) and brake mean effective pressure (BMEP) for the three fuel blends. One of the concerns with the use of ethanol is the lower fuel economy (i.e., vehicle miles per gallon) due to the lower heating value of ethanol compared with gasoline (see **Table A1**). The results in **Figure 3.6** show mid-level ethanol blends like E30 can approach the BSFC (and thus the fuel economy) comparable to E0 at higher MAPs.

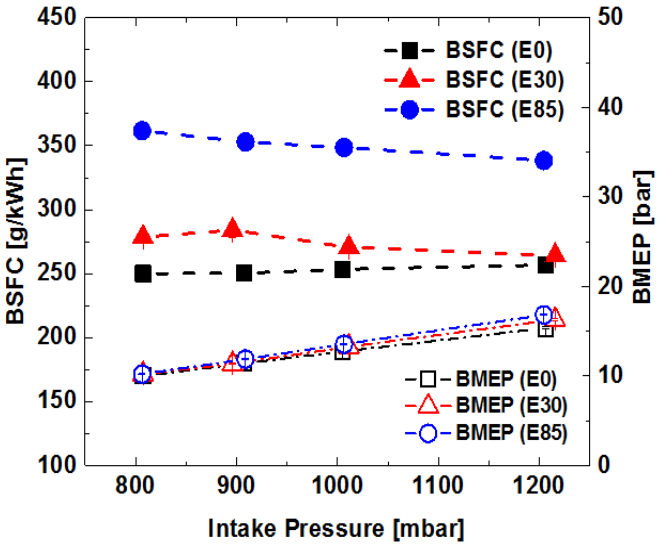

Figure 3.6. Comparison of BSFC and BMEP for different fuel blends tested with single fuel injection events.

3.5.2 Multiple Fuel Injection Events- Equal Fuel Mass

The results for brake thermal efficiency (BTE) for the multiple injection experiments with equal fuel mass in each injection event are presented in **Figure 3.7** for E0 and a MAP of 1000 mbar. The results for the single injection events, from previous section, are provided in the figure for comparison. The error bars in all figures are the standard deviations of the recorded combustion cycles unless stated otherwise (the methodology used for determining error bars is included in the Appendix). Multiple injection events systematically improved BTE above the single injection baseline for all injection timings later than 260 ^{o}bTDC; however, there was little sensitivity to the specific number of multiple injection events.

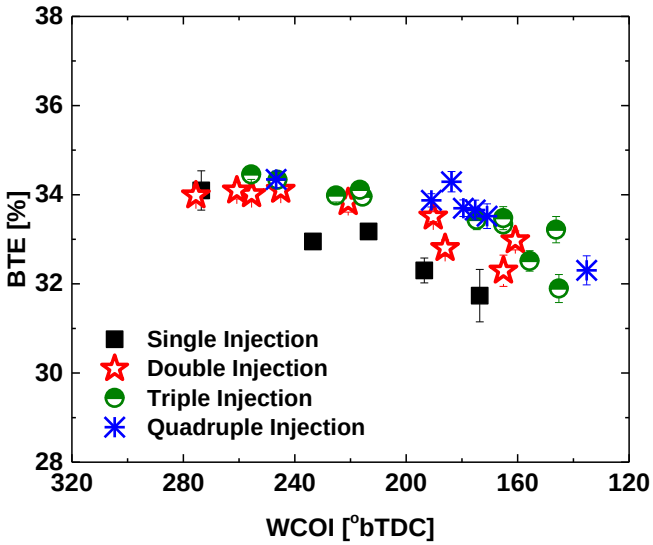

Figure 3.7. Comparison of BTE for multiple and single fuel injection events for E0 and MAP = 1000 mbar.

Figures 3.8 through **3.11** compare the engine performance for BTE, and the engine-out emissions of CO, THC and NOx, respectively. The fuel was E0 with a MAP of 1000 mbar. In the figures, the best results for each parameter were plotted, and the multiple injection results were not differentiated by the number of injection events. For example, the data of **Figure 3.8** are down-selected from the results presented in **Figure 3.7**. The improvement in BTE achieved via multiple injections is more apparent in **Figure 3.8**. **Figures 3.9** and **3.10** show multiple injections can lower CO (15-25%) and THC emissions (~30%). However, NOx emissions were either unaffected or slightly higher with multiple injections for E0 at 1000 mbar, as shown in **Figure 3.11**.

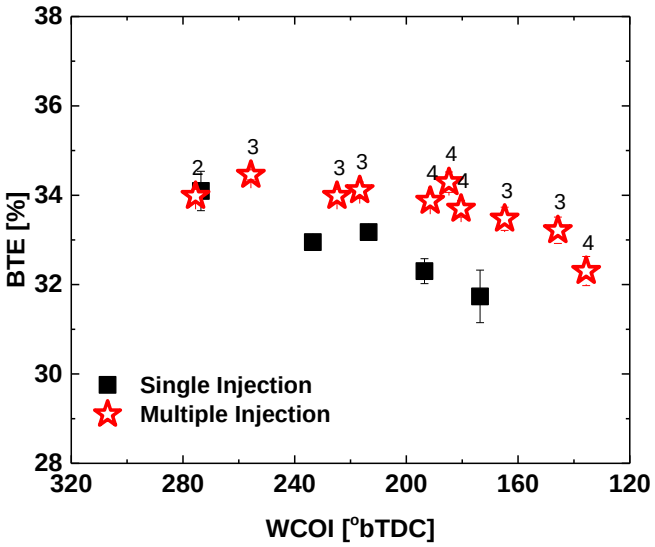

Figure 3.8. Maximum BTE Results from **Figure 3.7** filtered for comparison between single and multiple fuel injection events (E0 and MAP = 1000 mbar). The labels adjacent to the 'Multiple Injection' symbols are the number of injections.

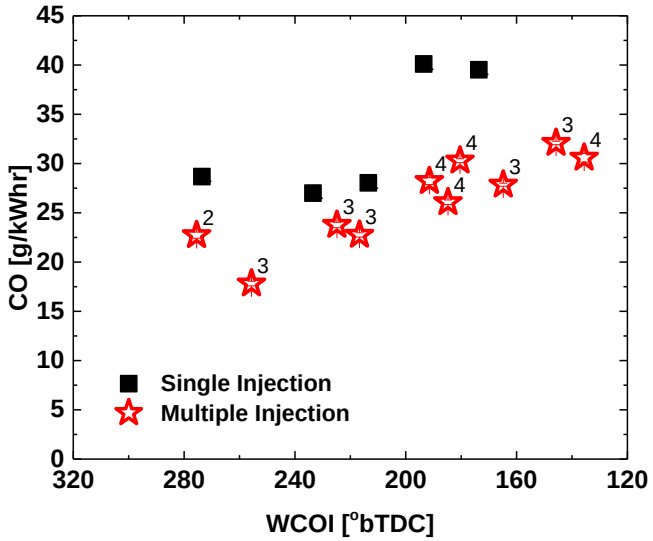

Figure 3.9. Comparison of CO emissions for single and multiple fuel injection events for E0 and MAP = 1000 mbar. The labels adjacent to the 'Multiple Injection' symbols are the number of injections.

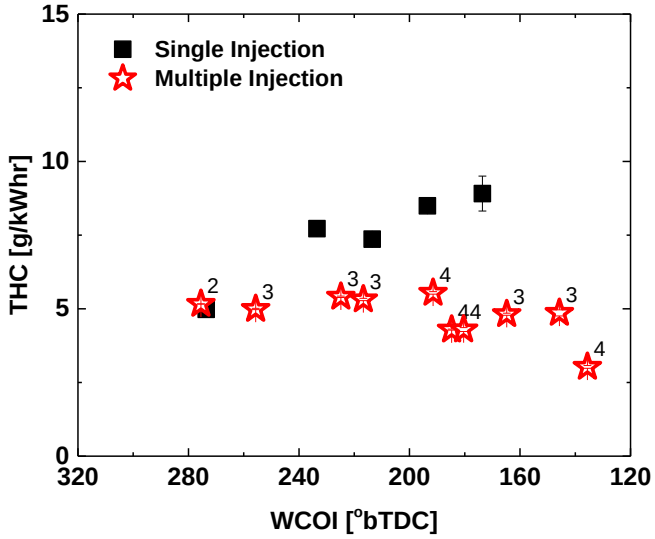

Figure 3.10. Comparison of THC emissions for single and multiple fuel injection events for E0 and MAP = 1000 mbar. The labels adjacent to the 'Multiple Injection' symbols are the number of injections.

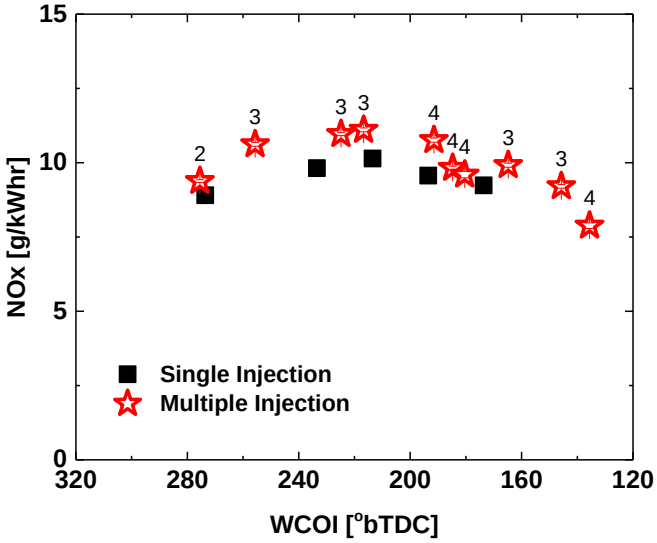

Figure 3.11. Comparison of NOx emissions for single and multiple fuel injection events for E0 and MAP = 1000 mbar.

The improvement in BTE, and lower CO and THC emissions for E0 are attributed to improved mixing achieved with multiple injections for the same WCOI. Similarly, Imaoka et al. [52] show an improvement in the Homogeneity Index as well as fuel consumption with the use of triple injection compared with single injection.

Results for BTE for E30 and E85 are shown in **Figure 3.12** for MAP of 1000 mbar. Like results with E0, multiple injections improve BTE for some more stratified (i.e., later WCOI) conditions. The results for the gaseous emissions for E30 and E85 are presented in **Appendix 2**. Briefly, only CO emissions were affected significantly for E30 (decreased by 15%).

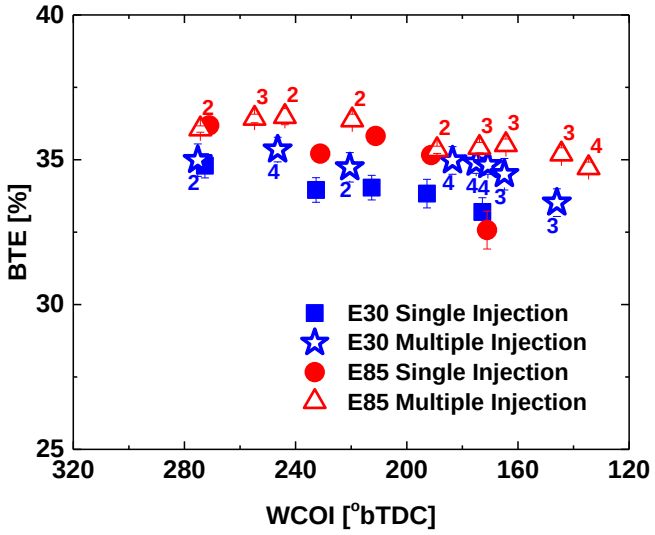

Figure 3.12. Comparison of maximum BTE for single and multiple fuel injection events for E30 and E85 and MAP = 1000 mbar. The labels adjacent to the 'Multiple Injection' symbols are the number of injections.

The use of multiple injection events systematically improved BTE in comparison with single injection events for more stratified, i.e., later WCOI timing, for all intake air pressures studied. **Figure 3.13** shows the maximum relative improvement achievable in BTE as a function of MAP for the three fuels at WCOI ~ 173°bTDC. The improvement in BTE was higher for higher MAPs for all fuels. The higher levels of MAP require longer injection duration to maintain stoichiometric air-fuel ratios, and multiple injection events likely enhanced homogeneity under these conditions.

The lower sensitivity of BTE improvement for the E30 blend could be due to the non-linear behavior of the fuel blend properties such as the vapor pressure and the distillation curve. For ethanol-gasoline blends, some of the parameters critical to fuel/air mixing, like vapor pressure and the distillation curve, exhibit nonlinear behavior with ethanol content [34]. Blends ranging from E10 to E30 have a vapor pressure that is higher than that of both gasoline and ethanol. This could lead to easier evaporation of fuel, and thus lower sensitivity of BTE to multiple injections.

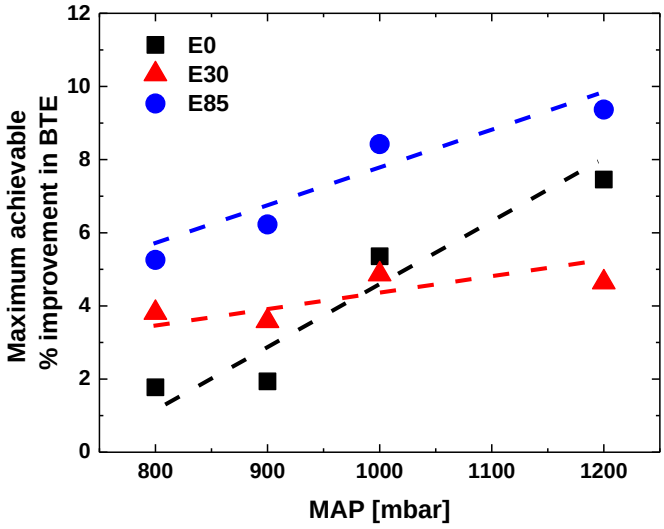

Figure 3.13. Maximum improvement in BTE achievable using multiple injections relative to the baseline of single injection for WCOI ~ 173°bTDC.

3.5.3 Multiple Fuel Injection Events- Variable Fuel Mass

Previous studies with split injection [47], [48] have shown both the amount of fuel injected and the timing of the injections can impact engine performance significantly. In the preceding section, equal fuel mass was injected in each event. In order to explore the effects of varying the fuel mass distribution, a triple injection strategy was used where the injection timings (SOI1, SOI2 and SOI3) were fixed, and the fuel mass in each injection event was varied. Triple

injection was selected as the BTE values were slightly better than for double injection and there was little difference between triple and quadruple injection results, as seen in **Figure 3.7**. For the first and second injections, fuel mass was varied from 0 to 100% of the total, and for the third injection, the fuel mass was varied from 0 to 50%, based on the combustion stability limit of maximum 5% COV of IMEP.

The injection timing was selected based on the results of the previous section. As seen in **Figure 3.7** for multiple injection events, maximum BTE values were similar for WCOI from approximately 220 ^{o}bTDC to 280 ^{o}bTDC. So SOI1 was set at 280 to allow a larger range of timing for SOI2 and SOI3. SOI2 was set at 220 ^{o}bTDC because there was a slight decrease in BTE for later WCOI as seen in **Figure 3.7**. SOI3 was set at a late timing of 30 ^{o}bTDC as previous studies [47], [52] suggest retarded injection timing, closer to firing TDC, has a larger cooling effect which may be able to prevent knock and improve efficiency. All experiments were conducted using E0 (as it was the most sensitive to the use of multiple injections), and no emissions measurements were made for this part of the study. The experimental matrix, including the fuel mass distributions considered, the corresponding values of WCOI and resulting BTE, is provided in the **Table 3.4**.

Table 3.4. Input parameters and range of values considered for triple fuel injection with fixed injection timing and variable fuel mass distribution

Parameter	**Value**
MAP (mbar)	800, 1000, 1200
Fuels Tested	E0
Timing of Injection Events (^{o}bTDC)	SOI1 = 280, SOI2 = 220, SOI3 = 30

Fuel Mass Distribution (%, event 1: event 2: event 3), and corresponding WCOI and WIS values	

Fuel Split	WCOI	WIS	BTE @1000 mbar
100:0:0	273.1	0	33.5%
0:100:0	213.1	0	33.2%
50:50:0	246.3	60	34%
0:50:50	120.4	192	31.3%
25:50:25	185.0	161	32.6%
50:25:25	196.7	176	32%
50:40:10	222.7	104	33.6%
40:50:10	217.1	95	33.6%
50:0:50*	151.8	250	N/A
*Not possible due to exhaust temperature limits			

The maximum BTE for all MAPs was obtained when the fuel was equally split between the first and second injection events and the third injection event was not used. Furthermore, injecting 25% or more of the total fuel mass in the third injection event considerably lowered the BTE. The trend is attributed to higher stratification and poorer mixing resulting from injecting fuel so late in the cycle with the use of the third injection event. The results are consistent with previous studies [47], [48] which concluded that with a split injection strategy the best engine performance was achieved with both injections earlier in the intake stroke.

3.5.4 Multiple Fuel Injection Events-Variable Fuel Mass and Injection Timing (SOI 3)

The previous results showed little benefit to varying the mass in the third injection event based on BTE, but only one set of injection timings was considered. In the next series of multiple injection experiments, a triple injection strategy was explored with fixed total fuel mass,

fixed SOI1 and SOI2 timing, but both the fuel mass and the SOI3 timing of the third event were varied. SOI3 ranged from 15 to 75 ºbTDC and the fuel in the third injection event was varied from 0 to 30% of the total fuel mass. The fuel mass injected in the first and second events was fixed at equal portions, i.e. ranging from 50% to 35% of the total fuel mass. E0, E30 and E85 fuels were used at three MAPs of 800, 1000 and 1200 mbar for the experiments; the BTE and emissions measurements were made. **Table 3.5** in shows the experimental matrix used.

Table 3.5. Input parameters and range of values considered for triple fuel injection with variable fuel mass distribution and variable injection timing for SOI3

SOI1	SOI2	SOI3	FM(1)	FM(2)	FM(3)	WCOI	WIS
280	N/A	N/A	100	N/A	N/A	274	0
	220	N/A	50	50	N/A	246	60
		15	45	45	10	219	103
			40	40	20	195	160
			35	35	30	174	202
		30	45	45	10	221	100
			40	40	20	200	147
			35	35	30	179	188
		45	45	45	10	223	97
			40	40	20	204	136
			35	35	30	184	174
		60	45	45	10	225	93
			40	40	20	207	126
			35	35	30	189	161
		75	45	45	10	226	90
			40	40	20	212	114
			35	35	30	194	148
FM(i) represents the % fuel mass injected in the i^{th} injection							

The results for BTE are presented in **Figure 3.14** as a function of SOI3 for E0 and E85. As the SOI3 timing was advanced, the BTE values approached the baseline of the single injection data irrespective of the amount of fuel mass injected in the third event. The performance decreased from the baseline as SOI3 approached TDC firing (15º bTDC) and as the

fuel mass injected in the third event increased. While BTE for some of the triple injection data were slightly higher than the single injection baseline, the improvement was within the standard deviation of the results. Thus, changing the injection timing and fuel mass in the third injection event had small effect on BTE. For clarity, the E30 data are not included in the figure, but has been shown in **Figure A2.9** in **Appendix 2**. Similar trends were observed with E30 fuel as well.

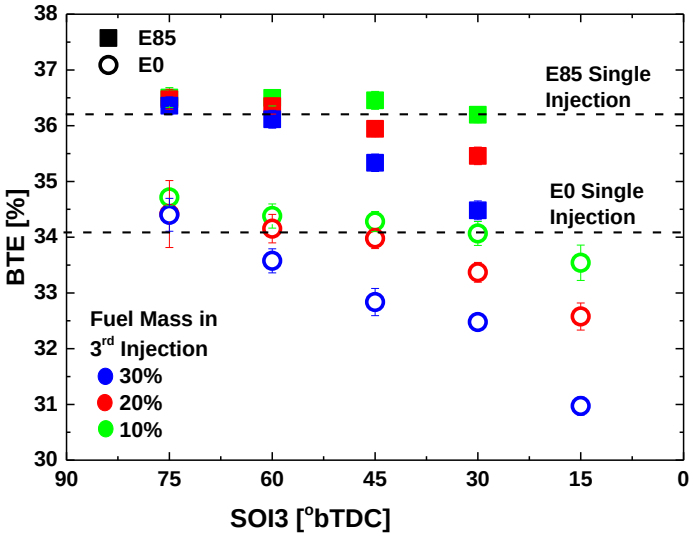

Figure 3.14. Effects of SOI3 timing and fuel mass on BTE for E0 and E85 and MAP = 1000 mbar. The results for single injection are provided for comparison as the dashed lines.

The results for the engine-out CO, THC and NOx emissions are presented in **Figure 3.15** for E0. THC emissions were systematically reduced with retarded SOI3 injection and increasing fuel mass in the third injection event for all fuel blends. However, CO emissions increased with later injection and increasing fuel mass in the third injection event. The results are consistent with later injection timing leading to increased stratification and less time for mixing and combustion. Similar sensitivity and trends with respect to SOI3 timing and the distribution of fuel mass was observed for E30 and E85 and for the other MAPs tested. Corresponding results

for MAP of 1000 mbar for E30 and E85 are provided in the **Figures 3.16** and **3.17** respectively, which follow similar trends as E0 fuel.

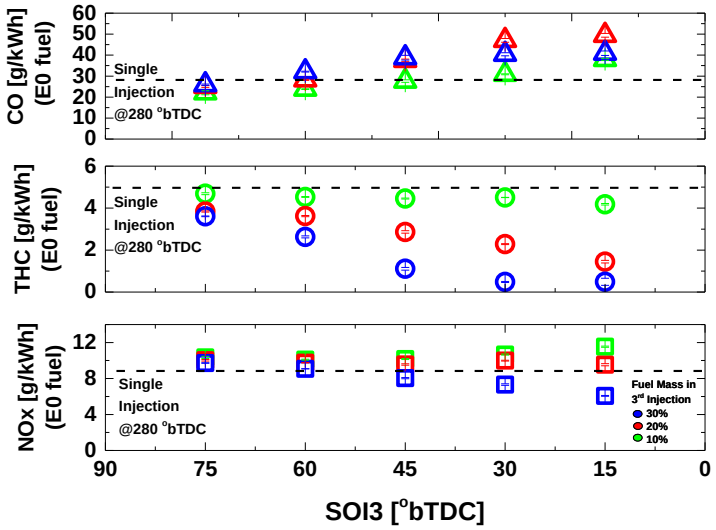

Figure 3.15. Effects of SOI3 timing and fuel mass on CO, THC and NOx emissions for E0 and MAP = 1000 mbar. The results for single injection are provided for comparison as the dashed line. The color legend is same as for **Figure 3.14**.

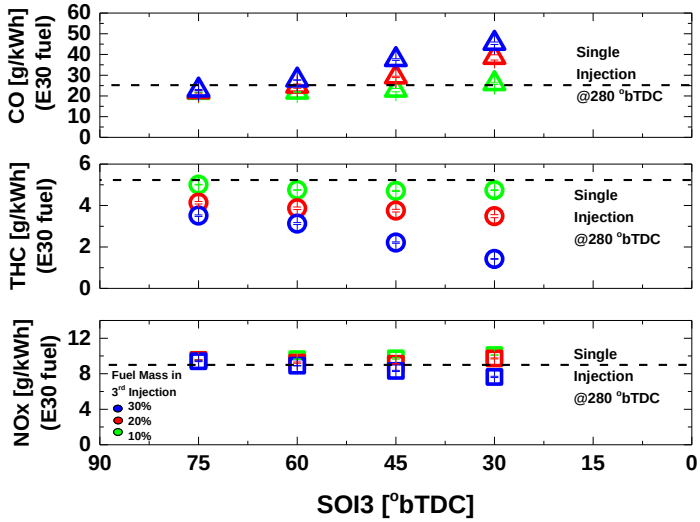

Figure 3.16. Effects of SOI3 timing and fuel mass on CO and THC emissions for E30 and MAP = 1000 mbar. The results for single injection are provided for comparison as the dashed line.

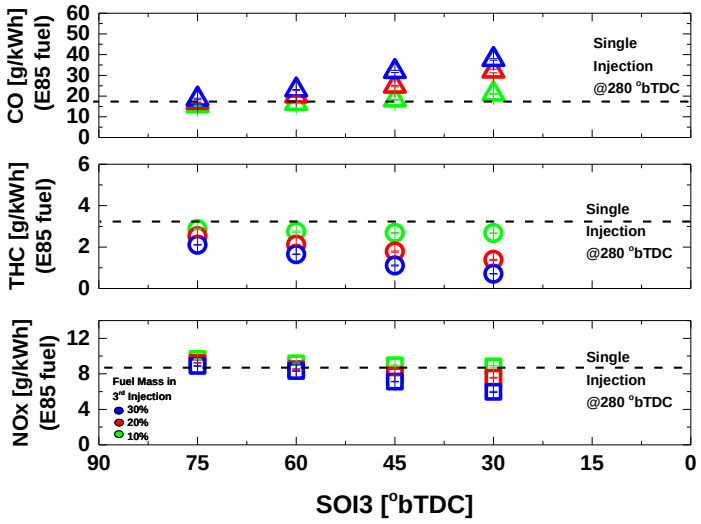

Figure 3.17. Effects of SOI3 timing and fuel mass on CO and THC emissions for E85 and MAP = 1000 mbar. The results for single injection are provided for comparison as the dashed line.

3.5.5 Injection Strategies to Reduce Particulate Emissions

The effects of the different injection strategies on particulate number emissions are presented here. While PN emissions were measured for many operating conditions, for conciseness, a summary of the results is presented here. The data are based on the experiments of the previous section, where variable fuel mass distribution and variable timing for SOI3 were investigated.

A comparison of the single, double and triple injection strategies on the PN size distribution as a function of particle size for E0 and MAP of 1000 mbar is presented in **Figure 3.18**. For the comparison, the injection timings and fuel mass distributions shown in **Figure 3.19** were used. These injection strategies yielded comparable BTE (see **Figure 3.14**) and CO emissions with lower THC emissions (see **Figure 3.15**) for the triple injection strategy. The timing and fuel mass distribution used for the triple injection strategy were the conditions that yielded the lowest total PN emissions.

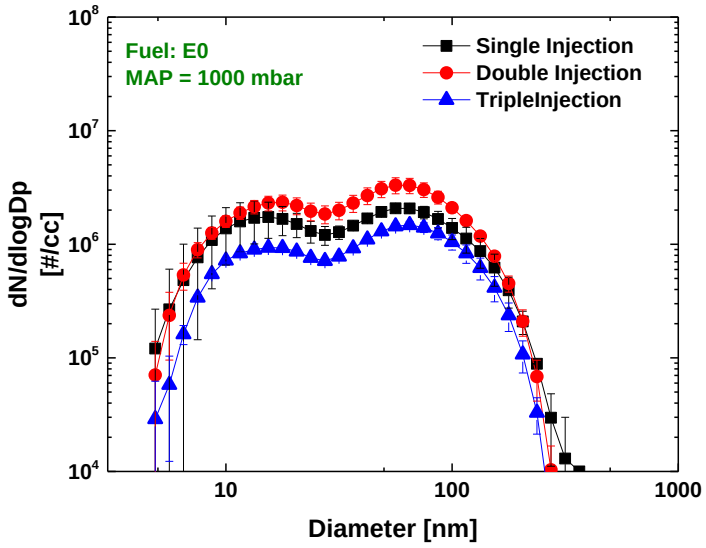

Figure 3.18. PN size distributions for E0 and MAP = 1000 mbar using the injection strategies presented in **Figure 3.19**. The error bars represent the standard deviations of the average recorded PN distribution for two days.

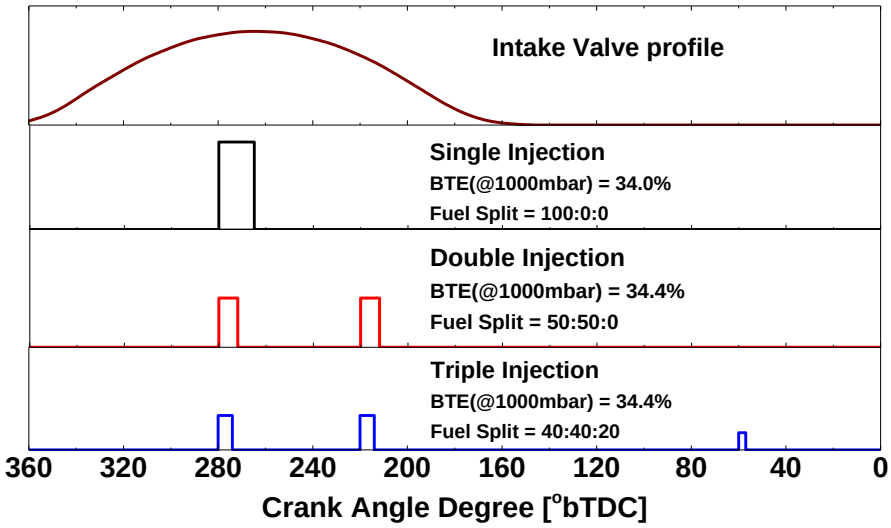

Figure 3.19. Injection strategies used for comparison of the PN emissions distribution presented in **Figure 3.18**. The areas of the bars represent the relative mass in each injection event.

The data in **Figure 3.18** show the triple injection strategy reduced the PN emissions for E0 for all size particles, yielding a 30% reduction in total PN concentration for the triple injection strategy in comparison with the single injection event. The same trends were observed

for E0 for the other intake air pressures studied, as seen in the total PN results presented in **Figure 3.20**. The data in **Figure 3.20** also show increasing MAP from 800 mbar to 1200 mbar increased PN for all injection strategies by almost an order of magnitude (note the decade log scale used in the figure). The increase in PN with increase in MAP or engine load is consistent with results from previous studies [53]. Increased load requires longer fuel injection duration to maintain stoichiometric combustion. The increase in fuel injection duration leads to higher spray tip penetration and thus higher potential for wall and piston impingement and the formation of fuel films. Fuel films are well known sources of particulate emissions [54].

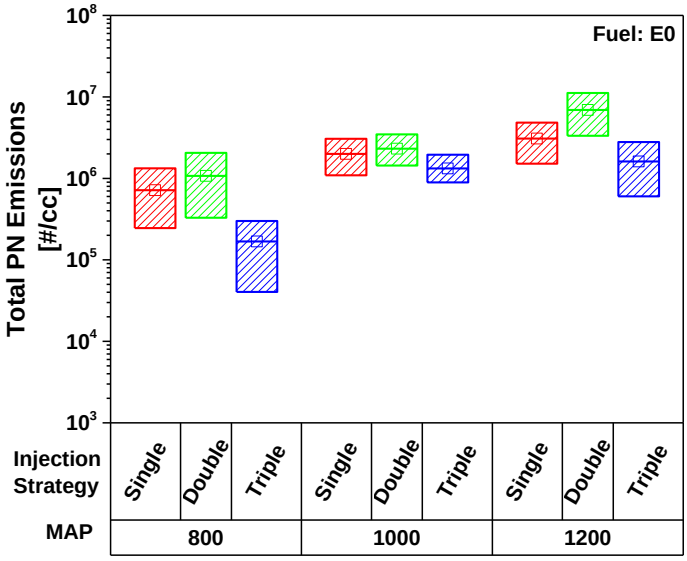

Figure 3.20. Total PN emissions for E0 as a function of MAP and the injection strategies presented in **Figure 3.19**. The limits of each box are the 10th and 90th percentiles, and the square marker is the mean of each condition.

Figures 3.21 presents the particle size distributions for E0, E30 and E85 at MAP of 1000 mbar for the triple injection strategy presented in **Figure 3.19**. Increasing ethanol content decreased the PN emissions at all sizes. **Figure 3.22** shows the total PN for each fuel and the effects of the different injection strategies. The multiple injection strategies combined with E85 decreased the total PN emission concentration by over an order of magnitude compared with E0.

The triple injection strategy reduced total PN for all fuels, but was more effective at reducing total PN for the ethanol blends.

In this work, the triple injection strategy decreased the fuel mass injected in both the first and second injection events compared with the double injection strategy. There may have been less wall wetting with the triple strategy due to the shorter injection durations. The triple injection strategy may have also resulted in better fuel air mixing. Note the differences in the PN emissions from the single and double injection strategies were small, with considerable overlap between the 10th and 90th percentiles of each distribution.

An additional consideration is fuel injector tip wetting which can lead to particulate emissions. Fischer et al. [55] reported a split injection increased fuel injector tip sooting compared with a single injection. This could be due to more injector opening and closing events which may lead to higher wetting of the fuel injector tip. The significant decrease in PN emissions with the triple injection strategy observed in the current work indicates fuel injector tip wetting is not a significant source of PN for the conditions studied.

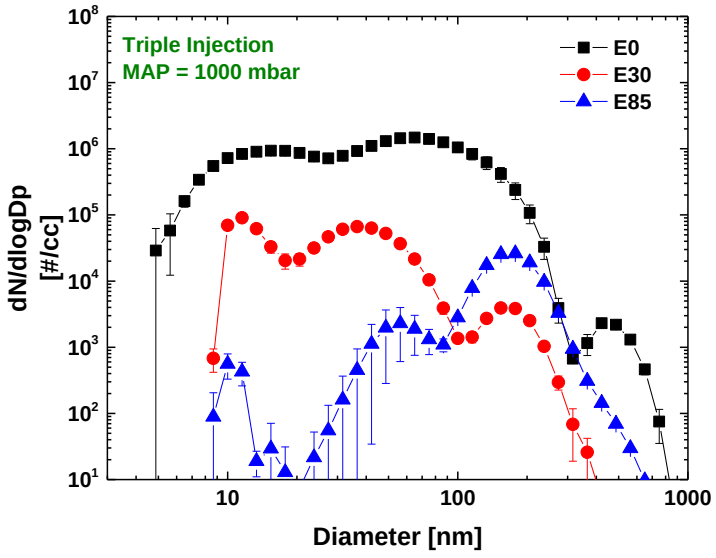

Figure 3.21. PN size distributions for E0, E30 and E85 at MAP = 1000 mbar using the triple injection strategy shown in **Figure 3.19**. The error bars represent the standard deviations of the average recorded PN distribution for two days.

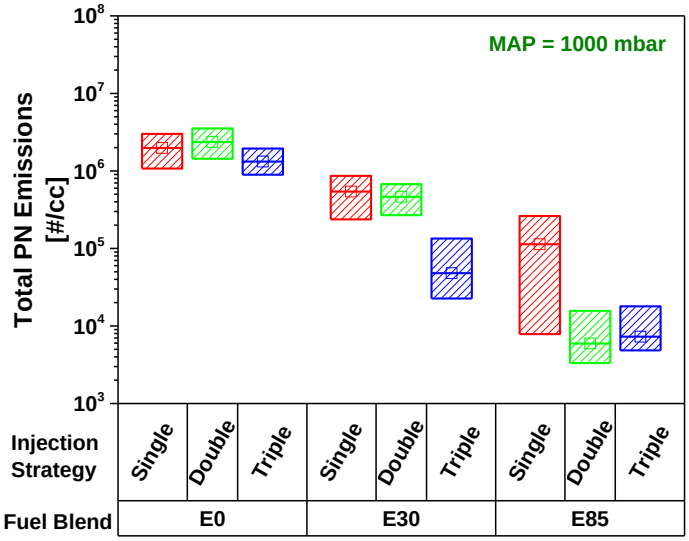

Figure 3.22. Total PN emissions for E0, E30 and E85 at MAP = 1000 mbar and using the injection strategies of **Figure 3.19**. The limits of each box are the 10th and 90th percentiles, and the square marker is the mean of each condition.

As seen in **Figure 3.21,** the PN emissions corresponding to larger diameters are higher for E85 compared with E30 fuel. Larger particles will contribute more to particulate mass (PM) emissions. The effects of injection strategy and fuel composition on PM emissions were estimate using the PN data. Assuming the soot particles were spherical and using an effective particle density co-relation from Liu et al. [56], the total PM was calculated. The results are presented in **Figure 3.23,** with the caveat that the PN data were collected after removal of particles larger than 1 μm. The removal of the larger particles will significantly affect the total PM; however, the estimates provide information on the trends for the PM in the size range up to 1 μm. The results in **Figure 3.23** show the ethanol significantly reduced PM for single injection

conditions; and both ethanol blends (E30 and E85) yield similar reduction in PM with use of triple injection strategy.

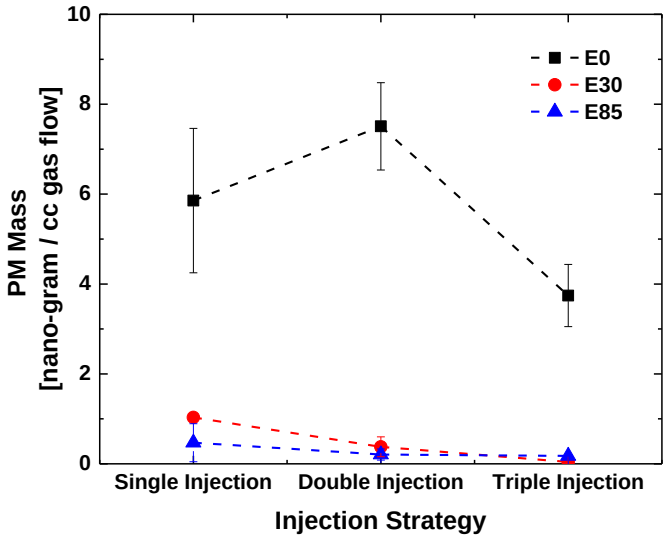

Figure 3.23. Estimates for particulate mass based on the size-resolved PN data for MAP = 1000 mbar.

The reduction in PN emissions observed with triple injection for E0 is consistent with results of the previous studies [49] which attributed the decrease in PN to reduced fuel spray penetration and thus lower piston and wall impingement. Previous literature also reported reduction in PN and PM emissions with increase in ethanol content in the fuel [57]. Westbrook et al. [58] in their chemical kinetic modeling study found a direct relation between the fraction of oxygen (ethanol) in diesel fuel and reduction in percent of fuel carbon converted to soot precursors, indicating a strong chemical pathway to reducing particulates. Similarly, Chen et al. [59] reported lower PN emissions with E25 compared with gasoline and attributed the low particulate formation to chemical effects of ethanol. However, Chen et al. [59] also reported the higher heat of vaporization of ethanol results in high evaporative cooling which enhances

formation of residual liquid film mass, which is a source of particulates and thus PN formation also depends on operating conditions.

Figure 3.24 summarizes the effects of the different fuels and injection strategies on the engine performance metrics for the conditions that yielded the greatest reduction in total PN (SOI1 =280; SOI2 = 220; SOI3 = 60; fuel distribution = 40:40:20). All ethanol blends yielded improvements in all metrics, except NOx which was mostly unaffected in comparison with E0. Additionally, multiple injection strategies improved the performance further for each fuel blend in comparison with single injection strategies.

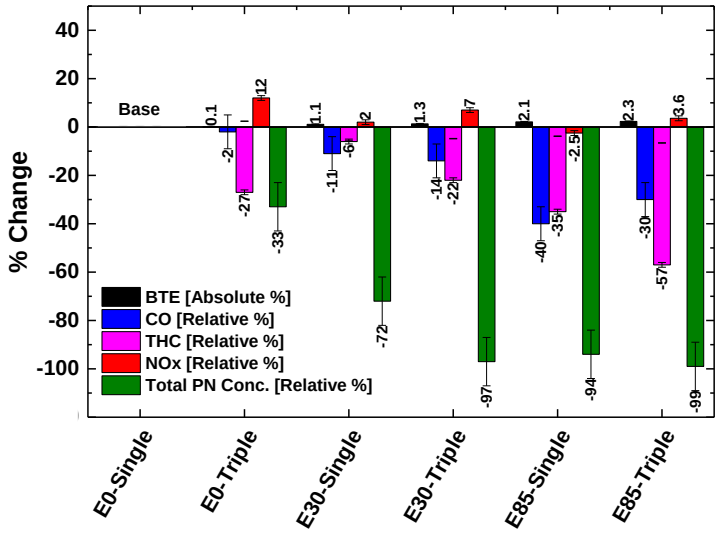

Figure 3.24. Comparison of single and multiple injection strategies that yielded the highest reduction in PN.

3.5.6 Engine sensitivity to different fuel blends

The weighted center of injection enabled comparing single injection data with the results of the multiple injection strategies using the WCOI as a representative injection timing. Some of the engine metrics showed greater sensitivity to WCOI, like BTE for E0, than other parameters, like BTE for E30. The timing of the injection strategy is an indication of the homogeneity of the

fuel/air mixture; however, WCOI does not completely capture the distribution of the fuel mass in the injection events. Fuel mass distribution also affects stratification and mixing of the fuel/air mixture. To evaluate the role of mass distribution, the results of the study were evaluated using a new parameter defined as the weighted injection spread (WIS). Here the spread refers to the timing of the different injection events relative to the WCOI. The definition is based on the mass-weighted average relative to the WCOI timing:

$$WIS = 2 * \sum_{i=1}^{N} IS_i * ID_i / \sum_{i=1}^{N} ID_i$$

where IS_i is the spread of i^{th} injection = $|COI_i - WCOI|$. Note WIS is zero for a single injection event.

Generally, earlier WCOI leads to more homogeneous mixtures and later WCOI leads to more stratified mixtures; however, the spread of injection affects stratification as well. For example, higher WIS at later WCOI timing will reduce stratification. For reference, schematics illustrating different values of WCOI and WIS are provided in through **Figures 3.25**, **3.26** and **3.27**.

Figure 3.25 presents the experimental matrix studied in the current work corresponding to conditions presented in **Table 3.3**, for E0 as a function of WCOI and WIS at MAP = 800 mbar.

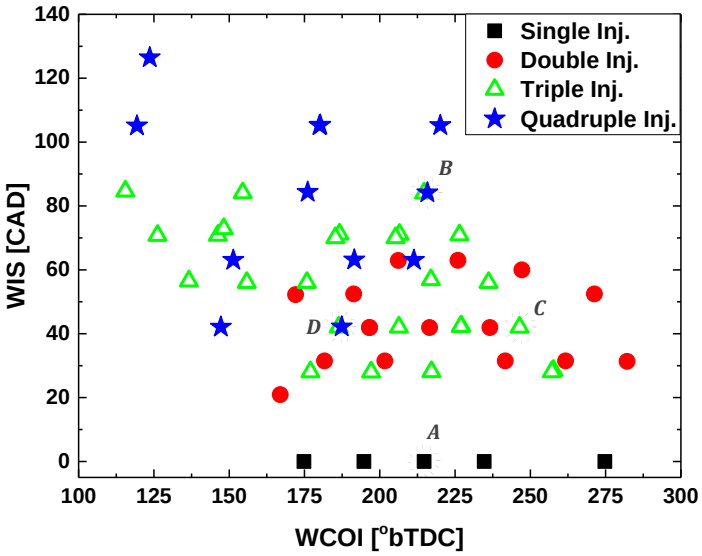

Figure 3.25. Experimental matrix evaluated for E0 fuel at 800 mbar. Schematics illustrating the timing of the injection strategies for the points labeled A, B, C and D are provided in the **Figures 3.26** and **3.27.**

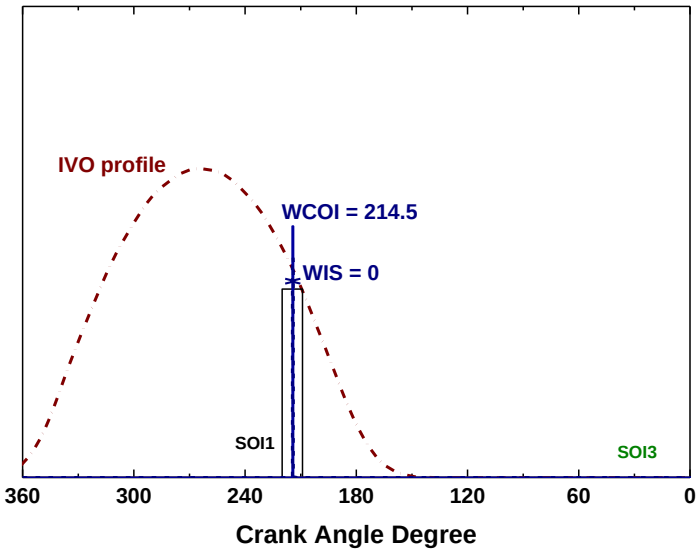

A

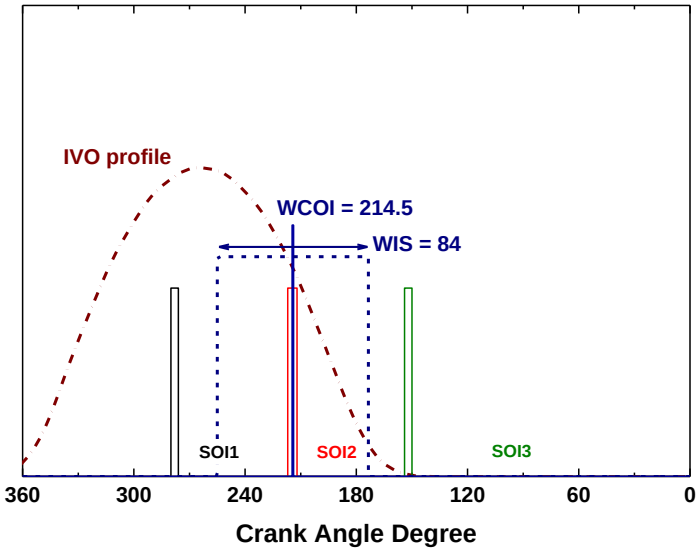

B

Figure 3.26. Comparison of injection strategies with the same WCOI and different WIS values, corresponding to the points labeled A and B in **Figure 3.25.**

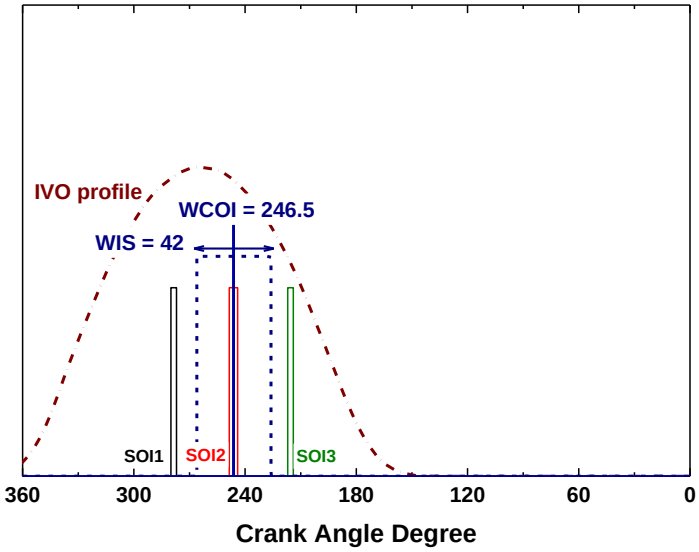

C

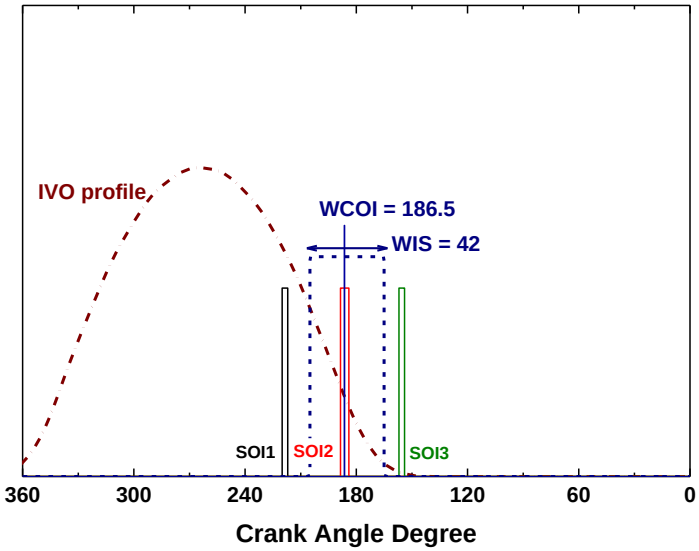

Figure 3.27. Comparison of injection strategies with the same WIS and different WCOI values, corresponding to the points labeled C and D in **Figure 3.25.**

Figure 3.28 presents the BTE, CO, THC and NOx emissions data for E0 as a function of the overall injection characteristics WCOI and WIS. Some clear trends are apparent in the figure. Very retarded WCOIs lead to poor efficiency with moderate emissions benefits. The highest BTE values correspond to mid-range WCOIs (~225° bTDC), not the most advanced injection timing and importantly, for fixed mid-range WCOI, the maximum benefits in terms of efficiency and emissions are found at the maximum values of WIS. The mid-range WCOI timing and higher WIS indicate favorable performance is achieved by allowing more time for fuel and air mixing and minimizing stratification as much as possible through higher values of WIS. Also, the large range of variability in performance possible for a fixed mid-range WCOI as a function of WIS, indicates the value of using WIS to characterize the fueling strategies.

Interestingly, the lowest NOx and THC emissions occurred at the maximum WIS considered in the study with a WCOI of ~175° bTDC. These conditions correspond to higher

fuel mass injected closer to firing TDC, which may contribute to lower peak in-cylinder temperatures [52] and thus lower NOx emissions.

Figure 3.29 and **3.30** presents the results for E30 and E85 respectively, as a function of WCOI and WIS. In comparison with E0 all metrics improve with ethanol blending. An important conclusion of comparing the data for E0, E30 and E85 is the similar sensitivity of the engine performance to the different fuel blends. The consequence of the similar fuel response facilitates translation of the engine control calibrations between different ethanol and gasoline fuel blends.

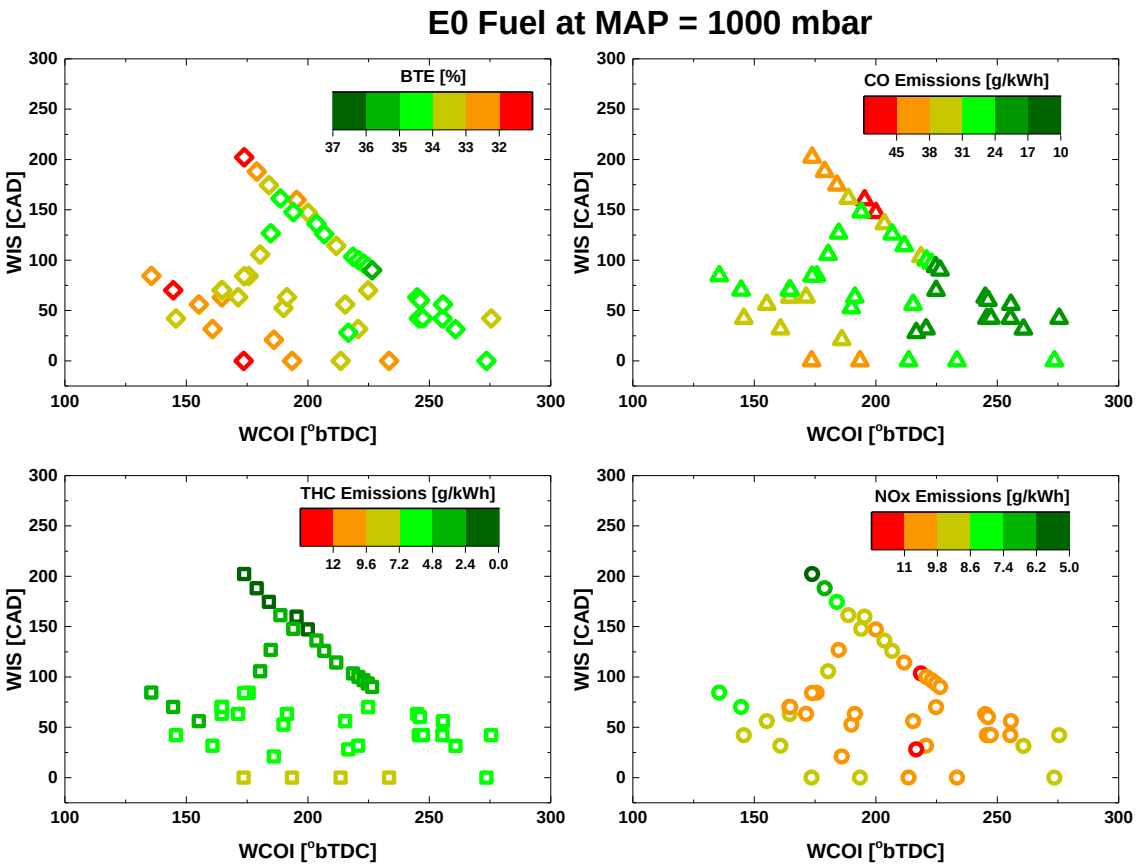

Figure 3.28. E0 results for MAP = 1000 mbar.

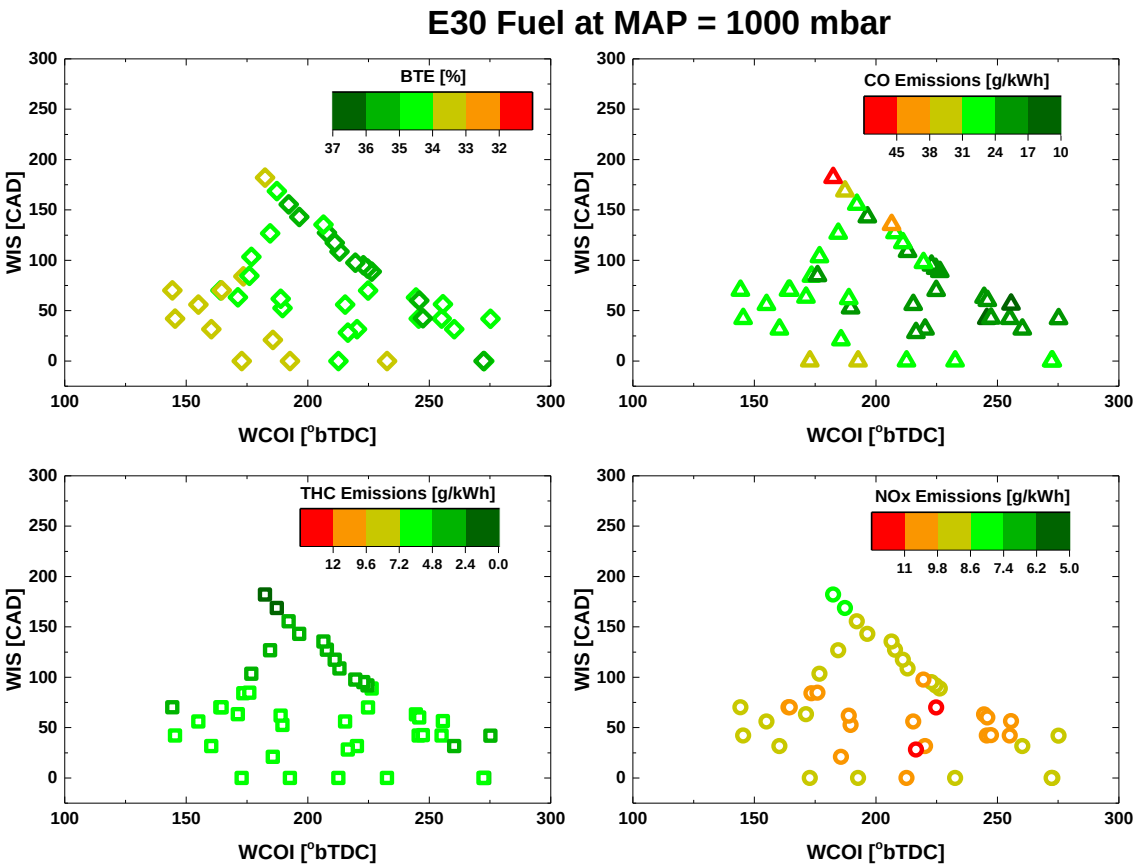

Figure 3.29. E30 results for MAP = 1000 mbar.

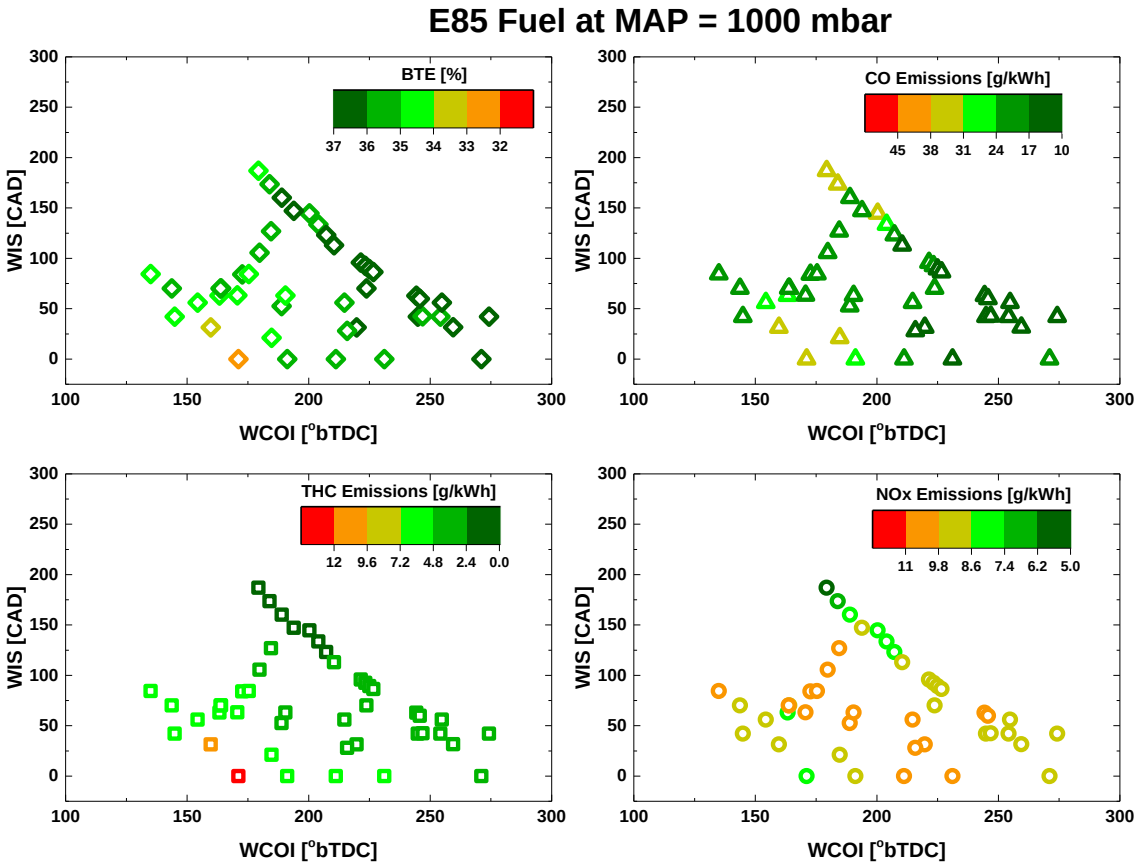

Figure 3.30. E85 results for MAP = 1000 mbar.

3.6 Conclusions

The key objective of the study was to quantify the effects of multiple fuel injection events and ethanol fuel blends on engine performance in comparison with a single fuel injection event for gasoline. The large parametric space of different multiple injection strategies had not been previously considered for ethanol blends. Key conclusions based on the experimental results are:

- A combined application of ethanol blends with a multiple injection strategy can help achieve considerable improvement in engine emissions while maintaining engine BTE. In particular, compared to single injection of E0, a multiple fuel injection strategy using E85 fuel resulted in more than 90% reduction in total PN emission concentration, 50%

reduction in THC, 35% reduction in CO on a relative basis, with 2.4% absolute improvement in BTE.

- The ethanol blends out-performed E0 for all metrics considered, and the ethanol blends exhibited similar response and sensitivity to the different injection strategies as E0. Thus, indicating injection strategies (e.g., number of injections, injection timing, etc.) can be readily translated from one fuel to another.
- Multiple injection strategies are more effective at improving performance at higher MAPs.
- The results of the study showed engine performance was very sensitive to more than just one characteristic of the injection strategy. For example, the timing and the distribution of fuel mass of the different injection events were all contributors to engine performance. A new parameter, the weighted injection spread (WIS), was introduced to characterize the different important parameters of multiple fuel injection strategies. When WIS was combined with a previously defined parameter of weighted center of injection, the results were more clearly differentiated and trends were clearly observable. Favorable engine performance was achieved using a mid-range value of weighted center of injection timing with higher values of weighted injection spread.

3.7 Acknowledgements

The authors would like to thank Andrew Karpin, Engine Calibration Engineer at Robert Bosch LLC for technical support. The authors gratefully acknowledge the support of the U.S. Department of Energy Vehicle Technologies Office.

3.8 Abbreviations

BTE - Brake Thermal Efficiency
BSFC - Brake Specific Fuel Consumption
COI - Center of Injection
CoV - Coefficient of Variance (for IMEP)
ECU - Engine Control Unit
EPA - Environmental Protection Agency
GDI - Gasoline Direct Injection
ID - Injection Duration
MAP - Manifold Absolute Pressure
MBT - Maximum Brake Torque
MPG - Miles Per Gallon
PFI - Port Fuel Injection
RFS - Renewable Fuel Standard
SOI - Start of Injection
TDC - Top Dead Center
WCOI - Weighted Center of Injection
WIS - Weighted Injection Spread

References

33. Singh, R., Burch, T., Lavoie, G., Wooldridge, M., and Fatouraie, M. (2017). Effects of Fuel Injection Events of Ethanol and Gasoline Blends on Boosted Direct-Injection Engine Performance. *SAE Technical Paper No. 2017-01-2238.*

34. Stein, R. A., Anderson, J. E., and Wallington, T. J. (2013). An overview of the effects of ethanol-gasoline blends on SI engine performance, fuel efficiency, and emissions. *SAE International Journal of Engines, 6(1), 470-487 (SAE Paper 2013-01-1635).*

35. Jung, H. H., Leone, T. G., Shelby, M. H., Anderson, J. E., and Collings, T. (2013). Fuel Economy and CO_2 Emissions of Ethanol-Gasoline Blends in a Turbocharged DI Engine. *SAE International Journal of Engines, 6(1), 422-43. (SAE Paper 2013-01-1321).*

36. Leone, T. G., Olin, E. D., Anderson, J. E., Jung, H. H., Shelby, M. H., and Stein, R. A. (2014). Effects of fuel octane rating and ethanol content on knock, fuel economy, and CO2 for a turbocharged DI engine. *SAE International Journal of Fuels and Lubricants, 7(1), 9-28 (SAE Paper 2014-01-1228).*

37. Jo, Y. S., Lewis, R., Bromberg, L., and Heywood, J. B. (2014). Performance Maps of Turbocharged SI Engines with Gasoline-Ethanol Blends: Torque, Efficiency, Compression Ratio, Knock Limits, and Octane. *SAE Technical Paper No. 2014-01-1206.*

38. Liu, H., Wang, Z., Long, Y., Xiang, S., Wang, J., and Fatouraie, M. (2015). Comparative study on alcohol–gasoline and gasoline–alcohol Dual-Fuel Spark Ignition (DFSI) combustion for engine particle number (PN) reduction. *Fuel*, *159*, 250-258.

39. The International Council on Clean Transportation (2016). A technical summary of Euro 6/VI vehicle emission standards, available from (https://www.theicct.org/sites/default/files/publications/ICCT_Euro6-VI_briefing_jun2016.pdf); [accessed 05 May 2017].

40. Catapano, F., Di Iorio, S., Lazzaro, M., Sementa, P., and Vaglieco, B. M. (2013). Characterization of ethanol blends combustion processes and soot formation in a GDI optical engine. *SAE Technical Paper No. 2013-01-1316*.

41. Vuk, C., and Vander Griend, S. J. (2013). Fuel property effects on particulates in spark ignition engines. *SAE Technical Paper No. 2013-01-1124*.

42. Ricci-Ottati GA, Bosch RH, inventors; Delphi Technologies Inc, assignee (2002). Method for controlling fuel rail pressure using a piezoelectric actuated fuel injector. *United States patent US 6,345,606.*

43. Moreno, C. J., Stenlaas, O., and Tunestal, P. (2017). Influence of Small Pilot on Main Injection in a Heavy-Duty Diesel Engine. *SAE Technical Paper No* 2017-01-0708.

44. Moreno, C. J., Stenlaas, O., and Tunestal, P. (2017). Investigation of Small Pilot Combustion in a Heavy-Duty Diesel Engine. *SAE International Journal of Engines, 10(2017-01-0718), 1193-1203. (SAE Paper 2017-01-0718).*

45. Mingfa, Y., Hu, W., Zunqing, Z., and Yan, Y. (2009). Experimental study of multiple injections and coupling effects of multi-injection and EGR in a HD diesel engine. *SAE Technical Paper No. 2009-01-2807*.

46. Cheng, X., Chen, L., Yan, F., Hong, G., Yin, Y., and Liu, H. (2013). Investigations of split injection strategies for the improvement of combustion and soot emissions characteristics based on the two-color method in a heavy-duty diesel engine. *SAE Technical Paper No. 2013-01-2523.*

47. Yang, J., and Anderson, R. W. (1998). Fuel injection strategies to increase full-load torque output of a direct-injection SI engine. *SAE Technical Paper No. 980495*.

48. Daniel, R., Wang, C., Xu, H., and Tian, G. (2012). Split-injection strategies under full-load using DMF, a new biofuel candidate, compared to ethanol in a GDI engine. *SAE Technical Paper No. 2012-01-0403*.

49. Su, J., Xu, M., Yin, P., Gao, Y., and Hung, D. (2015). Particle number emissions reduction using multiple injection strategies in a boosted spark-ignition direct-injection (SIDI) gasoline engine. *SAE International Journal of Engines, 8(1), 20-29 (SAE paper 2014-01-2845).*

50. Schmidt, L., Seabrook, J., Stokes, J., Zuhdi, M. F. A., Begg, S., Heikal, M., and King, J. (2011). Multiple injection strategies for improved combustion stability under stratified part load conditions in a spray guided gasoline direct injection (SGDI) engine. *SAE Technical Paper No. 2011-01-1228.*

51. Hagena, J. R., Filipi, Z., and Assanis, D. N. (2006). Transient diesel emissions: analysis of engine operation during a tip-in. *SAE Technical Paper No. 2006-01-1151*.

52. Imaoka, Y., Shouji, K., Inoue, T., and Noda, T. (2015). A study of a multistage injection mechanism for improving the combustion of direct-injection gasoline engines. *SAE International Journal of Engines, 8(3), 1080-1087 (SAE Paper 2015-01-0883).*

53. Whitaker, P., Kapus, P., Ogris M., & Hollerer, P. (2011). Measures to reduce particulate emissions from gasoline DI engines. *SAE International Journal of Engines (SAE Paper 2011-01-1219*)

54. Fatouraie, M., Wooldridge, M., & Wooldridge, S. (2013). In-cylinder particulate matter and spray imaging of ethanol/gasoline blends in a direct injection spark ignition engine. *SAE International Journal of Fuels and Lubricants. (SAE paper 2013-01-0259).*

55. Fischer, A., & Thelliez, M. (2018). Methodology and Tools to Predict GDI Injector Tip Wetting as Predecessor of Tip Sooting. *SAE Technical Paper No. 2018-01-0286, 2018.*

56. Liu, Z. G., Vasys, V. N., Dettmann, M. E., Schauer, J. J., Kittelson, D. B., and Swanson, J. (2009). Comparison of strategies for the measurement of mass emissions from diesel engines emitting ultra-low levels of particulate matter. *Aerosol Science and Technology*, *43*(11), 1142-1152.

57. Storey, J. M., Barone, T., Norman, K., and Lewis, S. (2010). Ethanol blend effects on direct injection spark-ignition gasoline vehicle particulate matter emissions. *SAE International Journal of Fuels and Lubricants*, *3*(2), 650-659 (*SAE Paper 2010-01-2129).*

58. Westbrook, C. K., Pitz, W. J., and Curran, H. J. (2006). Chemical kinetic modeling study of the effects of oxygenated hydrocarbons on soot emissions from diesel engines. *The journal of physical chemistry A*, *110*(21), 6912-6922.

59. Chen, Y., Zhang, Y., and Cheng, W. K. (2018). Effects of Ethanol Evaporative Cooling on Particulate Number Emissions in GDI Engines. *SAE Technical Paper No. 2018-01-0360*.

Chapter 4

Beyond the Engine Technology

4.1 Introduction

The history of ethanol fueled engines goes back to 1896, when Henry Ford built his first automobile: the Ford Quadricycle, which was designed to operate using pure ethanol. Since then, numerous studies, including this thesis work, have demonstrated the benefits of ethanol for spark-ignition engines [60], [61], [62]. Thus, the engine architecture for use of ethanol as a fuel, though not optimized, has been available since the 1900s. However, the use of ethanol fuel consumption across the globe accounts to less than 2% of that of gasoline; in the U.S. the percentage is around 10%. So the relatively low usage of ethanol is not due to lack of prior art or issues intrinsic to the engine architecture.

It is observed that globally the history of ethanol fuel production and use has been a history of policies enacted by governments to move towards greater energy independence and control air pollution. These policies include subsidies or laws guided by the national energy security, price of oil or other political state of affairs. This chapter briefly reviews the policies around the globe which have promoted ethanol use, with a special focus on how policies in the U.S. have guided the ethanol fuel use.

World ethanol consumption as a fuel for the transportation sector has been growing with several countries introducing mandates to promote ethanol blending in conventional automotive fuels. **Brazil** had the first largest successful program in the world to promote biofuels in their country. The history of ethanol fuel in Brazil dates back to 1970s with the launch of *PróÁlcool (pro-alcohol)* program [63]. The program focused on production of anhydrous ethanol from sugarcane to displace fossil based automotive fuels. In 1976 the government made 11% ethanol blending mandatory for automotive fuels. At present, the automobiles in Brazil run on fuel blended with 20% to 27% ethanol as per the government mandate. The **European Union (EU)** adopted its first biofuels policy in 2003. Today all gasoline sold in the EU typically contains up to 5% ethanol [64], with countries like Germany, France, Finland, Belgium leading with 10% ethanol blends available. The **Chinese** government has also been strongly promoting the National Fuel Ethanol Program, since 2002 [65]. In 2004, the Chinese government introduced a mandate to use E10 blend in five cities and now plans to expand the program nationally by 2020. **India** launched its Ethanol Blended Petrol (EBP) program in January 2003. The program was directed towards supplying of 5% ethanol blended with gasoline in nine states [66]. The country targets to meet 8-10% ethanol blend levels nationally by 2022 [67]. The renewable fuel regulations in **Canada** require fuel producers and importers to have an average renewable fuel (ethanol) content of at least 5% based on the volume of gasoline that they produce or import into Canada [68].

The leader of the global ethanol production market is the **United States**, with 15,800 million gallons of annual production in 2017 [69]. The history of corn-derived ethanol as a fuel in the U.S. began in the mid-1800s when it started replacing whale oil as a fuel for lamps. The timeline of U.S. ethanol use from the mid-1800s until today is presented in **Table 4.1** [70], [71],

[72]. **Figure 4.1** presents the annual U.S. fuel ethanol consumption since 1980. Currently, 95% of the gasoline sold in the U.S. is blended with 10% ethanol (E10) [73].

Table 4.1. U.S. Timeline of Ethanol Use

Year	Policy / Law Enacted / Event	Ethanol annual consumption (million gallons)
1800	***Ethanol for Lamp Oil*** Ethanol starts displacing whale oil as a fuel for lamps.	Data not available
1862	***Ethanol Tax*** The Union Congress put a $2 per gallon excise tax on ethanol to help pay for the Civil War. The cost of ethanol increased too much to be used as illuminating oil.	Data not available
1896	***Ford's Engine*** Henry Ford built his first automobile, the quadricycle, to run on pure ethanol. Ford believed ethanol to be the fuel of future.	Data not available
1906	***Tax Free*** Over 50 years after imposing the tax on ethanol, the U.S. congress removed it, making ethanol a cost competitive alternative fuel to gasoline as a motor fuel.	Data not available
1908	***Ford's FFV*** Henry Ford produced the Model-T as a flexible fuel vehicle (FFV). As a FFV it could run on ethanol, gasoline, or a combination of the two.	Data not available
1917	***World War I*** During World War I, the need for fuel increased ethanol demand to 50–60 million gallons per year.	Data not available

Year	Policy / Law Enacted / Event	Ethanol annual consumption (million gallons)
1930	***Midwest Market*** Fuel ethanol gained a market in the Midwest. Over 2,000 gasoline stations in the Midwest sold gasoline blended with 6% to 12% ethanol.	Data not available
1941-45	***World War II*** Ethanol production for fuel use increased, owing to a massive wartime increase in demand for fuel, but most of the increased demand for ethanol was for non-fuel wartime applications like production of synthetic rubber	Data not available
1947-78	***Ethanol Dip*** Once World War II ended, with reduced need for war materials and with the low price of gasoline, ethanol use as a fuel was drastically reduced.	Data not available
1975	***Lead Banned*** The U.S. begins to phase out lead (used as octane booster) in gasoline, owing to its hazardous nature. Ethanol became a more attractive additive.	Data not available
1978	***Gasohol*** The term gasohol was defined for the first time as a blend of gasoline with at least 10% alcohol by volume in the Energy Tax Act of 1978.	Data not available
1980	***Promoting Ethanol Production*** ● The Energy Security Act of 1980 offered insured loans for small ethanol producers. ● The Gasohol Competition Act of 1980 banned retaliation against ethanol resellers. ● The Crude Windfall Tax Act of 1980 extended the ethanol–gasoline blend tax credit.	Data not available

Year	Policy / Law Enacted / Event	Ethanol annual consumption (million gallons)
1984	***Peak Production*** There were 163 ethanol plants in the United States.	**495**
1985	***Another Dip*** Gasoline prices dropped and many ethanol producers went out of business, despite the subsidies. Only 74 of the 163 commercial ethanol plants remained operating.	**600**
1988	***Alternative Motor Fuels Act (AMFA)*** To incentivize alternative fuel vehicle development, AMFA established vehicle manufacturer incentives in the form of Corporate Average Fuel Economy (CAFE) credits [74].	**808**
1992	***E85 as Alternative Fuel*** The Energy Policy Act of 1992 defined ethanol blends with at least 85% ethanol (E85) as an alternative transportation fuel. The Act also provided tax deductions for purchasing Flex-Fuel Vehicles.	**956**
1997	***Flex Fuel Vehicles (FFVs)*** Major U.S. auto manufacturers began mass production of FFVs capable of operating on E85, gasoline, or blends of both. Most of these vehicles used gasoline as their only fuel because of the scarcity of E85.	**1222**
2000	***MTBE Phase-Out*** The EPA recommended that methyl tert-butyl ether (MTBE, which dominated the market as an octane booster) to be phased out nationally due to environmental concerns. Ethanol was again an attractive additive.	**1610**
2002	***The Farm Bill*** The Farm Security and Rural investment Act (U.S. Farm	**2018**

Year	Policy / Law Enacted / Event	Ethanol annual consumption (million gallons)
	Bill) promoted establishing a competitive grant program to support development of biorefineries [75].	
2003	***Reformulated Gasoline*** California began switching from MTBE to ethanol to make reformulated gasoline, resulting in a significant increase in ethanol demand. A total of 18 States had passed legislation that would eventually ban MTBE.	**2752**
2004	***Volumetric Ethanol Excise Tax Credit (VEETC)*** American Jobs Creation Act implemented VEET to combine two historic subsidies (a tax credit for ethanol and an excise tax that exempted ethanol-blended gasoline) [76].	**3460**
2005	***The Renewable Fuels Standard (RFS)*** The Energy Policy Act of 2005 was responsible for regulations that ensured gasoline sold in the United States contained a minimum volume of renewable fuel, called the Renewable Fuels Standard.	**3954**
2007	***The EISA*** The Energy Independence and Security Act (EISA) of 2007 expanded the Renewable Fuels Standard to require that 36 billion gallons of ethanol and other fuels be blended into gasoline, diesel, and jet fuel by 2022. EISA established four separate categories of renewable fuels: renewable fuel, advanced biofuel, biomass-based diesel, and cellulosic biofuel [77].	**6710**
2008	***1st Generation biofuel Challenge*** The U.S. government and international agencies speculated the 1st generation biofuels (produced from corn) caused higher food prices. The 'food vs fuel' debate intensified during the 2008 Farm Bill. ***The Great Recession***	**9435**

Year	Policy / Law Enacted / Event	Ethanol annual consumption (million gallons)
	The ethanol industry came under financial stress due to the 2008 economic crisis.	
2009	***The Recovery Act*** In response to the great recession the American Recovery and Reinvestment Act was signed into law. It allocated supplemental appropriations for biofuel research, development and demonstration projects [78].	**10734**
2010	***VEETC extended*** The Tax Relief, Unemployment Insurance Reauthorization, and Job Creation Act of 2010 extended the business tax credits for alternative fuels, such as the VEETC [79].	**12522**

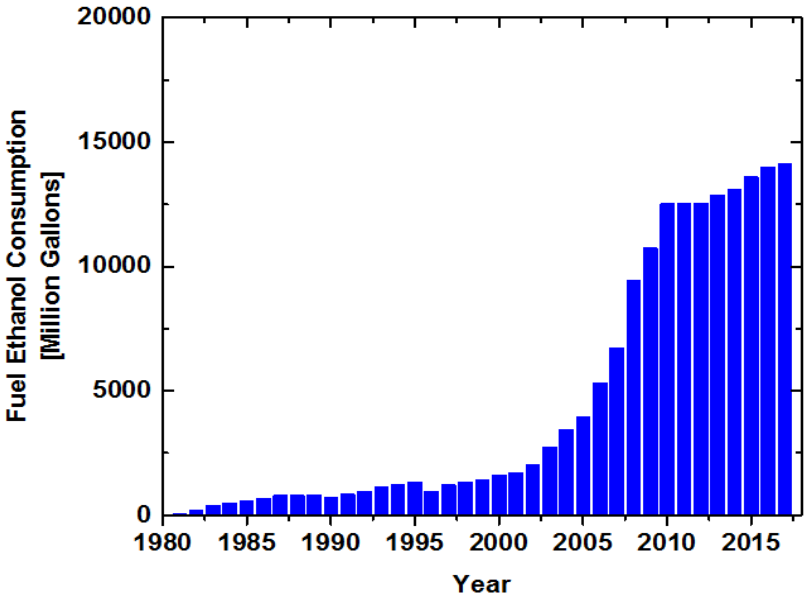

Figure 4.1. Annual U.S. Fuel Ethanol Consumption [80]

The timeline is a brief sample of the policies that molded ethanol use as a fuel. Each policy decision has its own 'behind the scene' story. A recent example is the formulation of the

RFS program, which played a key role in the emergence of the U.S. biofuels industry. The program historically and to date is a subject of dispute between interested stakeholders, such as the oil industry and automakers on one side, and the corn farmers, biofuel producers and environmental groups on the other. Several technical components of the program have been challenged—even in court—by both oil industry and biofuel lobby groups [81] [82].

4.2 Moving forward with ethanol as an alternative fuel

Different social, political and environmental events can shape the policies guiding ethanol fuel use in a country. Thus, it is essential to look beyond the engine technology and optimizing the engine parameters for the fuel. At present, two vital concerns of any nation trying to implement or expand an ethanol fuel program are the interrelated concerns of the feedstock and processing required to produce the ethanol and the infrastructure required to gather the feedstock and distribute the ethanol produced from the biorefineries. These topics are discussed briefly in the following sections.

4.2.1 Ethanol production from main food crop (Generation-I Biofuels)

As mentioned above, speculations were raised that the increase in corn price in 2008 in the U.S. was caused by ethanol production. Though this was proved incorrect [83], the rapid expansion of the U.S. ethanol program has led to dramatic increase in corn use for ethanol [84], and this has provoked concerns regarding unintended adverse effects on other sectors [85], [86]. In many developing countries, the concerns regarding food security and land-use change with ethanol production from main food crops (also known a gen-I ethanol) are of even greater concern than in the U.S.

These issues and others with gen-I ethanol have directed interest towards cellulosic ethanol (also known as gen-II ethanol), which is produced using non-food feedstocks such as crop residues. Gen-II ethanol does not complete with food crops and moreover, has been reported to have significantly lower lifecycle greenhouse gas emissions than gen-I ethanol [87].

In the U.S., the RFS program is promoting production of cellulosic ethanol by adding explicit definitions for the fuels to qualify as 'renewable'. For example, the following definitions have been added to the standard:

- **Biomass-based diesel** must meet a 50% lifecycle GHG reduction
- **Cellulosic biofuel** must be produced from cellulose, hemicellulose, or lignin and must meet a 60% lifecycle GHG reduction
- **Advanced biofuel** can be produced from qualifying renewable biomass (except cornstarch) and must meet a 50% GHG reduction
- **Renewable (or conventional) fuel** typically refers to ethanol derived from corn starch and must meet a 20% lifecycle GHG reduction threshold

Under this revised RFS program (also known as RFS-II), all renewable fuel must be made from feedstocks that meet a revised definition of renewable biomass. **Figure 4.2** shows the expected contribution from each category to meet the 36 billion gallon target volume set for 2022 by the RFS-II. Most of the target volume requirement beyond 2017 is expected to be met through biofuels under the cellulosic and advanced categories; the 'renewable' category which consists of corn-starch ethanol is capped at 15 billion gallons.

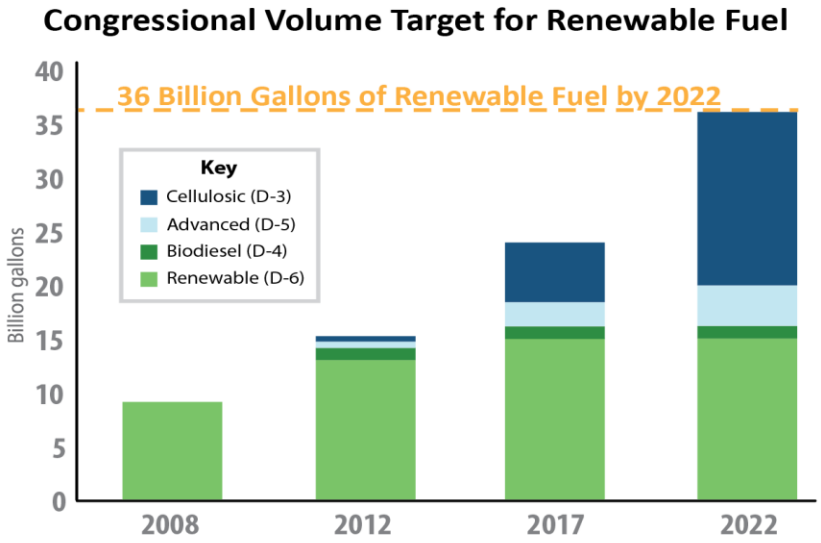

Figure 4.2. Renewable fuel volume targets under RFS-II program [88]

Driven by the RFS-II policy, the cellulosic ethanol sector in the U.S. is increasing commercial scale production. However, a major barrier to cellulosic fuel production is that the production costs still remain significantly higher than for corn/starch-based ethanol. Currently, various production processes for conversion of cellulosic feedstocks into motor fuel are prohibitively expensive, including physical, chemical, enzymatic, and microbial treatment [89]. The National Renewable Energy Laboratory (NREL) estimated the cost of producing cellulosic ethanol as 1.5 to 2 times the cost of corn-based ethanol. The current technological and economic issues in cellulosic ethanol production have led to shut down of projects like the DuPont refinery in Iowa and the Abengoa refinery in Kansas, U.S. However despite the uncertainties and challenges associated with these U.S. demonstrations, cellulosic ethanol production has been demonstrated successfully on commercial scale at other plants. The Raizen Energia refinery in Brazil produces cellulosic ethanol from sugarcane bagasse. A successful leading example in the U.S. is the project Liberty by Poet-DSM Advanced Biofuels, LLC, in Emmetsburg, Iowa; which

began producing cellulosic ethanol from corn stover in 2014. The biorefinery has the capacity to produce up to 25 million gallons of cellulosic ethanol annually [90].

Cellulosic ethanol is being widely recognized as a unique transportation fuel. The powerful environmental and social benefits of cellulosic ethanol can be realized with government policies to overcome the perceived risk of first application. Several nations are advancing towards local cellulosic ethanol production. Canada [91], Denmark [92] and Brazil [93] have operational cellulosic biorefineries. China has pilot scale plants and has added subsidies for cellulosic ethanol production and processing to promote biofuel development which does not compete for arable land designated for food crops [94]. India inaugurated its first demonstration scale cellulosic ethanol production plant in April 2016 [95].

4.2.2 Inadequate infrastructure for ethanol distribution

In addition to concerns about feedstock for ethanol production, slow development of ethanol distribution infrastructure is also a deterrent to widespread adoption of the biofuel. According to IHS Markit [96], there are nearly 20 million flex fuel vehicles (FFVs) on U.S. roads today, capable of running with gasoline fuel ethanol levels of up to 85% by volume. However only 10-15% of these vehicles use ethanol blends other than E10. This is attributable to lack of infrastructure available for ethanol distribution: only 3% of total gas stations in the U.S. provide refueling options with fuel higher than 10% ethanol blending [97].

The policies to date have been centered on fuel production and vehicle end-use technologies. There has been significantly less effort focused on the infrastructure decisions [98]. Ethanol does present challenges for infrastructure, such as being corrosive at high concentrations, and thus may damage existing pipelines [99]. However, development of effective policies and support programs like the Biofuels Infrastructure Partnership (BIP) which provide

financial support to accelerate development of ethanol infrastructure can help address issues associated with ethanol distribution.

4.3 A case study set in Ghana

Transition to cellulosic (gen-II) ethanol production with an adequate infrastructure is a requirement for developing a sustainable biofuel program in any country. In the U.S., a number of studies have been carried out to estimate the potential of gen-II ethanol production from feedstocks like corn stover [100], [101]. There are also studies focused on infrastructure recommendations for production and distribution of cellulosic ethanol, especially for the mid-west part of the country [102]. However, these studies are missing for the developing regions of the world, like Africa, which are projected to have greater contribution to increase in global energy use.

As part of this dissertation study, a unique opportunity was presented to explore the cellulosic ethanol production potential provided by agricultural waste in Ghana, Africa. Ghana intends to integrate 20% biofuels into the transportation fuel mix by 2030 [103]. To support that effort and explore the potential methods for siting biorefineries in Ghana, extensive analysis of the supply- and demand-sides of ethanol use in Ghana was conducted. Outcomes of the work include recommendations for biorefinery locations and fuel blending infrastructure on the basis of minimizing transportation costs involved with biomass residue feedstock collection and with distribution of the ethanol produced by the biorefineries. The results of the study are presented and discussed in **Chapter 5**. This study provides valuable input for future work and policy framing which includes an integrated assessment of the social, economic and environmental aspects of cellulosic ethanol for the transportation sector in Ghana. Moreover, Ghana being an

agrarian economy can present a good model for other developing agrarian nations in Africa and Asia.

References

60. Van Hartesveldt, C. H. (1949). ANTIDETONANT INJECTION. *SAE Technical Paper No. 490196*.

61. Scheller, W. A. (1973). *Agricultural alcohol in automotive fuel: Nebraska GASOHOL* (No. CONF-7310124-1). Nebraska Univ., Lincoln (USA). Dept. of Chemical Engineering.

62. Powell, T. (1975). Racing experiences with methanol and ethanol-based motor-fuel blends. *SAE Technical Paper No. 750124*.

63. Soccol, C. R., Vandenberghe, L. P., Costa, B., Woiciechowski, A. L., Carvalho, J. C. D., Medeiros, A. B., and Bonomi, L. J. (2005). Brazilian biofuel program: an overview.

64. European Renewable Ethanol, available from (https://epure.org/about-ethanol/fuel-market/fuel-blends/); [accessed on 11/26/2018].

65. Koizumi, T., and Ohga, K. (2006). Impacts of the Chinese Fuel-Ethanol Program on the World Corn Market: An Econometric Simulation Approach. *The Japanese Journal of Rural Economics, 8, 26-40.*

66. Vikaspedia. Ethanol Blended Petrol Programme - India, available from (http://vikaspedia.in/energy/policy-support/renewable-energy-1/ethanol-blended-petrol-programme); [accessed on 11/26/2018].

67. Times of India. New Policy to go a long way in ethanol blending programme, available from (https://timesofindia.indiatimes.com/business/india-business/new-policy-to-go-a-long-way-in-ethanol-blending-programme/articleshow/64861653.cms); [accessed on 11/26/2018].

68. Government of Canada. Renewable fuel regulations, available from (https://www.canada.ca/en/environment-climate-change/services/managing-pollution/energy-production/fuel-regulations/renewable.html); [accessed on 11/25/2018].

69. Renewable fuels association. Fuel Ethanol Production, available from (https://ethanolrfa.org/resources/industry/statistics/#1537559649968-e206480c-7160); [accessed on 11/20/2018].

70. Ethanol History, available from (http://www.ethanolhistory.com/) [accessed on 10/15/2018].

71. U.S. Energy Information Administration, available from (https://www.eia.gov/KIDS/energy.cfm?page=tl_ethanol); [accessed on 10/15/2018].

72. North Dakota State University, History of ethanol production and policy, available from (https://www.ag.ndsu.edu/energy/biofuels/energy-briefs/history-of-ethanol-production-and-policy); [accessed on 10/15/2018].

73. U.S. Energy Information Administration. Today in Energy, available from (https://www.eia.gov/todayinenergy/detail.php?id=26092); [accessed on 10/25/2018].

74. Alternative Fuels Data Center. Key Federal Legislation, available from (https://afdc.energy.gov/laws/key_legislation); [accessed on 09/20/2018].

75. United States Department of Agriculture. 2002 Farm Bill, available from (https://web.archive.org/web/20150907223955/http://www.ers.usda.gov/media/264008/ap022_6_.pdf); [accessed on 10/20/2018].

76. The Volumetric Ethanol Excise Tax Credit. History and Current policy, available from (https://www.taxpayer.net/agriculture/the-volumetric-ethanol-excise-tax-credit-history-and-current-policy/); [accessed on 10/20/2018].

77. United States Environmental Protection Agency. Renewable Fuel Standard Program, available from (https://www.epa.gov/renewable-fuel-standard-program/renewable-fuel-standard-rfs2-final-rule); [accessed on 11/18/2018].

78. 111th Congress. American Recovery and Reinvestment Act of 2009, available from (https://www.congress.gov/bill/111th-congress/house-bill/1/text/enr); [accessed on 10/22/2018].

79. Zimmerman C., House Passes Tax Bill with Biofuel Incentives, available from (http://energy.agwired.com/2010/12/16/house-passes-tax-bill-with-biofuel-incentives/); [accessed on 10/22/2018].

80. U.S. Energy Information Administration. Monthly Energy Review, available from (https://www.eia.gov/totalenergy/data/monthly/index.php#renewable); [accessed on 10/25/2018].

81. Houston Chronicle. Ethanol wins a round with its battle with oil, available from (https://www.houstonchronicle.com/business/article/Ethanol-wins-a-round-in-its-battle-with-oil-11274353.php); [accessed on 11/25/2018].

82. Living History Farm. Oil vs. Ethanol, available from (https://livinghistoryfarm.org/farminginthe50s/crops_05.html); [accessed on 11/24/2018].

83. Mueller, S. A., Anderson, J. E., and Wallington, T. J. (2011). Impact of biofuel production and other supply and demand factors on food price increases in 2008. *Biomass and Bioenergy*, *35*(5), 1623-1632.

84. United States Department of Agriculture. U.S. Ethanol: An Examination of Policy, Production, Use, Distribution, and Market Interactions, available from (*https://www.usda.gov/oce/reports/energy/EthanolExamination102015.pdf*); [accessed on 11/24/2018].

85. Solomon, B. D., Barnes, J. R., and Halvorsen, K. E. (2007). Grain and cellulosic ethanol: History, economics, and energy policy. *Biomass and Bioenergy*, *31*(6), 416-425.

86. Soratana, K., Harden, C. L., Zaimes, G. G., Rasutis, D., Antaya, C. L., Khanna, V., and Landis, A. E. (2014). The role of sustainability and life cycle thinking in US biofuels policies. *Energy Policy*, *75*, 316-326.

87. Wang, M., Wu, M., and Huo, H. (2007). Life-cycle energy and greenhouse gas emission impacts of different corn ethanol plant types. *Environmental Research Letters*, *2*(2), 024001.

88. United States Environmental Protection Agency. Overview of Renewable Fuel Standard Program, available from (https://www.epa.gov/renewable-fuel-standard-program/overview-renewable-fuel-standard); [accessed on 10/18/2018].

89. Congressional Research Service. Renewable Fuel Standard (RFS) (2013). Overview and Issues, available from (https://fas.org/sgp/crs/misc/R40155.pdf); [accessed on 11/25/2018].

90. Office of Energy Efficiency and Renewable Energy. POET-DSM Project Liberty (https://www.energy.gov/eere/bioenergy/poet-dsm-project-liberty); [accessed on 11/30/2018].

91. Enerkem Alberta Biofuels, available from (https://enerkem.com/facilities/enerkem-alberta-biofuels/); [accessed on 11/26/2018].

92. Inbicon. Inbicon Biomass Refinery Cellulosic Ethanol Technology Platforms, available from (https://www.eia.gov/biofuels/workshop/pdf/paul_kamp.pdf); [accessed on 11/24/2018].

93. Biomass Magazine. Brazilian president official opens cellulosic ethanol plant, available from (http://biomassmagazine.com/articles/12226/brazilian-president-officially-opens-cellulosic-ethanol-plant); [accessed on 11/20/2018].

94. China Biofuels Annual. Growing Interest for Ethanol Brightens Prospects, available from (https://gain.fas.usda.gov/Recent%20GAIN%20Publications/Biofuels%20Annual_Beijing_China%20-%20Peoples%20Republic%20of_10-20-2017.pdf); [accessed on 11/25/2018].

95. Department of Biotechnology – India. India's first cellulosic alcohol technology demonstration plant inaugurated, available from (http://www.dbtindia.nic.in/india%E2%80%99s-first-cellulosic-alcohol-technology-demonstration-plant-inaugurated/); [accessed on 11/20/2018].

96. Alternative Fuels Data Center. Flexible Fuel Vehicles, available from (https://afdc.energy.gov/vehicles/flexible_fuel.html); [accessed on 10/25/2018].

97. Alternative Fuels Data Center. Ethanol Fueling Station Locations, available from (https://afdc.energy.gov/fuels/ethanol_locations.html#/find/nearest?fuel=E85); [accessed on 11/23/2018].

98. Wakeley, H. L., Griffin, W. M., Hendrickson, C., and Matthews, H. S. (2008). Alternative transportation fuels: Distribution infrastructure for hydrogen and ethanol in Iowa. *Journal of Infrastructure Systems*, *14*(3), 262-271.

99. Congressional Research Service (2007). Ethanol and Biofuels: Agriculture, Infrastructure, and Market Constraints Related to Expanded Production , available from (http://nationalaglawcenter.org/wp-content/uploads/assets/crs/RL33928.pdf); [accessed on 11/25/2018].

100. Graham, R. L., Nelson, R., Sheehan, J., Perlack, R. D., and Wright, L. L. (2007). Current and potential US corn stover supplies. *Agronomy Journal*, *99*(1), 1-11.

101. Somma, Dan, Hope Lobkowicz, and Jonathan P. Deason. "Growing America's fuel: an analysis of corn and cellulosic ethanol feasibility in the United States." *Clean Technologies and Environmental Policy* 12, no. 4 (2010): 373-380.

102. Kang, S., Önal, H., Ouyang, Y., Scheffran, J., and Tursun, Ü. D. (2010). Optimizing the biofuels infrastructure: Transportation networks and biorefinery locations in Illinois. In *Handbook of bioenergy economics and policy* (pp. 151-173). Springer, New York, NY.

103. Iddrisu, I., and Bhattacharyya, S. C. (2015). Ghana′ s bioenergy policy: Is 20% biofuel integration achievable by 2030?. *Renewable and Sustainable Energy Reviews*, *43*, 32-39.

Chapter 5

Locational Analysis of Cellulosic Ethanol Production and Distribution Infrastructure for the Transportation Sector in Ghana

This chapter was published as Singh, R., Kemausuor, F., & Wooldridge, M. (2018). Locational analysis of cellulosic ethanol production and distribution infrastructure for the transportation sector in Ghana. *Renewable and Sustainable Energy Reviews*, *98*, 393-406. (doi: *https://doi-org.proxy.lib.umich.edu/10.1016/j.rser.2018.09.017*)

5.1 Abstract

Owing to the high availability of crop residues in Ghana, ethanol produced from cellulosic feedstock provides an opportunity to achieve energy security without competing with food crops. This study applied methods to identify the best locations in Ghana for biorefineries with 100 ML and 50 ML annual production capacity for cellulosic ethanol by minimizing transportation costs involved in the biomass residue feedstock collection and distribution of the ethanol produced by the biorefinery. The potential for ethanol production in the 10 regions of Ghana from 11 major crop residues was determined. Brong Ahafo and Eastern were identified as the regions with the highest ethanol production potential from single crop residues (with ethanol production potential of >120 ML/yr), and residue from maize crop was identified as the biomass with the highest potential as source material. Two ethanol distribution scenarios were

considered assuming the ethanol would be mixed with gasoline to produce an E10 fuel blend (10% ethanol by volume). In one scenario, all ethanol from the biorefineries was transported to Tema and then distributed using the existing gasoline infrastructure. In the second scenario, ethanol was delivered from the biorefineries directly to the major demand cities. Total transportation costs were used to identify which of nine candidate locations for the biorefineries and which ethanol distribution scenario led to the lowest costs. The results showed the best configuration to meet supply- and demand-side constraints was to use three biorefineries of 50 ML/yr capacity each to supply individual demand locations across the country, and biorefineries located in Koforidua in Eastern and Sunyani in Brong Ahafo led to the lowest transportation costs regardless of distribution scenario. The recommended biorefinery locations showed low sensitivity to important input assumptions, indicating a low risk to the development of biorefineries at Koforidua and Sunyani based on minimizing transportation costs.

5.2 Introduction

In 2016, Ghana was the 10th largest producer of oil in Africa [104]; however, Ghana is almost entirely dependent on imported oil and petroleum products due to the lack of refining capacity currently within the country. Reducing the dependence on foreign imports and transitioning towards energy independence is a high priority for Ghana. Additionally, Ghana is a member of the Paris Agreement of the United Nations Framework Convention on Climate Change (UNFCCC). As per the National Inventory Report submitted by Ghana to the UNFCCC [105], the Ghana energy sector contributed 13.5 million metric tonnes of CO_2-equivalent (MT CO_{2e}) to greenhouse gas emissions which included 6.46 MT CO_{2e} from the transportation sector. The Strategic National Energy Plan developed by Ghana's Energy Commission targets 10% of petroleum fuels to be displaced by renewable biofuels by 2020 [106]. One approach to reducing

the dependence on fuel imports while simultaneously reducing greenhouse gas emissions is to develop the national supply of renewable biofuels produced from crop residues sourced in Ghana.

Many nations around the globe are focusing on ethanol as an alternative fuel to reduce dependence on fossil fuels while also decreasing CO_2 emissions. While displacing 100% of gasoline or diesel demand is challenging for most countries, blends of ethanol and gasoline from 10% ethanol by volume (E10) to 85% ethanol by volume (E85) have been successfully demonstrated at commercial scales in several countries including Brazil, Canada and the U.S. Most of the ethanol currently produced around the world is considered "first generation," i.e. produced from direct food sources such as corn and sugarcane. Second and higher generation biofuels are produced using non-food feedstocks. In Ghana, producing biofuels from first generation feedstocks presents social challenges like land grabbing [107]. Also, the production of biofuels from food feedstocks could lead to food shortages and negative environmental impacts, including soil degradation, biodiversity reduction and eutrophication [108]. According to Wang et al. [109], in a study focused on U.S. ethanol production, ethanol produced from lignocellulosic biomass is more attractive from a long-term sustainability perspective due to significantly lower lifecycle greenhouse gas emissions (compared with grain ethanol) and the potential to address the conflict of food versus fuel. Several studies of Ghana resources indicate significant potential for producing ethanol from food and non-food feedstocks [110], [111], [112], [113].

Commercial scale biorefineries for the production of ethanol from crop residues have been successfully demonstrated in the U.S. and Brazil and plants are planned in several other countries [114]. A disadvantage of cellulosic ethanol production is the higher investment and

operating costs required compared with first-generation bioethanol [115]. Thus, successful development of cellulosic biofuels is critically sensitive to minimizing associated costs, and economic studies show a dramatic sensitivity of the profitability of cellulosic biorefineries to feedstock costs (including transportation costs), which account for 40-60% of plant operating costs) [116]. While previous studies of bioresidue have shown significant potential for biofuel production in Africa in general [1133], [117] and Ghana in particular [110], [111], [112] there are no previous studies to propose specific locations for 2nd generation biorefineries in Ghana. The study by Osei et. al. [110] concluded that Ghana has the capacity to embark on a biofuels program specifically using ethanol production. Osei et. al. [110] identified ethanol production potential from first-generation food crops: cassava, yam and maize, but food crops have significant social and environmental challenges, as discussed above. A recent study by Kemausuor et al. [112] estimated Ghana's production potential for ethanol from lignocellulosic crop residues to be 2300 ML/yr, which is significantly more than the projected requirements to meet the Strategic National Energy Plan goal of 10% displacement of petroleum fuel (estimated at 336 ML [112]). Importantly, crop residues are the lignocellulosic parts of the plants that are inedible. Thus, the use of crop residues to produce ethanol does not compete with food production and instead, provide an additional value stream to the inedible cellulosic materials. The current study expands the work by Kemausuor et al. [112] from identifying the potential of cellulosic ethanol to assessing and recommending crucial infrastructural developments. Such an investigation has not been conducted previously and is vital for informing public- and private-sector development of a biofuel infrastructure in Ghana. In view of this, the objective of this study was to identify optimal locations for cellulosic ethanol production in Ghana based on transportation costs associated with feedstock supply and the distribution of the ethanol product.

The approach leverages the regional data available for agricultural production (feedstock supply) and vehicle use (fuel demand) in Ghana.

5.3 Methodology and Results

The analysis initially considered the supply and demand sides separately to estimate maximum ethanol production potential and gasoline fuel demand; both on regional and district levels. Once the gasoline fuel demand was determined, demand for ethanol was calculated assuming all fuel would be mandated to be a blend of 10% ethanol and 90% gasoline by volume (E10). The E10 blend level was selected for the case study due to the compatibility of E10 with the powertrain technology of most passenger vehicles and with most gasoline distribution infrastructure. After the regional information was determined for ethanol supply and demand, the total transportation costs including crop residue and ethanol transport were minimized to identify optimal biorefinery locations. The analysis used 2012 data, unless noted otherwise.

5.*3.1 Regional potential to produce cellulosic ethanol*

The regional potential of ethanol production from crop residues followed the same procedures used by Kemausuor et al. [112]. The process is briefly reviewed here; additional details are provided in Kemausuor et al. [112]. Ethanol production from lignocellulosic residues is estimated using regional crop production data (denoted as *p* variables) and applying a series of multipliers based on assumed values for yields (denoted as *Y* variables), efficiencies (denoted as η variables) and concentrations (denoted as *c* variables) for the different collection and processing steps. The steps for the lignocellulose conversion to ethanol are grouped as pretreatment, hydrolysis and fermentation with assumed efficiencies and yields. **Figure 5.1** provides a schematic, representing the overall process from crop residue collection to cellulosic

ethanol production and the associated calculations and parameters used. The definitions of the parameters shown in **Figure 5.1** are provided in **Table 5.1**. The values for the parameters in **Figure 5.1** are specific to ethanol production from maize stalks in the Brong Ahafo region, with a known annual maize crop production of 0.57 MT/yr. The overall calculation of the potential cellulosic ethanol production from a specific crop residue is represented by **Eqn. (1)** from Kemausuor et al. [112]:

$$p_{eth} = p_{crop} * Y_{RPR} * Y_{RF} * c_{glu} * Y_{hyd} * Y_{eth} * \eta_{pre} * \eta_{enzy} / \rho_{eth} \quad (1)$$

The amount of crop residue available for ethanol processing includes an estimate of reasonable recovery relative to the theoretical maximum crop residue available from the crop production defined as the recoverability yield (Y_{RF}). As noted in Kemausuor et al. [112], the potential amount of biomass that can be recovered is expected to be lower than the values used here if additional social or economic factors like methods and technologies for feedstock collection, cultural implications of crop residue use, cost of feedstock collection etc. are considered. Consequently, the results of this work represent a reasonable upper bound for ethanol production potential.

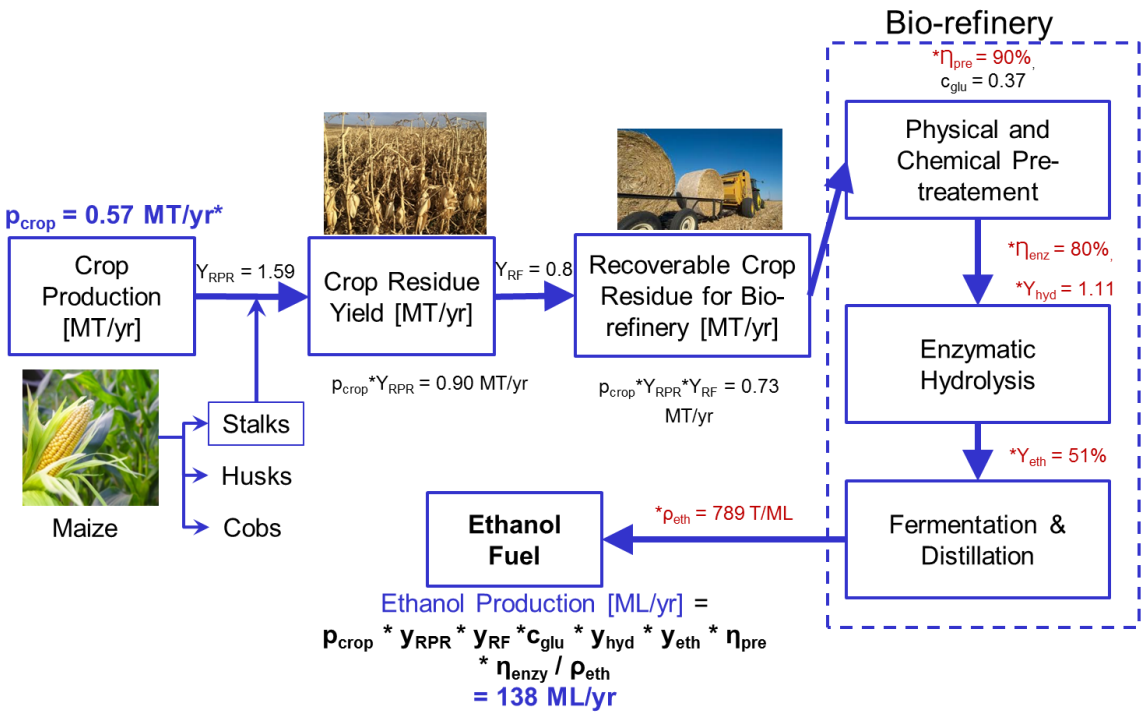

Figure 5.1. Schematic of the method used to estimate the potential of cellulosic ethanol production from a single type of crop residue. Data for maize stalks from the Brong Ahafo region of Ghana are highlighted in this example. The definitions of the variables in the schematic are provided in **Table 5.1**. The values in red are constant for all types of crop residue. The values in black are crop specific. The values in blue are the annual input and output of the calculations.

Table 5.1. Variables presented in **Figure 5.1** and used in **Eqn. (1)** to estimate the potential ethanol production from cellulosic processing of maize stalks for Brong Ahafo region. All fixed parameters were taken from [112].

Variable	Definition	Unit
ρ_{eth}	annual ethanol production	ML
p_{crop}	annual crop production	MT
Y_{RPR}	residue to product ratio	kg/kg
Y_{RF}	recoverability factor	kg/kg
c_{glu}	concentration of glucan (cellulose or starch) in a specific residue	g/100 g total solids
Y_{hyd}	stoichiometric yield from hydrolysis	1.11 g/g
Y_{eth}	stoichiometric yield from fermenting	0.51
η_{pre}	conservation of glucan in pretreatment	90%
η_{enz}	enzymatic conversion efficiency for glucan	80%
ρ_{eth}	ethanol density	789 T/ML

Using the available data for annual regional agricultural production (MT/yr), the annual regional potential to produce cellulosic ethanol (ML/yr) was determined using **Eqn. (1)** for 11 crops. The 11 crops are cassava, cocoyam, cowpea, groundnuts, maize, millet, plantain, rice, sorghum, soybean and yam. The yields from hydrolysis and fermentation and the efficiencies for glucan during pretreatment and for enzymatic pretreatment were fixed at the values presented in **Table 5.1** for all crops considered in the study. **Table 5.2** shows the values of the parameters that were specific to the different types of crops. The only parameter that varied by location was the annual crop production, p_{crop}, where the regional data were obtained from [118] for 2012.

Table 5.2. Crop specific parameters used in **Eqn. (1)** to estimate cellulosic ethanol production. All data were taken from [112].

Food crop	p_{crop} [MT/yr]	crop residue	c_{glu} [g/100 g total solids]	Y_{RPR} [kg/kg]	Y_{RF} [kg/kg]
Cassava	14.5	Stalk	0.33	0.06	0.8
		Peelings	0.56	0.25	0.2
Cocoyam	1.27	Straw	0.25	0.50	0.8
Cowpea	0.23	Shells	0.08	1.75	1.0
Groundnuts	0.47	Shells	0.36	0.37	1.0
		Straw	0.37	2.15	1.0
Maize	1.95	Stalks	0.37	1.59	0.8
		Husks	0.35	0.20	1.0
		Cobs	0.34	0.29	1.0
Millet	0.18	Stalks	0.27	1.83	0.8
Plantain	3.55	Trunks and leaves	0.34	0.50	0.8
Rice	0.50	Straw	0.38	1.66	0.3
		Husk	0.31	0.26	1.0
Sorghum	0.28	Straw	0.42	1.99	0.8
Soybean	0.15	Straw and pods	0.38	3.50	0.8
Yam	6.63	Straw	0.25	0.50	0.8

Ghana, located in the sub-region of West Africa along the Gulf of Guinea and the Atlantic Ocean, consists of ten regions. **Figure 5.2** shows the ethanol production potential on a regional map of Ghana and the corresponding data is provided in **Table 5.3**. The total potential ethanol production including all crop residues is presented, as well as the maximum ethanol potential using a single crop type. The results of **Figure 5.2** show the Brong Ahafo, Northern and Eastern regions have the highest ethanol production potential on total residue, single crop residue and per area bases, with maize (Brong Ahafo and Eastern regions) and groundnuts (Northern region) as the crops with the highest potential. **Figure 5.3** shows the total ethanol potential based on all crop residue available in the country and on a per cropped-area basis. While residue from soybean has a much higher ethanol yield on a cropped-area basis compared with maize and groundnuts, the total ethanol production potential from soybean residue in Ghana is low. On the other hand, both the total potential and the ethanol yield per cropped area are high for maize and historical data points to this trend continuing (see **Figure A3.1** of the **Appendix**).

Table 5.3: Estimates of regional cellulosic ethanol production

Region	Total crop residue (MT/yr)	Ethanol production potential (ML/yr)	Maximum ethanol production using residues from single crop (ML/yr)	Crop with residues having maximum production potential
Ashanti	1.35	238	69.6	Plantain
Brong Ahafo	2.80	468	188	Maize
Central	0.60	118	63.2	Maize
Eastern	1.90	346	133	Maize
Greater Accra	0.03	5.52	2.32	Rice
Northern	2.87	470	110	Groundnuts
Upper East	0.60	106	31.6	Groundnuts
Upper West	1.18	193	69.0	Groundnuts
Volta	0.59	103	28.7	Cassava
Western	0.57	101	37.5	Plantain

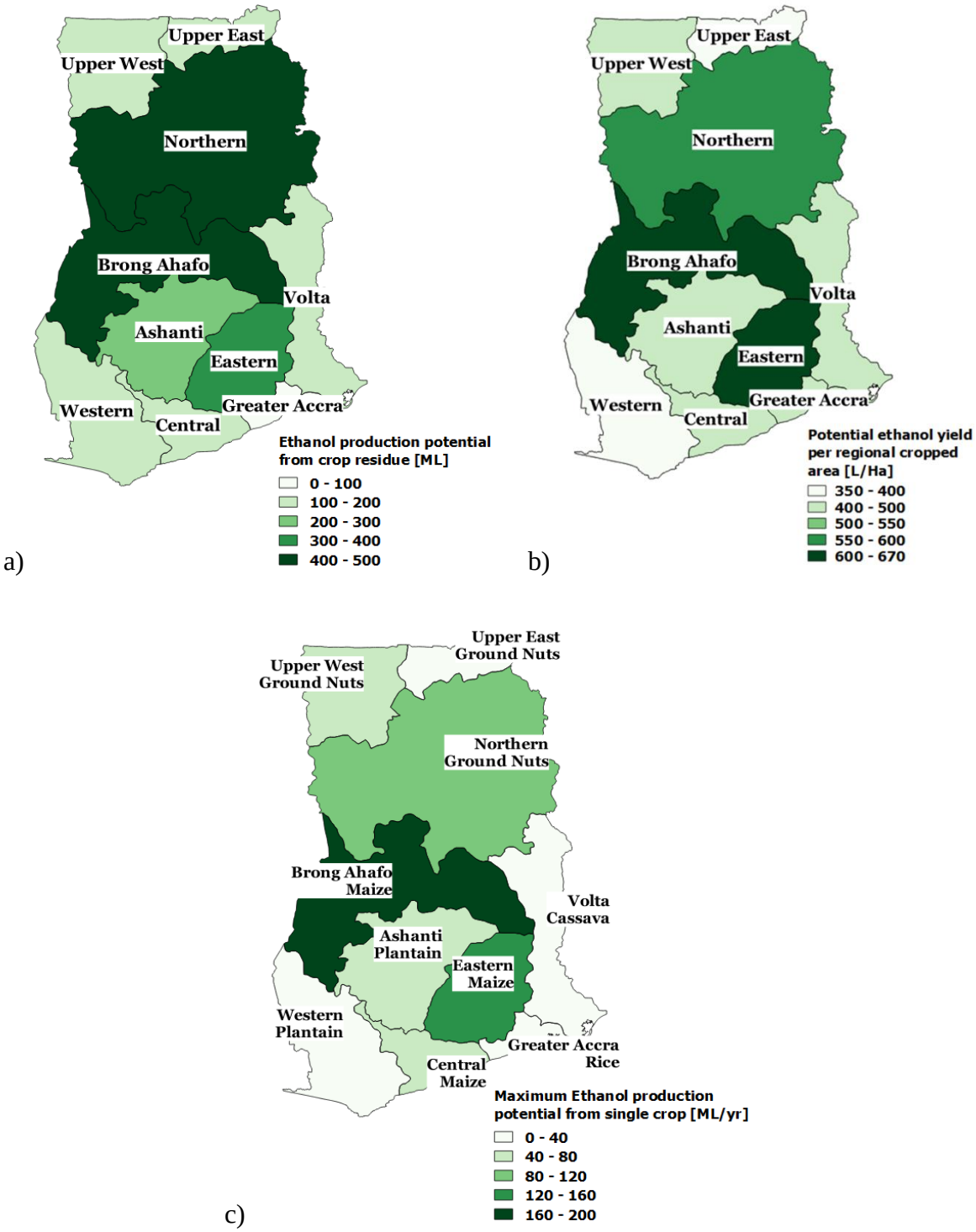

Figure 5.2. Regional ethanol production potential using a) all crop residues, b) all crop residues per cropped area basis, and c) single crop residue with maximum mass.

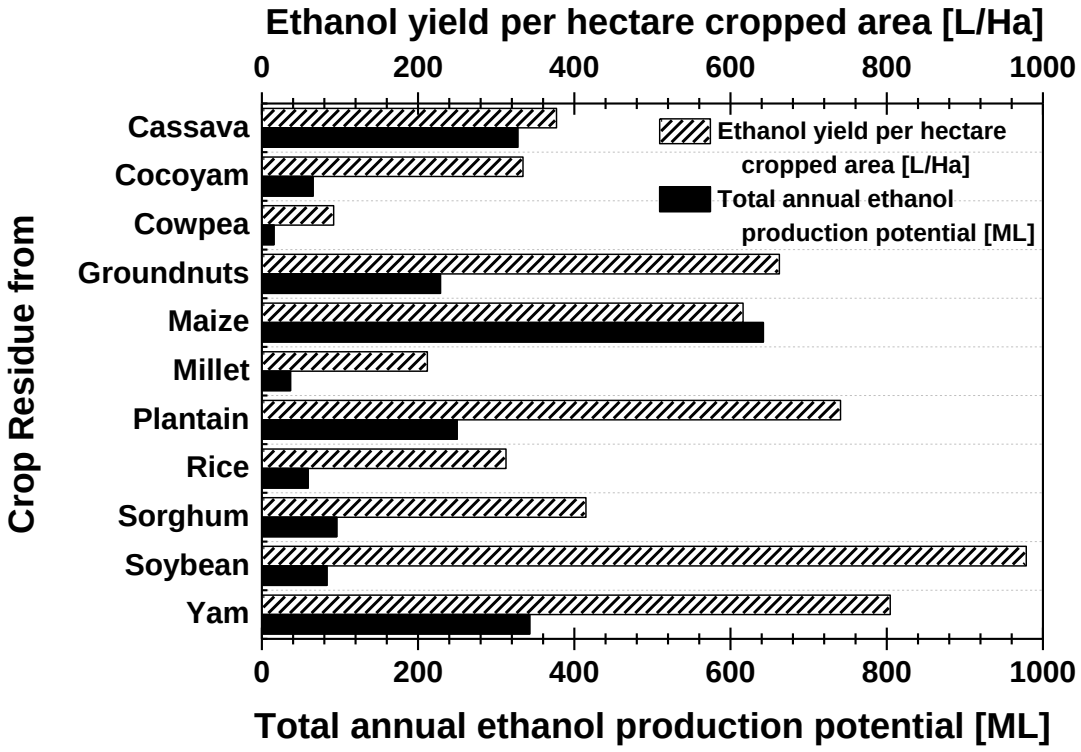

Figure 5.3 Ethanol yield per hectare of cropped area [L/Ha] and total annual ethanol production potential [ML] from the inedible crop residues for selected crops

5.3.2 Projected regional ethanol consumption

To estimate the ethanol volume required to create an E10 blend, the gasoline consumption was determined for the major cities and districts of Ghana with the assumption that local consumption of gasoline was directly proportional to the fraction of vehicles at the location relative to the national total. National gasoline consumption data was obtained from Ghana's national energy statistics [119], which reported the annual gasoline consumption for the year 2012 as 1332.5 ML. The local consumption of gasoline was then determined using the number of vehicles with roadworthy certificates classified by major cities and districts relative to the national total using data from the Ghana Statistical Service [120] (note that the major cities and districts account for ~65% of the national total of registered vehicles). Because the heating value

(or energy density) of E10 fuel is lower compared with gasoline, a larger volume of ethanol is needed to meet the same energy demand as gasoline. Thus, the ethanol volume required to displace gasoline consumed at each location in Ghana with an E10 blend was determined on an energy basis using **Eqn (2)**

$$V_{eth} = 0.10 * Y_{veh}*(\rho_{gas}*e_{gas})/(\rho_{E10}*e_{E10})*V_{gas} \quad (2)$$

where V_{eth} is the volume of ethanol (ML), V_{gas} is the volume of gasoline (ML, national total =1332.5 ML [119]), e_{gas} is the lower heating value of gasoline (44 MJ/kg [121]), ρ_{gas} is the density of gasoline (745 kg/m^3, [122]), ρ_{E10} is the density of E10 (749.4. kg/m^3, calculated using the mass fractions and density values for gasoline [122] and ethanol [123]), e_{E10} is the lower heating value of E10 (42 MJ/kg, calculated using the mass fractions and the heating values of gasoline [122] and ethanol [123121]) and Y_{veh} is the fraction of certified vehicles in the region or district. The total ethanol volume required to meet the national demand for E10 is 138 ML/yr. The results for the locational consumption of gasoline based on vehicle registrations and the required ethanol volume to create E10 are presented in **Figure 5.4.** A total of 23 cities and towns were considered as locations with significant demand for ethanol, and the list includes at least one location in every region of Ghana. The supporting data is provided in **Table A3.2** in the **Appendix 3**. As expected, the two largest cities, Accra and Kumasi, consume the largest volumes of gasoline and require the largest volumes of ethanol. The Greater Accra region has the highest demand for ethanol.

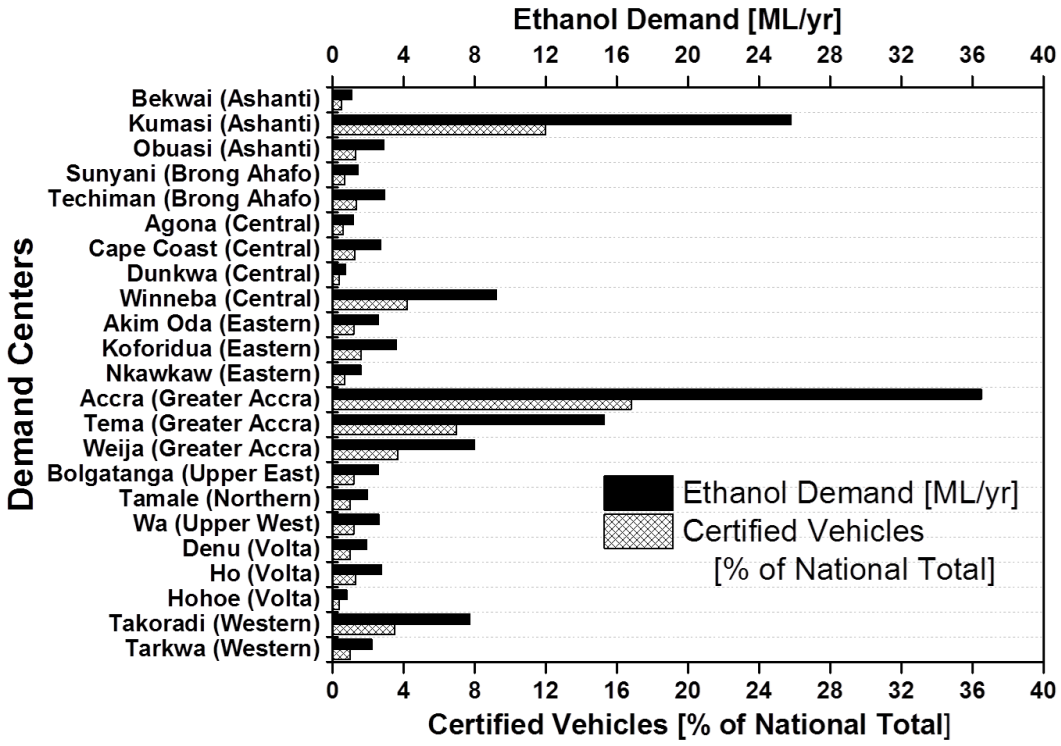

Figure 5.4. Distribution of certified vehicles and estimated ethanol required to meet E10 demand for the major cities and towns in Ghana.

5.3.3 Method to identify candidate biorefinery locations

The location for biorefineries is a strong function of the planned capacity of the plant [124]. Recently constructed commercial-scale facilities and facilities currently under construction have planned capacities in the range of 10-150 ML/yr [114]. Based on this range, and the assumption that economics and efficiencies are better with higher capacities, two capacities of 50 ML/yr and 100 ML/yr were considered in this study. The total ethanol requirement to meet the national demand for E10 fuel is 138 ML/yr. This demand can be met using two biorefineries, one with a 100 ML/yr capacity and another with a capacity of 50 ML/yr, or using three biorefineries of 50 ML/yr capacity each. Studies [109] have shown the ethanol yield from different biomass residues depends upon the methods and conditions employed for

pre-treatment and hydrolysis. Thus, a refinery can be optimized for a single type of crop residue, and although it can still produce ethanol from other residues, the most efficient operation would be for one type of residue. For this reason, only regions where cellulosic ethanol production of more than 50 ML/yr is achievable with a single crop residue were considered in this analysis. The regions and crop combinations which meet the criteria are highlighted in **Table 5.4**. As seen in **Table 5.4**, this selection criterion eliminates the Western, Greater Accra, Volta and Upper East regions as sources of crop residues. Within the remaining six regions, the crops with sufficient residue are maize, cassava, yam, plantain, groundnuts and soybean. Cocoyam, cowpea, millet, rice, and sorghum crops do not produce sufficient residue for further consideration.

The next state of the analysis considered specific locations (e.g. cities or districts) within the regions which could support a biorefinery. A cellulosic ethanol plant requires supporting infrastructure. Koikai et al. [125] identified proximity to farms for feedstock supply, close access to major roads or railway networks, water, power, and proximity to developed areas as some important factors for biorefinery site selection. In this work, two criteria were applied to select specific biorefinery locations within a region. The first was the distance to highway access to ensure transportation availability, and the second was a threshold number of industrial establishments as an indicator of the availability of other infrastructure. Cities and towns with over 600 industrial companies between 2004 and 2015 were considered viable biorefinery locations [126]. Applying these criteria leads to the list of nine candidate locations presented in **Table 5.5** and shown geographically in **Figure 5.5**. Note the large population centers of Tema and Accra do not meet the criteria of producing sufficient crop residue within the region of Greater Accra, so these cities are not candidate locations for the proposed biorefineries.

Table 5.4. Regional ethanol production potential from crop residues from major crops grown in Ghana. Highlighted data are region and crop combinations that meet the threshold criterion of ethanol production potential greater than 50 ML/yr.

SOURCE OF CROP RESIDUE (inedible biomass) ↓	**Cellulosic ethanol production potential (ML/yr)**									
/ REGION→	**Ashanti**	**Brong Ahafo**	**Central**	**Eastern**	**Greater Accra**	**Northern**	**Upper East**	**Upper West**	**Volta**	**Western**
Cassava (stalk, peeling)	50	66	40	94	1.7	31	0	0	29	16
Cocoyam (straw)	18	18	2.5	13	0	0	0	0	2.7	12
Cowpea (shell)	0.2	0.5	0	0.2	0	8.2	1.3	4.9	0.3	0
Groundnuts (shell)	4	6.9	0	6.9	0	110	32	69	0	0
Maize (stalk, husk, cob)	68	190	63	130	1.5	69	22	43	28	27
Millet (stalk)	0	0	0	0	0	16	10	9.7	0	0
Plantain (trunk & leaves)	70	68	11	59	0	0	0	0	5.3	38
Rice (straw, husk)	3.4	0.8	0.4	3	2.3	20	14	0.9	10	3.1
Sorghum (straw)	0	0.3	0	0	0	43	20	30	1.8	0
Soybean (straw, pod)	0	0	0	0	0	66	6.5	8.4	2.3	0
Yam (straw)	25	120	0.9	37	0	110	0	27	24	4.9

Table 5.5: Candidate biorefinery locations based on highway access, available industrial resources and potential to provide a minimum of 50 ML/yr of ethanol (listed alphabetically by region).

City (Region)	Number of industrial companies	Nearest highway*	Source of inedible crop residue	Local ethanol production potential [ML] / crop residue [MT]
Obuasi (Ashanti)	787	22.1 km from N8	Maize Plantain	68 / 0.36 70 / 0.40
Kumasi (Ashanti)	5895	Direct access to N6, N8 & N10	Maize Plantain	68 / 0.36 70 / 0.40
Sunyani (Brong Ahafo)	749	Direct access to N12	Maize Yam Cassava Plantain	190 / 1.00 120 / 0.93 66 / 0.28 67 / 0.38
Techiman (Brong Ahafo)	637	Direct access to N10 & N12	Maize Yam Cassava Plantain	190 / 1.00 120 / 0.93 66 / 0.28 67 / 0.38
Cape Coast (Central)	608	Direct access to N1 & N8	Maize	63 / 0.34
Awutu Breku (Central)	603	Direct access to N1	Maize	63 / 0.34
Koforidua (Eastern Region)	833	Direct access to N4	Maize Cassava Plantain	130 / 0.71 60 / 0.26 59 / 0.33
Tamale (Northern Region)	1351	Direct access to N10 & N9	Groundnuts Yam Maize	110 / 0.57 110 / 0.81 69 / 0.37
Wa (Upper West)	~600	Direct access to N12	Groundnuts	69 / 0.36

*N# is the National Highway designation in Ghana

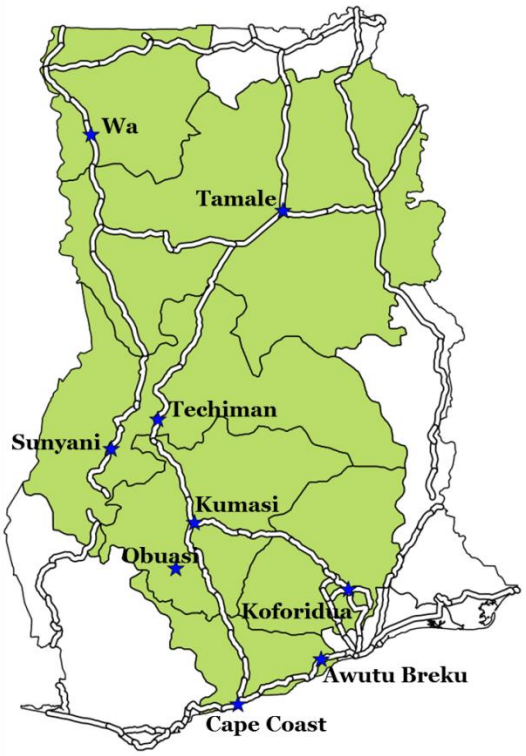

Figure 5.5 Geographic locations for the nine candidate cities for biorefineries within the 6 regions (highlighted in green) which meet the minimum crop residue requirement to produce over 50 ML of ethanol per year, have good access to major highways (shown as double lines), and have access to industry resources.

Once the candidate biorefinery locations were identified, the next step in the analysis was to determine which of the locations could optimally supply the 150 ML/yr required. The selection process can involve various engineering, social, environmental and economic considerations. In this study, only the transportation costs were applied as the selection criterion. The transportation costs represent an important economic factor in the success of the cellulosic biorefineries, and the costs are directly related to the energy costs of transportation and the associated CO_2 emissions. The transportation costs were considered a function of load (mass of crop residue and volume of ethanol) and distance traveled. While transportation costs in Africa may also be a function of the region and the condition of roads [127], [128] such data were not

available for this study and were not considered in the analysis. Instead, a fixed cost based on the local currency of Ghana Cedis per kilometer and per ton of 12 GHC/km-T was used [127].

5.3.4 Residue transportation costs

The transportation costs to bring the crop residues from the collection centers to the candidate biorefinery locations were calculated at the district level for each combination of region and crop residue with ethanol production potential higher than 50 ML/yr (the highlighted data in **Table 5.4** and the highlighted regions in **Figure 5.5**). The biomass residue available and ethanol production potential for each district was estimated using the same approach applied for estimating the regional ethanol production potential. The analysis assumed the crop residue for each district would be available at the district capital and the residue would be transported from the capital to the location of the biorefinery. Further, the analysis assumed each biorefinery received biomass residue only from districts within the same region where the biorefinery was located and not from any districts outside the region. No international transport was considered.

An example of the results of the district level ethanol production potential from maize crop residue is presented in **Figure 5.6** for the Brong Ahafo region. As listed in **Table 5.5**, two candidate biorefinery locations meet the selection criteria of resources for industry support with good highway access in the Brong Ahafo region: Sunyani and Techiman. The location of the cities is highlighted in **Figure 5.6**, in addition to the capitals for each district.

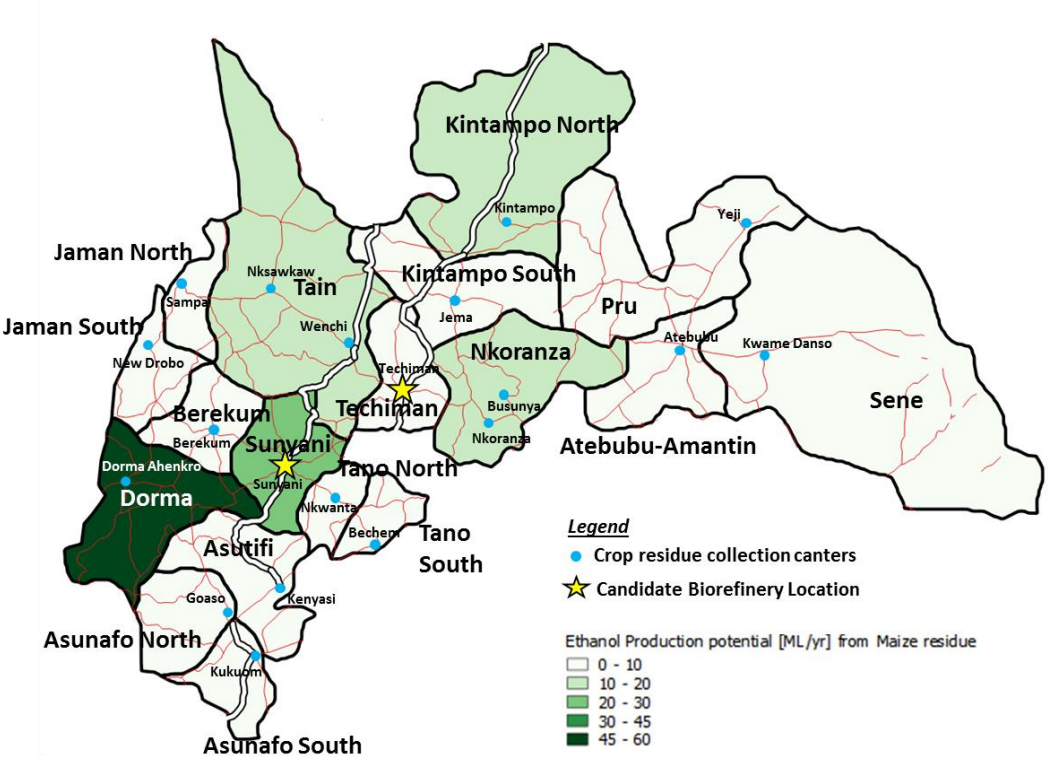

Figure 5.6. District level ethanol production potential from maize residues for the Brong Ahafo region. The district names are in bold. The district capitals are marked with blue dots and the proposed refinery locations are marked with yellow stars. The highways (double black lines) and secondary roads through the region (single red lines) show access to the candidate biorefinery locations.

Table 5.6 lists the distances between the district capitals in the Brong Ahafo region and the candidate biorefinery location in Sunyani. Google Maps was used to find the shortest distances for each pair of locations. The amount of maize crop residue available at the district level and the corresponding ethanol production potential are also provided in **Table 5.6**. The transportation costs were estimated as a product of these data (i.e. the residue mass and the distance traveled), and the fixed transportation cost factor of 12 GHC/km*T. Crop residue is not required from all the districts to meet the target of producing 50 ML/yr or 100 ML/yr of ethanol. There are several criteria that can be applied to select which districts are used for the feedstock residues. Selecting districts by closest proximity to the biorefinery or districts with maximum biomass available are each reasonable criterion. Minimum total transportation costs are found with the first criterion, where the crop residues are transported from the closest districts until the

ethanol capacity is met. For example, for the data shown in **Table 5.6**, the first eight out of the 22 districts listed can supply enough maize residue to produce 104 ML/yr of ethanol with a total transportation cost of 304,000,000 GHC. If the districts with the maximum residue are considered, five districts (Wamfie, Dormaa Ahenkro, Odumase, Busunya and Kintampo) are required to produce 101 ML/yr of ethanol with total transportation cost of 470,000,000 GHC. Thus, using the closest districts represents a 35% savings in transportation costs.

The calculations were repeated for each region, corresponding candidate biorefinery location and type of crop residue to identify the minimum transportation costs to produce a total of 150 ML/yr of ethanol using either two biorefineries (with capacities of 100 ML/yr and 50 ML/yr) or three biorefineries (each with a capacity of 50 ML/yr). When only a portion of the residue from a district was necessary to meet the plant capacity of either 50 ML or 100 ML per year, the transportation costs reflected the lower mass from that location. The results of the analysis are provided in the supply side of the ribbon diagrams which are presented and discussed later in the results section.

Table 5.6. Costs to transport maize residue from each district capital in Brong Ahafo to one of the candidate biorefinery locations for this region, Sunyani. The districts are listed from the closest to the farthest from Sunyani. The last two columns provide cumulative totals for the ethanol production potential and the transportation costs as a function of distance from Sunyani.

District of crop residue	District capital	Distance from bioref. location [km]	Maize residue avlbl. [kT]	Ethanol production potential [ML]	Residue transportation costs [MGHC]	Cumulative ethanol production potential [ML]	Cumulative transportation costs [MGHC]
Sunyani Municipal	Sunyani	1	49	9.0	0.58	9.0	0.58
Sunyani West	Odumase	7.4	75	14	6.65	23	7.23
Tano North	Nkwanta	36	19	3.5	8.09	27	15.3
Berekum	Berekum	38	43	8.0	19.3	35	34.6
Tano South	Bechem	51	20	3.7	11.9	38	46.5

District of crop residue	District capital	Distance from bioref. location [km]	Maize residue avlbl. [kT]	Ethanol production potential [ML]	Residue transportation costs [MGHC]	Cumulative ethanol production potential [ML]	Cumulative transportation costs [MGHC]
Dorma East	Wamfie	61	250	46*	179	84	226
Tain	Wenchi	61	55	10	40.3	94	266
Techiman	Techiman	63	50	9.4**	23.3	100	289
Jaman South	New Drobo	80	21	3.8	19.7	Not required for 100 ML biorefinery	Not required for 100 ML biorefinery
Dorma Municipal	Dorma Ahenkro	82	61	11	59.6		
Asunafo North	Goaso	82	18	3.4	17.8		
Tain	Nsawkaw	90	7.9	1.5	8.55		
Nkoranza South	Nkoranza	91	55	10	60		
Asunafo South	Kukuom	98	16	3.0	18.9		
Kintampo South	Jema	100	38	7.1	46.9		
Nkoranza North	Busunya	110	66	12	86.3		
Jaman North	Sampa	120	9.2	1.7	13.1		
Kintampo North	Kintampo	120	95	18	139		
Asutifi	Kenyasi	130	20	3.8	31.8		
Atebubu - Amantin	Atebubu	200	6.4	1.2	15.7		
Sene	Kwame Danso	240	27	5.1	77.6		
Pru	Yeji	260	9.6	1.8	30.5		

*Only 11.8 ML of the 46 ML potential required to meet 50 ML demand. The total transportation costs scaled for a 50 ML capacity biorefinery are 58 MGHC.

**Only 5.8 ML of the 9.4 ML potential required to meet 100 ML demand. The transportation costs are scaled accordingly.

5.3.5 Ethanol distribution costs

The costs to transport the ethanol produced at the biorefinery to the demand centers considered two distribution scenarios. In the first case, all ethanol produced at the local

biorefineries was supplied to one distribution center located at Tema. Tema was selected for centralized distribution because it is home to the largest port in Ghana which handles shipping and distribution of all gasoline in Ghana [129]. In the second scenario, the local distribution of ethanol within the region of the feedstock source residue was considered.

5.3.5.1 Ethanol supplied for centralized distribution in Tema

For first distribution scenario, all ethanol produced at the regional biorefineries would be transported to Tema and blended with gasoline to create E10 for distribution. This approach leverages the existing gasoline distribution infrastructure. Using the ethanol volume to be produced at the biorefinery locations, the transportation costs to bring the ethanol to Tema were determined. Specifically, a 100 ML ethanol biorefinery would transport ethanol mass of 78,900 T and a 50 ML ethanol biorefinery would transport ethanol mass of 39,450 T. A fixed transportation cost of 12 GHC/km*T [127] was used. **Table 5.7** shows the total transportation costs (i.e. including costs of transporting the crop residues and ethanol) for the different biomass feedstocks and different candidate biorefinery locations. Costs for both 50 ML/yr and 100 ML/yr capacity biorefineries are presented. The ethanol transportation costs scale by a factor of two for 50 ML/yr and 100 ML/yr biorefineries. However, the residue costs do not scale by a factor of two due to the different district sources required for the different capacity biorefineries. The minimum transportation costs for the 100 ML/yr and the 50 ML/yr capacity biorefineries are highlighted in **Table 5.7**. Combining the 100 ML/yr and 50 ML/yr results to represent the target of 150 ML of annual ethanol production yields a minimum transportation cost of 616,000,000 GHC. Combining the three lowest costs using 50 ML/yr biorefineries yields a minimum transportation cost of 586,000,000 GHC, or about a 5% savings. For both scenarios, the best location based on costs is Koforidua in the Eastern region producing cellulosic ethanol from

cassava, maize and plantain residues. A visual representation comparing the transportation costs for a 100 ML capacity biorefinery is presented in **Figure 5.7**. Note, only four of the candidate biorefinery locations have the crop residue required to produce 100 ML of ethanol annually. The cost estimates in **Figure 5.7** show the dramatic transportation savings achieved by locating the 100 ML/yr biorefinery at Koforidua.

Table 5.7. Total transportation costs for the candidate biorefinery locations and a single ethanol distribution center located in Tema. The lowest total costs for one 100 ML/yr biorefinery and three 50 ML/yr biorefineries are highlighted. The results are listed alphabetically by region.

Candidate biorefinery location (region)	Distance from Tema [km]	Crop residue	Biorefinery capacity [ML/yr]	Residue transportation costs [MGHC]	Ethanol transportation costs [MGHC]	Total transportation costs [MGHC]
Kumasi (Ashanti)	274	Maize	50	172	130	302
Obuasi (Ashanti)	261	Maize	50	301	124	424
		Plantain	50	269	124	392
Sunyani (Brong Ahafo)	398	Maize	100	289	377	666
			50	92.5	188	281
		Yam	100	1080	377	1450
			50	341	188	530
		Cassava	50	210	188	399
		Plantain	50	254	188	442
Techiman (Brong Ahafo)	389	Maize	100	308	368	676
			50	102	184	286
		Yam	100	727	368	1090
			50	143	184	327
		Cassava	50	231	184	415
		Plantain	50	325	184	509
Awutu Breku (Central)	66.3	Maize	50	257	31.4	288
Cape Coast (Central)	173	Maize	50	197	81.9	279
Koforidua (Eastern)	82.6	Maize	100	381	78.2	459
			50	129	39.1	168
		Cassava	50	118	39.1	157
		Plantain	50	222	39.1	261
Tamale	653	Groundn	50	157	309	466

Candidate biorefinery location (region)	Distance from Tema [km]	Crop residue	Biorefinery capacity [ML/yr]	Residue transportation costs [MGHC]	Ethanol transportation costs [MGHC]	Total transportation costs [MGHC]
(Northern)		uts	100	591	618	1210
		Yam	50	435	309	744
			100	1230	618	1850
		Maize	50	282	309	591
		Soybean	50	274	309	583
		Plantain	50	158	130	287
Wa (Upper West)	741	Groundnuts	50	138	351	489

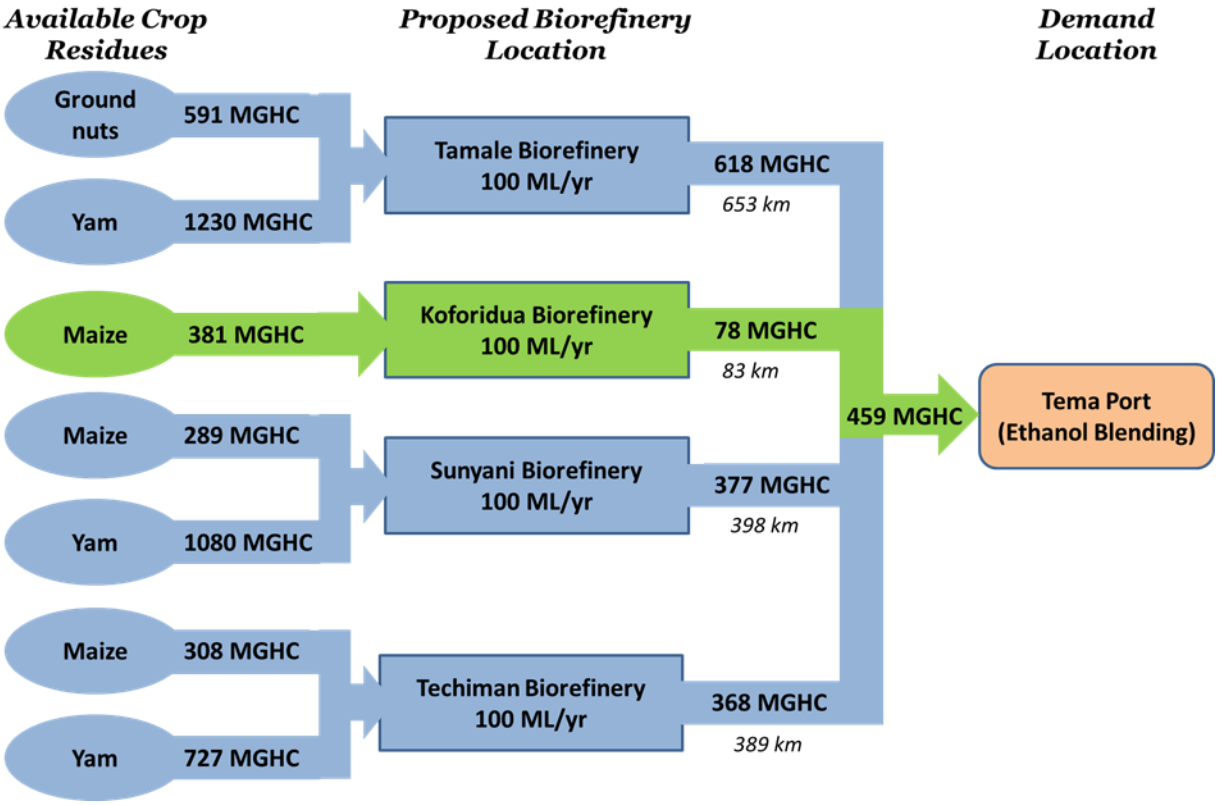

Figure 5.7. Transportation costs for the candidate locations for a 100 ML/yr biorefinery supplying ethanol to Tema.

5.3.5.2 Localized ethanol distribution throughout Ghana

In the second distribution scenario, the ethanol produced at the biorefineries would be transported directly to the demand cities listed in **Figure 5.4**. There are many permutations and combinations of supply and demand locations to consider, particularly when both 100 ML/yr and 50 ML/yr biorefineries are included in the analysis. An example of the process applied here is presented for a 50 ML/yr biorefinery at Sunyani supplying ethanol to Kumasi in Ashanti region. The ethanol demand for Kumasi is 25.8 ML (see **Figure 5.4** or **Table A3.2**). The transportation cost to collect the maize residue to produce 50 ML of ethanol at Sunyani is 92,500,000 GHC (see **Table 5.7**). The total Sunyani feedstock transportation costs are scaled by the ratio of 25.8 ML/50 ML to determine the specific costs for Kumasi which is 47,800,000 GHC for this example. The ethanol transportation cost, $C_{eth,Sunyani\text{-}Kumasi}$, from Sunyani to Kumasi is determined using the same methods described earlier where

$$C_{eth,i\text{-}j} = (12\ GHC/kmT) * \rho_{eth} * V_{eth}\ d_{i\text{-}j} \quad (3)$$

where $d_{i\text{-}j}$ is the distance between the ethanol biorefinery location i and the demand location j, which is 125 km for the Sunyani and Kumasi. For this example, the ethanol transportation cost is 30,600,000 GHC and the total transportation cost for a biorefinery at Sunyani and ethanol demand at Kumasi is 783,000,000 GHC.

This method for determining the total transportation costs for localized distribution of the ethanol from each of the biorefineries was systematically applied to the nine candidate locations for the biorefineries and the 23 regional ethanol demand locations. Furthermore, the two scenarios of (1) two biorefineries with capacities of 100 ML/yr and 50 ML/yr and (2) three biorefineries, each with a capacity of 50 ML/yr, were evaluated. Summaries of the results for the combinations with the lowest total transportation costs are presented in the form of ribbon diagrams in **Figure 5.8** and **5.9**. Some of the supporting data for **Figure 5.8** and **5.9** are provided in **Table A3.3** in the **Appendix 3** for reference. **Figure 5.8** and **5.9** show Koforidua and Sunyani are the biorefinery locations that lead to the lowest transportation costs when the localized distribution of ethanol is considered. Maize is the source feedstock for both biorefineries and cassava is included as a source for Koforidua with maize when three 50 ML/yr biorefineries are proposed. Because the biorefineries are only sourced with residue from the region in this case

study, only districts in Brong Ahafo and the Eastern Region provide crop residue to the biorefineries. If other regions that are close to Koforidua and Sunyani are included in the analysis, it is likely that further costs savings could be realized.

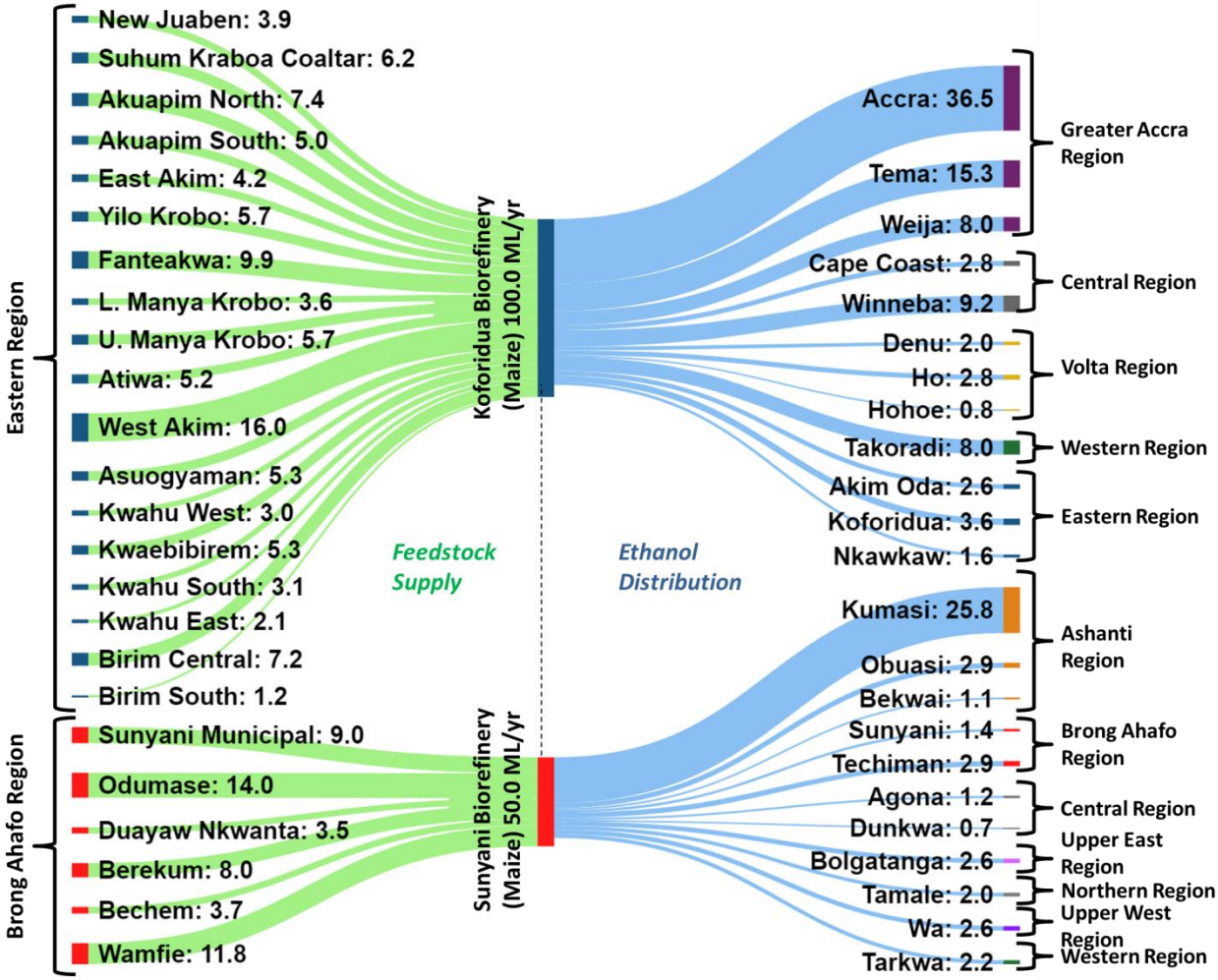

Figure 5.8. Crop residue supply and ethanol demand combinations resulting in minimum transportation costs of 610 MGHC for the scenario of one biorefinery with 100 ML/yr capacity and one with 50 ML/yr capacity. All values are ML/yr. The different colors of the nodes represent different regions.

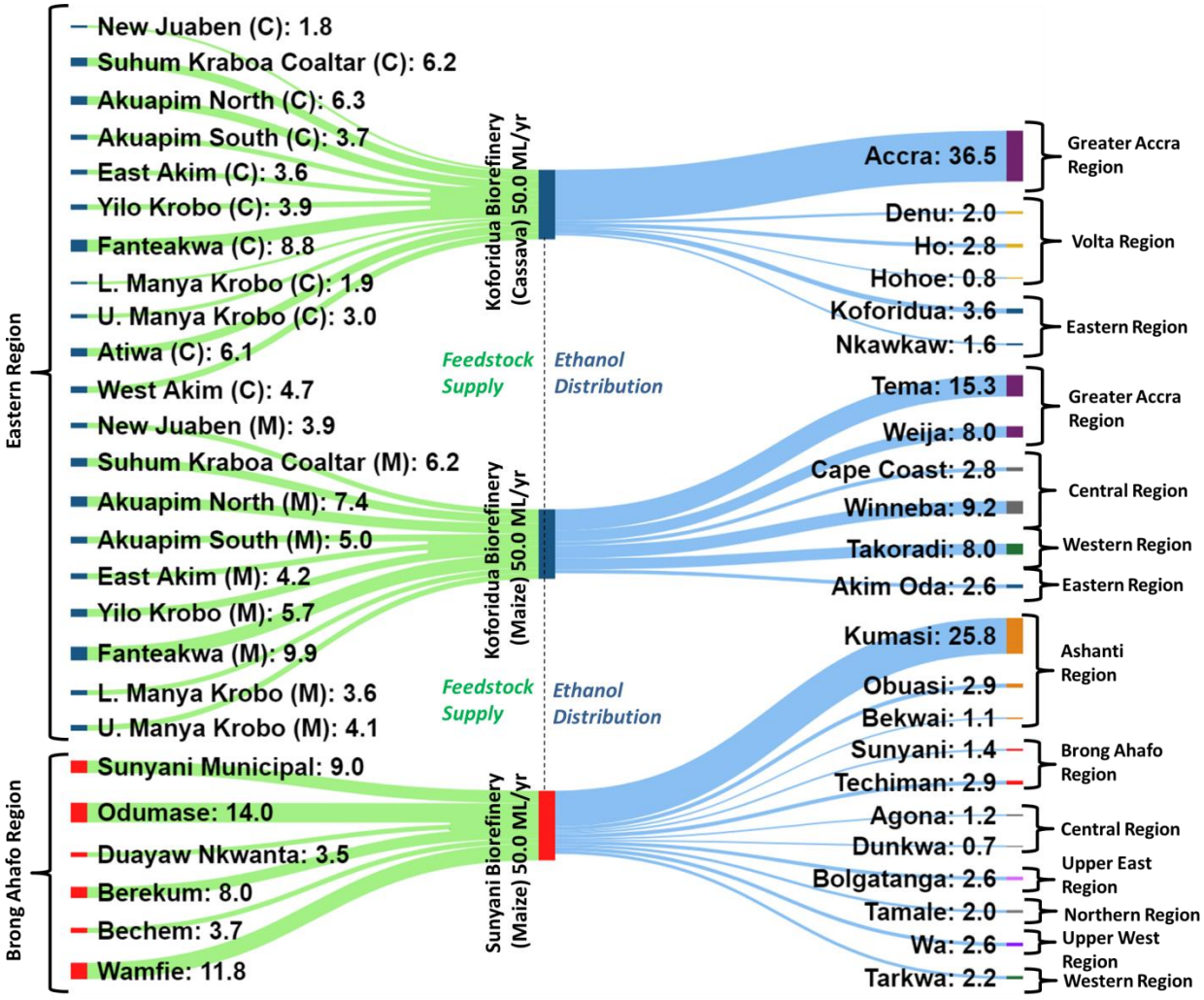

Figure 5.9. Crop residue supply and ethanol demand combinations resulting in minimum transportation costs of 490 MGHC for the scenario of three biorefineries each with 50 ML/yr capacity. All values are ML/yr. The different colors of the nodes represent different regions.

5.3.6 Comparison of results for different scenarios

A summary of the total transportation costs for the two biorefinery production and two distribution scenarios is presented in **Table 5.8**. Using two biorefineries of 100 ML/yr and 50 ML/yr yielded comparable total costs for local distribution and for centralized distribution. The least expensive option was the production of the cellulosic ethanol using three 50 ML/yr biorefineries combined with local distribution. The three smaller refineries had lower total costs

compared with using one 100 ML/yr capacity plant and one 50 ML/yr plant, for both centralized as well as local distribution cases. The results indicate smaller operations with more direct distribution yield significant transportation cost savings. However, it should be noted the analysis presented does not consider any additional costs of creating a local infrastructure for blending, or the costs of modifying the centralized infrastructure for handling ethanol. Capital costs for both would need further consideration, beyond the scope of this work.

Table 5.8. Summary of the results for the different supply and demand scenarios considered.

Scenario	Biorefinery locations (food crop residue, plant capacity)	Demand center locations	Total transportation costs [MGHC]
Production in two biorefineries with centralized distribution	Koforidua (maize, 100 ML/yr); Koforidua (cassava, 50 ML/yr)	Tema	616
Production in two biorefineries with local distribution	Koforidua (maize, 100 ML/yr) Sunyani (maize, 50 ML/yr)	23 cities listed in **Figure 5.4**	610
Production in three biorefineries with centralized distribution	Koforidua (cassava) Koforidua (maize) Koforidua (plantain)	Tema	586
Production in three biorefineries with local distribution	Koforidua (cassava) Koforidua (maize) Sunyani (maize)	23 cities listed in **Figure 5.4**	490

5.4 Sensitivity of results to key assumptions

The sensitivity of biorefinery locations and for transportation costs to key assumptions was evaluated to provide a quantitative understanding of the associated uncertainties. Biorefinery capacity, collection sequence of crop residue, different transportation scaling costs for biomass residue and ethanol, and different blends of ethanol and gasoline were independently investigated.

5.4.1 Biorefinery capacity

The effect of increasing biorefinery capacity on the crop residue collection costs is presented in **Figure 5.10**, for the two important locations of Koforidua and Sunyani. Feedstocks from crop residues of maize, cassava and plantain were considered. The costs to transport the biomass residue increase non-linearly with increasing plant capacity for all crops and for both cities. Plantain costs increase more dramatically than the other crop residues and the maximum plantain mass available to support a Koforidua biorefinery limits the maximum plant capacity to no more than 50 ML/yr of ethanol. While maize residue is notably less expensive to transport to Sunyani, maize and cassava yield almost identical transportation costs for Koforidua up to 80 ML/yr plant capacity. Overall, the results indicate smaller capacity biorefineries are more beneficial in terms of transportation costs. However, the higher capital and operating costs per volume of ethanol produced and lower efficiencies generally associated with smaller facilities must be balanced with the transportation costs to identify the optimum capacity of the biorefinery. Such an analysis is beyond the scope of this work.

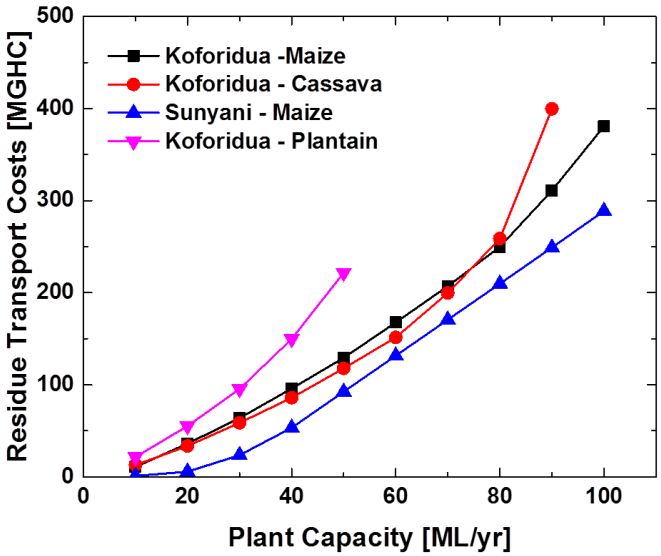

Figure 5.10. Transportation costs as a function of plant capacity for biorefineries at Koforidua and Sunyani.

5.4.2 Crop residue collection sequence

The results presented in **Section 5.2** assumed the biorefinery receives crop residue from the districts closest to the biorefinery first and the farthest location last. Another reasonable approach is to prioritize collecting residue from locations with the maximum ratio of residue available to distance from the biorefinery. Application of this method for collecting crop residue was considered for centralized distribution at Tema with three biorefineries of 50 ML/yr capacity each. The results for the different methods for collecting crop residue are compared in **Table 5.9**. The location of the first two 50 ML/yr biorefineries remains the same using the same crop residue; however, maximizing the ratio of residue to distance shifts the third refinery from Koforidua and plantain to Cape Coast and maize. Although the total transportation costs are significantly higher for the approach based on maximum residue-to-distance, the results also show the insensitivity of the location of the first two 50 ML/yr biorefineries to the sequence used

to collect the bioresidue. In addition, the total transportation costs for the first two biorefineries change by less than 10%.

Table 5.9. Effect of crop residue collection on transportation costs for three 50 ML/yr capacity biorefineries and centralized distribution of ethanol at Tema.

Crop residue collection sequence	Biorefinery location (food crop residue)	Residue transportation costs [MGHC]	Total transportation costs [MGHC]
Closest location to biorefinery first, to farthest location last	Koforidua (cassava) Koforidua (maize) Koforidua (plantain)	157 168 261	586
Locations with maximum ratio of residue available to distance first	Koforidua (cassava) Koforidua (maize) Cape Coast (maize)	160 182 283	625

5.4.3 Unequal transportation costs for ethanol and crop residue

The transportation costs for the previous analysis considered only cargo weight and distance traveled; however, crop residue and ethanol require different shipping and handling methods, and it is likely the transportation costs would differ between these products. As per the International Energy Agency [130], the transportation costs for second generation ethanol is higher than the costs of the input streams which includes the cost of feedstock transport and processing. To explore the effect of different transportation costs for ethanol and crop residue, the scenario of centralized distribution of ethanol from Tema using three 50 ML/yr biorefineries was considered first. The prior analysis based on equal scaling costs for crop residue and ethanol led to all three biorefineries at Koforidua using cassava, maize and plantain (see **Tables 5.7** and **5.8**). The results for Koforidua biorefineries based on cassava and maize residue were unchanged by increasing the costs of transporting ethanol. However, the location of the third biorefinery shifts from Koforidua and plantain to:

1) Awetu Breku using maize, when the ethanol transportation costs are greater than 10 times the residue transportation costs
2) Sunyani using maize, when residue transportation costs are greater than or equal to 1.5 times than the ethanol transportation costs.

When three 50 ML/yr biorefineries with local distribution of ethanol was considered, the locations and feedstocks remained unchanged (see **Table 5.8**) with biorefineries at Koforidua (cassava and maize) and Sunyani (maize), both when the residue transportation costs were greater than the ethanol transportation costs (by any amount), and when the ethanol transportation costs were up to two times the residue transportation costs. As with the residue collection, the results show the consistency of the recommendation for Koforidua for biorefinery operation using cassava and maize.

5.5 Practical Implications of Study

This study considered regional data of Ghana to identify locations for biorefineries for the production of cellulosic ethanol based on minimizing transportation costs for the crop residue and ethanol distribution. A summary of the recommended locations is presented in the regional map of Ghana in **Figure 5.11**. The Brong Ahafo and Eastern regions were identified as the regions with the highest potential for ethanol production based on single crop (maize) residues, and the comparison of the centralized distribution of ethanol with local distribution showed considerable costs savings for localized distribution. The results show the best configuration to meet supply- and demand-side constraints is to use three biorefineries of 50 ML/yr capacity each to supply individual demand locations across the country. Koforidua and Sunyani were identified as the best regional locations for the biorefineries regardless of localized versus

centralized ethanol distribution. Maize residues have the greatest potential for larger capacity biorefineries for both local and centralized ethanol distribution. Smaller capacity biorefineries are feasible with low transportation costs using multiple different feedstocks including maize, cassava and plantain. The results for transportation costs and therefore biorefinery location showed low sensitivity to key assumptions including scaling of transportation costs and methods to collect crop residue for 50 ML/yr biorefineries at Koforidua using cassava and maize crop residues. The results for higher ethanol capacity, i.e. a third biorefinery with 50 ML/yr capacity, showed higher sensitivity to the input assumptions of the analysis. The results indicate a low risk to the development of biorefineries at Koforidua and Sunyani based on minimizing transportation costs.

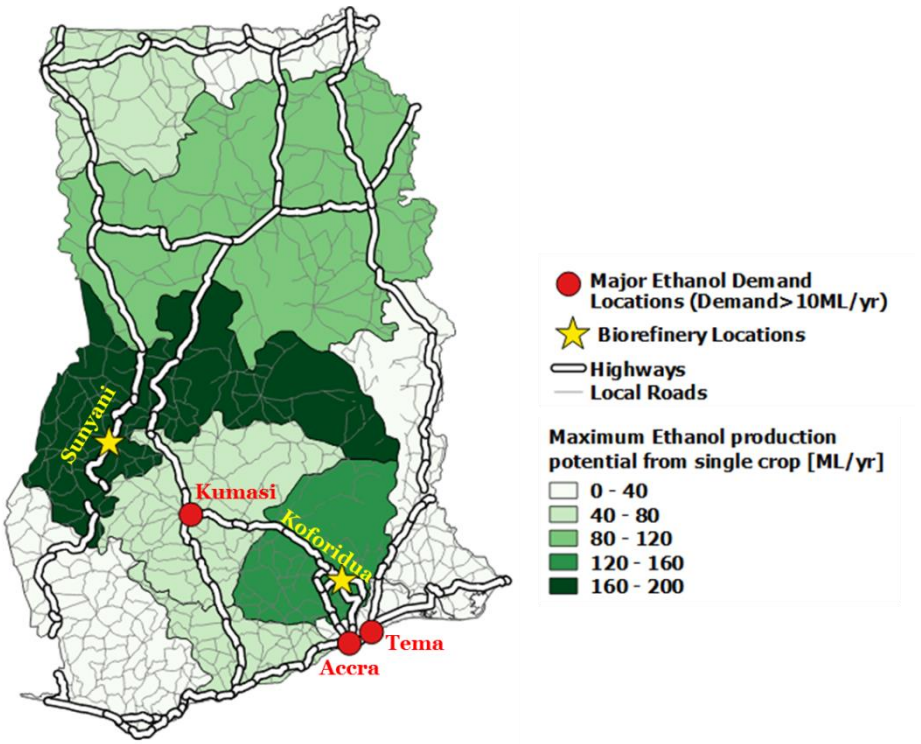

Figure 5.11. Recommended locations for biorefineries based on lowest transportation costs for crop residue feedstock and ethanol supply. See **Figure 5.2** for crop identification for each region.

The results of the study identified a specific geographical network for production and distribution of cellulosic ethanol by minimizing transport costs. Because transportation costs are directly linked to energy costs and CO_2 emissions from transportation, minimizing transportation costs will also reduce CO_2 emissions associated with cellulosic ethanol production. Small-scale or pilot scale projects are an excellent method for validating the findings of this project and other studies to transition Ghana towards a sustainable transportation fuel infrastructure. Such a project can mandate the blending of ethanol with gasoline at one of the major demand locations (say Accra, Tema or Kumasi), or even a particular captive fleet in these locations (e.g. vehicles of government agencies). The robustness of Koforidua (Eastern Region) as a biorefinery location to the different factors and scenarios tested makes Koforidua a favorable and lower risk location to start a pilot biorefinery facility. However, before such a pilot scale project is initiated, future work should consider other aspects of the bioethanol supply chain and additional optimization metrics like net reduction in CO_2 emissions using biomass feedstocks, aspects which are beyond the scope of the work presented here. For example, the analysis which includes using multiple modes of transport, like combinations of rail and truck, should indicate further savings in transportation costs [131]. Needs, methods and costs associated with storage of the crop residue and ethanol should be also considered. Lastly, maize has been identified as the crop with the greatest potential for the 100 ML/yr and 50 ML/yr biorefineries considered in this work and historical data points to this trend continuing (see **Figure A3.1** of the **Appendix 3**). However, trends in agricultural production should be considered as a function of time to understand the potential effects on siting the biorefineries and the source residues.

5.6 Policy Recommendations

The results of this study provide a significant step towards sound policy advocacy for the biofuels program in Ghana. The Ghana government's Strategic National Energy Plan (SNEP) [106] was proposed in Ghana in 2006, but the SNEP targets for renewable fuels have not been met to date. There have been fears that governments in Africa are promoting biofuels and making decisions without adequate policy and institutional frameworks to guide implementation. Several studies [132], [133], [134] point this out as well as ask for pragmatic measures to meet the intended targets. For example, previous studies on policies to promote biofuels [132132], [133], [134] recommend removal of subsidies and incentives on petroleum-derived fuels, providing grants and incentives to boost production of biofuels, and tax and import duty exemption on equipment involved in the collection of crop residues or production of ethanol. Although these policies may promote biofuel supply, the previous studies did not consider that most of the automotive fleet in Ghana is not compatible with ethanol blending at levels higher than 10%. Thus, higher levels of ethanol blending would require additional policies and incentives to expand the compatible fleet of vehicles in Ghana. The analysis provided in this study by itself is not sufficient to set policies on ethanol blend levels and infrastructure development. For example, because the study demonstrated crop residues from maize, cassava, and plantain are essential biomass feedstocks for cellulosic ethanol production in Ghana, policies which affect these crops should be considered both for unintended interactions and intentional consequences. Moreover, additional economic, social, and political indicators should be considered to set informed policy.

5.7 Conclusions

Historically, crop residue has been used for purposes other than as a cellulosic biofuel feedstock, e.g. as a source of fodder for animals or livelihood energy source, and studies have shown crop residues are an important source of soil and water quality. However, in many developing nations, advancements in technology have reduced other demands for crop residue (e.g., replacing livestock with powered equipment). Consequently, biomass is being discarded, burned in the fields, or used with low efficiency [135], [136]. Historical changes in biomass use show "redundant" crop residues (agriculture residues not in productive use for other applications like cattle forage) in rural areas of developing nations can be used to produce biofuels with positive societal and economic effects [137]. Conversion of crop residue into ethanol improves the energy density of the fuel (e.g. the energy density of ethanol is 27 MJ/kg compared with 15-20 MJ/kg for a typical biomass) and facilitates integration with the liquid fuels of the transportation infrastructure. Furthermore, cellulosic plants in developed nations have demonstrated a balance can be achieved between the amount of crop residue left to provide nutrients and benefit the soil and the amount of biomass provided as a fuel feedstock [138]. The results of this study show the feasibility of using crop residue in Ghana to provide a significant amount of biofuel to the nation. Progress in reducing the costs of cellulosic ethanol and alleviating concerns of competing applications for biomass will further improve the benefits of cellulosic ethanol in Ghana. This study provides a foundation for future work which includes an integrated assessment of the social, economic and environmental aspects of cellulosic ethanol for the transportation sector in Ghana.

5.8 Acknowledgements

The authors would like to acknowledge the generous support of the Rackham Global Engagement Program at the University of Michigan. The authors would like to thank Dr. Kathleen Sienko, Professor of Mechanical Engineering at the University of Michigan and Dr. Gabriel Takyi, Director of the Energy Center, Kwame Nkrumah University of Science and Technology for enabling the UM/KNUST visitor program.

5.9 Units

GHC- Ghana Cedis
Ha – Hectare
MGHC – Million Ghana Cedis
ML – Million liters
MT – Million ton
kT – Kilo ton
T – Ton = 1000 kg
ML/yr – Million liters per year

References

104. International Energy Statistics (2017). Total Petroleum and Other Liquids Production, available from: (https://www.eia.gov/beta/international/rankings/#?prodact=53-1andcy=2017); [accessed 06/05/17].

105. Republic of Ghana (2015). National greenhouse gas inventory report: 2014 national carbon accounting: Ghana Government Submission to the United Nations Framework Convention on Climate Change, available from: (https://unfccc.int/files/national_reports/non-annex_i_parties/biennial_update_reports/application/pdf/nir1_to_bur1_ghana.pdf); [accessed 05/02/18].

106. Energy Commission, Ghana (2006). Strategic national energy plan 2006-2020, available from (http://energycom.gov.gh/files/snep/PETROLEUM%20final%20PD.pdf); [accessed 05/22/17].

107. Boamah, F. (2014). How and why chiefs formalise land use in recent times: the politics of land dispossession through biofuels investments in Ghana. *Review of African Political Economy*, *41*(141), 406-423.

108. Soratana, K., Harden, C. L., Zaimes, G. G., Rasutis, D., Antaya, C. L., Khanna, V., and Landis, A. E. (2014). The role of sustainability and life cycle thinking in US biofuels policies. *Energy Policy*, *75*, 316-326.

109. Wang, M., Wu, M., and Huo, H. (2007). Life-cycle energy and greenhouse gas emission impacts of different corn ethanol plant types. *Environmental Research Letters*, *2*(2), 024001.

110. Osei, G., Arthur, R., Afrane, G., and Agyemang, E. O. (2013). Potential feedstocks for bioethanol production as a substitute for gasoline in Ghana. *Renewable Energy*, *55*, 12-17.

111. Kemausuor, F., Nygaard, I., and Mackenzie, G. (2015). Prospects for bioenergy use in Ghana using Long-range Energy Alternatives Planning model. *Energy*, *93*, 672-682.

112. Kemausuor, F., Kamp, A., Thomsen, S. T., Bensah, E. C., and Østergård, H. (2014). Assessment of biomass residue availability and bioenergy yields in Ghana. *Resources, Conservation and Recycling*, *86*, 28-37.

113. Bensah, E. C., Kemausuor, F., Miezah, K., Kádár, Z., and Mensah, M. (2015). African perspective on cellulosic ethanol production. *Renewable and Sustainable Energy Reviews*, *49*, 1-11.

114. Brown, T. R., Brown, R. C., and Estes, V. (2015). Commercial-scale production of lignocellulosic biofuels. *Chemical Engineering Progress*, *111*(3), 62-64.

115. National Renewable Energy Laboratory (2007). A national laboratory market and technology assessment of the 30x30 scenario. National Renewable Energy Lab Technical Report/TP-510-40942, available from: (https://www.nrel.gov/docs/fy07osti/40942.pdf); [accessed 06/12/17].

116. Mupondwa, E., Li, X., and Tabil, L. (2017). Large-scale commercial production of cellulosic ethanol from agricultural residues: A case study of wheat straw in the Canadian Prairies. *Biofuels, Bioproducts and Biorefining*, *11*(6), 955-970.

117. Amigun, B., Musango, J. K., and Stafford, W. (2011). Biofuels and sustainability in Africa. *Renewable and sustainable energy reviews*, *15*(2), 1360-1372.

118. Ministry of Food and Agriculture (MOFA) (2013). Agriculture: Facts and Figures.

119. Energy Commission of Ghana (2016). National Energy Statistics 2006-2015, available from (http://energycom.gov.gh/files/National%20Energy%20Statistics_2016.pdf); [accessed 07/26/17].

120. Ghana statistical service (2015). Statistical Yearbook 2010-2013, available from (http://www.statsghana.gov.gh/docfiles/publications/2013%20STATISTICAL%20YEARBOOK_website.pdf); [accessed 07/26/17].

121. Sonntag, R. E. (1998). Borgnakke C, and Van Wylen GJ. *Fundamentals of Thermodynamics. New York: Wiley*, 88-102.

122. Bell Fuels (2002). Gasoline - Material Safety Datasheet, available from: (https://web.archive.org/web/20020820074636/http:/www.sefsc.noaa.gov/HTMLdocs/Gasoline.htm); [accessed 07/22/17].

123. Pubchem (2004). Ethanol compound summary, available from: (https://pubchem.ncbi.nlm.nih.gov/compound/702#section=Top); [accessed 07/22/17].

124. Kang, S., Önal, H., Ouyang, Y., Scheffran, J., and Tursun, Ü. D. (2010). Optimizing the biofuels infrastructure: Transportation networks and biorefinery locations in Illinois. In *Handbook of bioenergy economics and policy* (pp. 151-173). Springer, New York, NY.

125. Koikai, J. S. (2008). Utilizing GIS-Based Suitability Modeling to Assess the Physical Potential of Bioethanol Processing Plants in Western Kenya.". *Saint Mary's University of Minnesota University Central Services Press, Winona, MN*.

126. Ghana Statistical Service (2016). Regional Spatial Business Report, available from: (http://www.statsghana.gov.gh/docfiles/IBES_Questionnaires/IBES%201%20reports/REGIONAL%20SPATIAL%20BUSINESS%20REPORT.pdf); [accessed 09/25/17].

127. Angmor E. (2012). The role of road transportation service in the development of traditional markets: a case study of Asesewa and Agormanya traditional markets in the Eastern Region. *Ghana. M.Sc. Thesis, Dep. Planning, KNUST*.

128. Taiwo, A., and Kumi, F. (2013). An appraisal of road condition effect on rural transportation in sekyere central district of the ashanti region of Ghana. *Journal of Transportation Technologies*, *3*(04), 266.

129. Ghana Ports and Harbours Authority, Tema Port, available from: (http://ghanaports.gov.gh/page/19/Port-Highlights); [accessed 07/27/17].

130. International Energy Agency (IEA) (2013). Production of alternative transportation fuels: influence of crude oil price and technology maturity, available from (https://webstore.iea.org/production-costs-of-alternative-transportation-fuels); [accessed 02/12/18]

131. Park, Y. S., Szmerekovsky, J., Osmani, A., and Aslaam, N. M. (2017). Integrated Multimodal Transportation Model for a Switchgrass-Based Bioethanol Supply Chain: Case Study in North Dakota. *Transportation Research Record: Journal of the Transportation Research Board*, (2628), 32-41.

132. Antwi, E., Bensah, E. C., Quansah, D. A., Arthur, R., and Ahiekpor, J. (2010). Ghana's biofuels policy: challenges and the way forward. *Int J Energy Environ*, *1*(5), 805-14.

133. Iddrisu, I., and Bhattacharyya, S. C. (2015). Ghana′ s bioenergy policy: Is 20% biofuel integration achievable by 2030?. *Renewable and Sustainable Energy Reviews*, *43*, 32-39.

134. COMPETE (INCO-CT-2006-032448) Second Periodic Activity Report – Annex 6-2-4 Performance Evaluation of National and Regional Biofuels Policies in SSA (2009), available from (https://www.compete-bioafrica.net/policy/Annex6-2-4-COMPETE-032448-2ndReport-PerformanceEvaluation-Final.pdf); [accessed 08/08/18]

135. Kemausuor, F., Bolwig, S., and Miller, S. (2016). Modelling the socio-economic impacts of modern bioenergy in rural communities in Ghana. *Sustainable Energy Technologies and Assessments*, *14*, 9-20.

136. Kemausuor, F., Addo, A., and Darkwah, L. (2015). Technical and socioeconomic potential of biogas from cassava waste in Ghana. *Biotechnology research international*, *2015*.

137. Zheng, Y. H., Li, Z. F., Feng, S. F., Lucas, M., Wu, G. L., Li, Y., and Jiang, G. M. (2010). Biomass energy utilization in rural areas may contribute to alleviating energy crisis and global warming: A case study in a typical agro-village of Shandong, China. *Renewable and Sustainable Energy Reviews*, *14*(9), 3132-3139.

138. Birrell, S. J., Karlen, D. L., and Wirt, A. (2014). Development of sustainable corn stover harvest strategies for cellulosic ethanol production. *BioEnergy Research*, *7*(2), 509-516.

Chapter 6

Conclusions and Recommendations for Future Work

6.1 Conclusions

The current work presents new analysis and results at the device and system scales valuable for enabling ethanol as a renewable transportation fuel. Physical experiments were carried out on two gasoline turbocharged direct injection (GTDI) engine experimental set-ups. The results demonstrated the benefit of using ethanol blends to improve engine thermal efficiency and lower engine-out emissions, with considerable improvements at boosted conditions for both engine architectures. The relative gain in thermal efficiency was found to be a function of the thermo-physical and chemical properties of the fuel blend. These properties also play significant role towards optimizing operating parameters like the fuel injection timing.

The following were the key novel conclusions from the engine studies in this work:

- The favorability of a mid-range ethanol blend (E30) based on performance benefits achievable and engine operational constraints, is a key recommendation from this work. It is known that increasing the ethanol volume fraction in the fuel increases the research octane number (RON) and thus the knock resistance of the fuel. However, this study confirmed that the peak in-cylinder pressure limits arrive prior to knocking onset for fuels with ethanol volume fractions of 30% (E30) and higher. Thus, component protection limited the performance gains achievable with higher ethanol blends.

- A combined application of ethanol blends with a multiple injection strategy can improve engine efficiency while lowering the engine out emissions considerably. For fuel injection strategies that use multiple injections, the engine performance was sensitive to overall injection timing and the distribution of fuel mass in the different injection events.
- Introducing a new parameter, the weighted injection spread (WIS), better characterized the injection strategies when combined with the weighted center of injection timing (WCOI) parameter (a parameter previously introduced in the literature).
- The ethanol blends exhibited similar response and sensitivity to the different injection strategies as gasoline. Thus, indicating engine fuel injection strategies can be readily translated from one fuel to another.
- Use of multiple injections is more effective in improving the engine performance at higher intake pressures and later WCOIs.

The physical experiments established the benefit of use of ethanol to improve the engine thermodynamic efficiency, as well as identified strategies to maximize the improvement achievable. The results from these experiments are useful for guiding the future design of engine architectures and fuel injection strategies the automotive manufacturers, as we move towards stringent emission regulations and higher biofuel blending mandates.

A sustainable biofuels program will require transitioning from gen-I to gen-II ethanol and an optimized infrastructure for the ethanol production and distribution. The system scale study conducted in this work using biomass residue and other data from Ghana, Africa was the first effort of its kind to recommend development of geographic infrastructure for introduction of 2nd generation ethanol in the Ghana transportation sector. The conclusions from the Ghana case-study showed:

- Crop residues collected regionally can be used to produce cellulosic ethanol in sufficient quantity to fuel the passenger vehicle fleet in Ghana with E10 (10% by volume ethanol blended with gasoline).
- Most of the automotive fleet in Ghana is not compatible with ethanol blending at levels higher than 10%. Thus, higher levels of ethanol blending would require additional policies and incentives to expand the compatible fleet of vehicles in Ghana.
- The Brong Ahafo and Eastern regions of Ghana were identified as the regions with the highest potential for ethanol production. Within these regions, Koforidua (Eastern region) and Sunyani (Brong Ahafo region) were identified as the best locations for ethanol production in Ghana, regardless of local versus centralized ethanol distribution. The recommendations of these cities had low sensitivity to the input assumptions used in the analysis.
- Crop residues from maize, cassava, and plantain are essential biomass feedstocks for cellulosic ethanol production in Ghana; with maize residues having greatest potential for larger capacity biorefineries. Thus policies which affect these crops should be considered both for unintended interactions and intentional consequences.
- Smaller capacity biorefineries (50ML/yr) with localized distribution result in the lowest overall transportation costs.

This study is an unprecedented step towards recommendations for cellulosic ethanol infrastructure development in Ghana. The results provide a foundation for future work towards a sustainable biofuels program, which could include an integrated assessment of the social, economic and environmental aspects of cellulosic ethanol for the transportation sector in Ghana.

6.2 Recommendations for Future Work

In this study we introduced an approach that identified favorable locations for bio-ethanol production in Ghana, Africa. The next step to identifying the favorable locations for bio-ethanol production would be conducting a detailed investigation into the process design and economics of cellulosic ethanol production in order to estimate a plant gate price for the fuel. The National Renewable Energy Laboratory (NREL) published a report in 2011 - *'Process Design and Economics for Biochemical Conversion of Lignocellulosic Biomass to Ethanol'* [139], which provides a detailed techno-economic model for estimating production cost for ethanol from corn stover. The report documents detailed material and energy balances and capital and operating costs developed for the entire process of conversion of corn stover to ethanol. The methodology developed in the NREL report serves as a good basis to estimate production cost of ethanol, necessary to assess the fuel competitiveness and market potential. Such analysis can also help make decisions on policies like tax credits/exemptions or biofuel subsidies to promote the use of cellulosic ethanol. Further, including greater modeling fidelity at the different steps involved in the cellulosic ethanol production cycle, e.g. methods and technologies for feedstock collection, cultural implications of crop residue use, the road conditions and regional transport cost variations etc., will reduce uncertainty in the recommendations.

From a vehicle application perspective, all the engine experiments conducted as part of this study have been at steady-state engine conditions where the engine coolant, oil, hardware, etc. is warm (temperatures over 50 ^{o}F). Such conditions are not entirely representative of real-world driving. In a real-world scenario, the engine operates over a range of temperatures and transient driving patterns. Consequently, the trends observed here may not be representative of on-road performance of the vehicle. Testing protocols like those used in federal vehicle

assessments (e.g. the U.S. Federal Test Procedure, US06, or the New European Driving Cycle) have been developed to capture transient driving patterns and certify exhaust emissions of vehicles. However in 2011, the research body of the European Commission, the Joint Research Centre (JRC), published a report highlighting the large and growing discrepancies between laboratory and on-road emissions [140]. The discrepancies emphasize the need to expand the benefits demonstrated at the laboratory scale to benefits achievable in real driving scenarios.

Also, the future powertrain is advancing towards hybridization of the vehicle technology from conventional internal combustion engine vehicles to hybrid electric vehicles (HEVs), with electric batteries coupled to the engine. These future powertrains may employ an engine technology other than conventional GDI [141] and may require different engine operating strategy than conventional for optimal performance [142]. Thus, it is of interest to identify the benefits and challenges cellulosic ethanol fuel will present for these advanced hybrid powertrains.

Apart from ethanol derived from cellulosic feedstock being recognized as a potent candidate for transportation fuel, with less environmental and social impact, there are other alternative fuels under development for use in alternative fuel vehicles and advanced technology vehicles. These fuels include biodiesel, hydrogen, natural gas (as compressed natural gas), propane (as liquefied petroleum gas), dimethyl ether (DME), etc. These fuels have potential to increase energy security, reduce emissions, improve vehicle performance, and stimulate the U.S. economy. However, to achieve market penetration for any of the next generation fuels under consideration, as with ethanol, information and policies are needed to overcome perceived and actual risks of first application. Detailed analysis at the local level is desired from production to fuel use. Policies, like the U.S. RFS program for biofuels, which specify acceptable pathways for

fuel production to ensure reduction in greenhouse gas emissions can be key enablers to decarbonizing the transportation sector.

An essential tool available for policy makers to assess the impact of a new biofuel or bioenergy pathway under consideration is the Global Bioenergy Partnership (GBEP) report of 2011 [143]. The report identified twenty-four sustainability indicators under the themes of environmental, economic and social impact assessments. The GBEP recognized the development and deployment of modern bioenergy should be based on a set of sustainability indicators, which integrate economic, social and environmental considerations, and can be applied by individual countries or communities to make informed decision-making. The degree of relevance of each of the twenty-four indicators might differ locally, and this is likely to be reflected in the choice of indicators that the countries or organizations use to inform their own analysis.

A key step to successful integration of any next generation fuel into the transportation infrastructure is engagement of public stakeholders, who are a critical consideration for the policy makers and an influential component of the policy-making process. This can be achieved by creating the necessary public awareness and understanding of how a consumer can play a role in this transition of infrastructure from fossil-based fuels to more efficient and non-fossil alternative fuels.

References

139. Humbird, D., Davis, R., Tao, L., Kinchin, C., Hsu, D., Aden, A., & and Sexton, D. (2011). Process design and economics for biochemical conversion of lignocellulosic biomass to ethanol: dilute-acid pretreatment and enzymatic hydrolysis of corn stover (No. NREL/TP-5100-47764). National Renewable Energy Lab (NREL), Golden, CO (United States).

140. International Council on Clean Transportation (2017). Real-Driving emissions test procedure for exhaust gas pollutant emissions of cars and light commercial vehicles in europe, available from (https://www.theicct.org/sites/default/files/publications/EU-RDE_policy-update_18012017_vF.pdf); [accessed 11/10/2018].

141. Triantopoulos, V. (2018). Experimental and Computational Investigation of Spark Assisted Compression Ignition Combustion Under Boosted, Ultra EGR-Dilute Conditions.

142. Burke, A. (1993). On-Off Engine Operation for Hybrid/Electric Vehicles. *SAE Technical Paper No. 930042*.

143. The global bioenergy partnership sustainability indicators for bioenergy (2011), available from (http://www.globalbioenergy.org/fileadmin/user_upload/gbep/docs/Indicators/The_GBEP_Sustainability_Indicators_for_Bioenergy_FINAL.pdf); [accessed 08/08/2018].

APPENDICES

Appendix 1: Supplemental material for single-cylinder engine study

Figure A1.1 shows the CA90 (crank angle position where 90% of the total heat is released) for all the ethanol blends. E100 exhibited systematically faster burn rates compared with the other fuels.

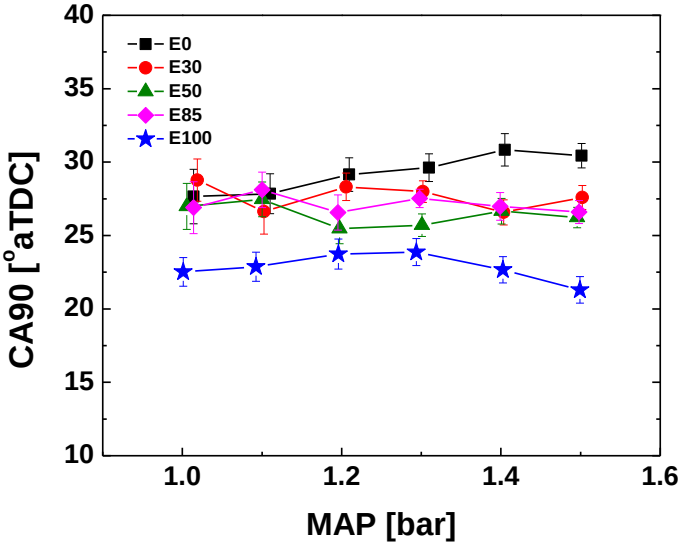

Figure A1.1: CA90 phasing corresponding to the data presented in **Figure 6.**

Figure A1.2 compares the 10-90% burn durations of the fuels. The burn durations were determined from the total heat release and do not account for unburnt fuel mass. Although the values of CA10, CA50 and CA90 are all later for E0 compared with E100, the 10-90% burn duration is shorter for E0 than for E100 at the higher MAP conditions.

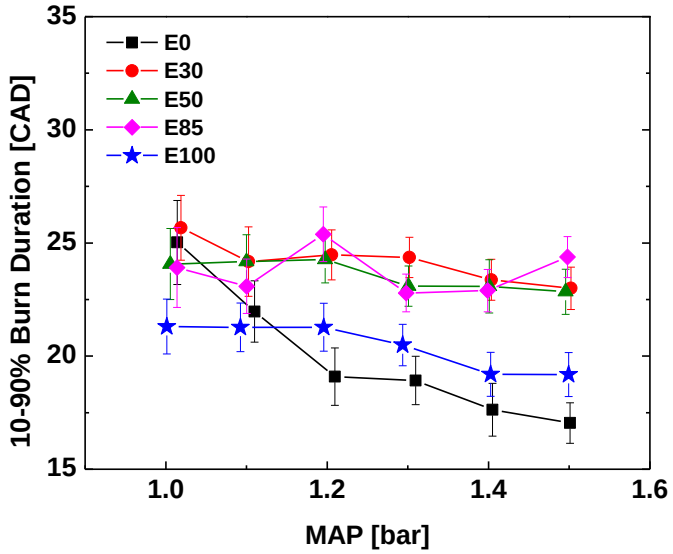

Figure A1.2: 10-90% burn duration results corresponding to the data presented in **Figure 6.**

Figures A1.3 to A1.8 present in-cylinder pressure data for each of the MAP conditions studied. Each pressure trace shown corresponds to an actual engine cycle for which the cycle GIMEP was closest to the average GIMEP at the tested condition. The data correspond to the results presented in **Figure 6**.

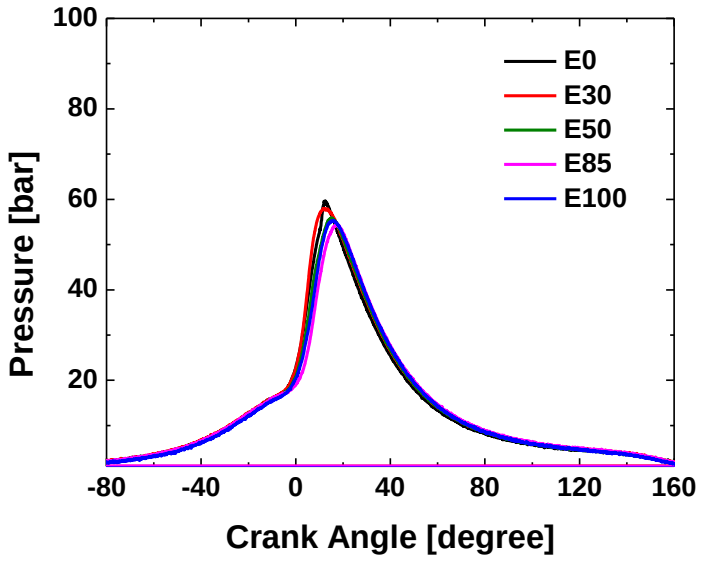

Figure A1.3: In-cylinder pressure data corresponding to MAP = 1 bar.

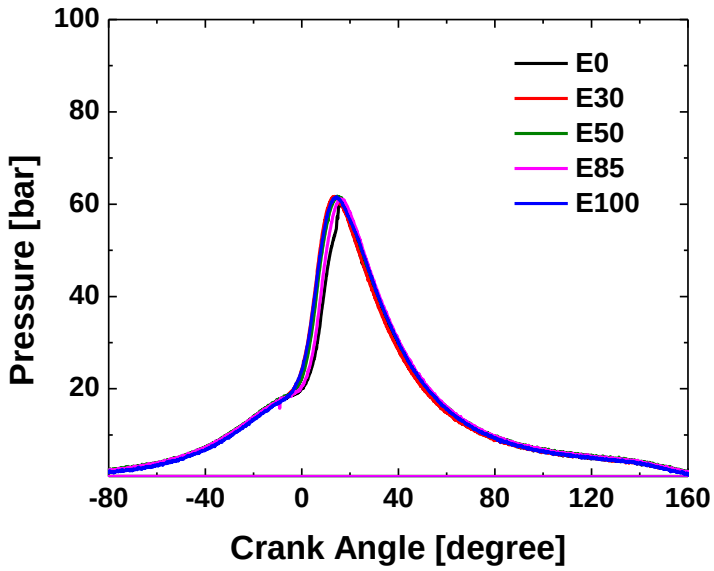

Figure A1.4: In-cylinder pressure data corresponding to MAP = 1.1 bar.

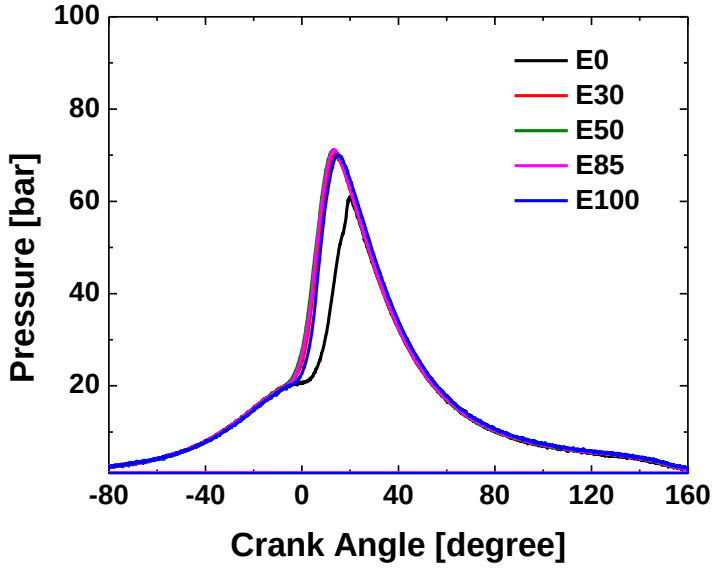

Figure A1.5: In-cylinder pressure data corresponding to MAP = 1.2 bar.

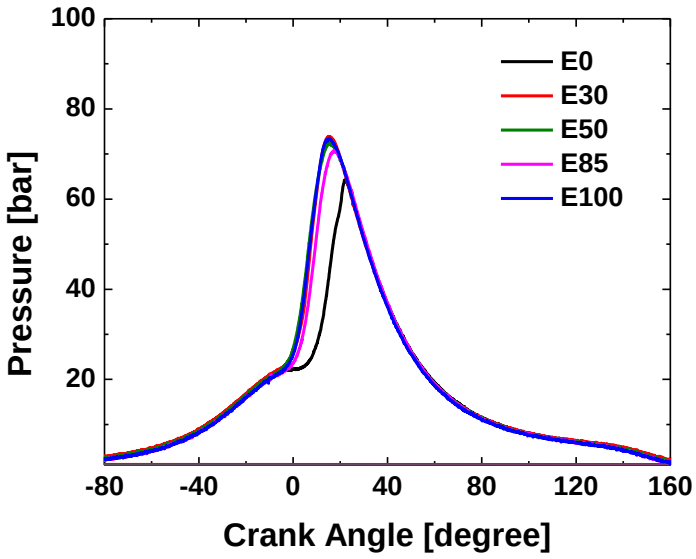

Figure A1.6: In-cylinder pressure data corresponding to MAP =1.3 bar.

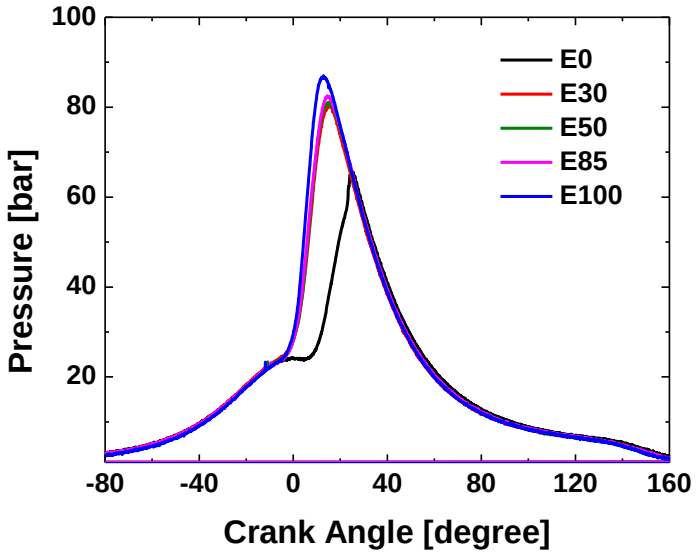

Figure A1.7: In-cylinder pressure data corresponding to MAP = 1.4 bar.

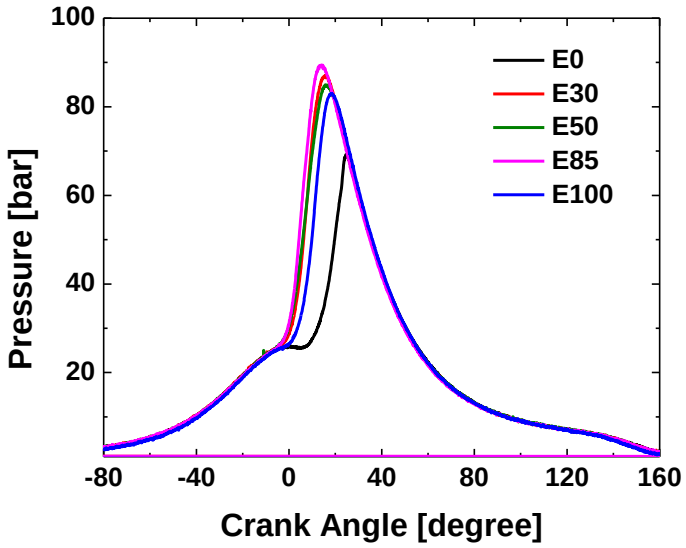

Figure A1.8: In-cylinder pressure data corresponding to MAP = 1.5 bar.

Figures A1.9 to A1.14 present the results for Heat Release Rate (HRR) corresponding to the engine cycle data presented in **Figures A1.3 – A1.8**.

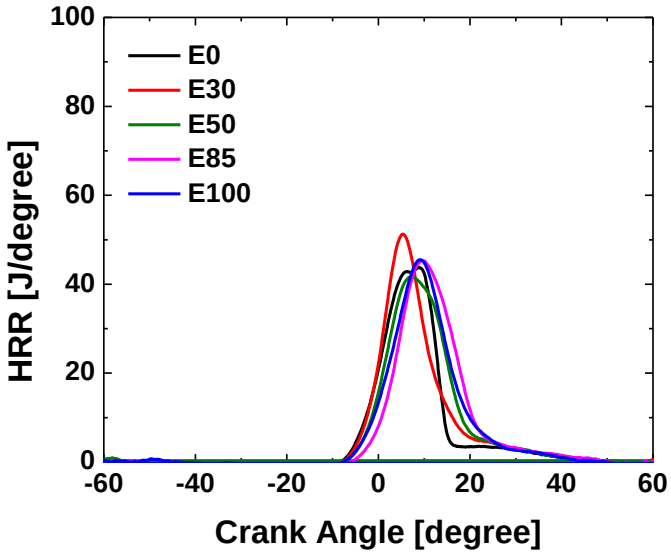

Figure A1.9: Heat release rate for MAP = 1 bar corresponding to the in-cylinder pressure data presented in **Figure A1.3**.

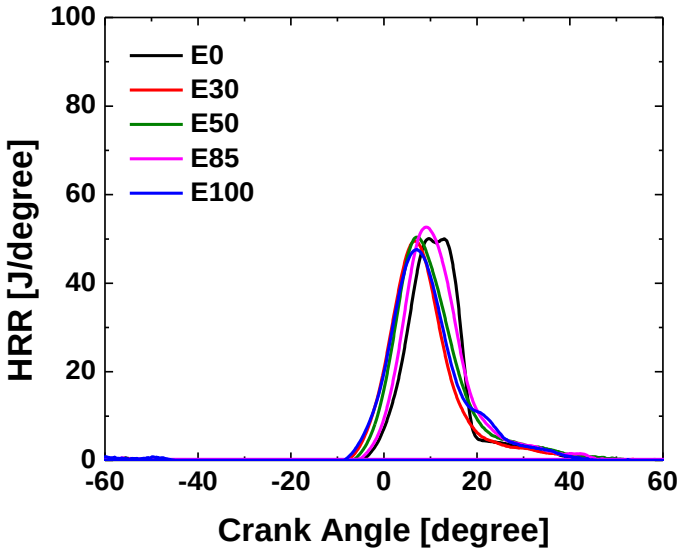

Figure A1.10: Heat release rate for MAP = 1.1 bar corresponding to the in-cylinder pressure data presented in **Figure A1.4**.

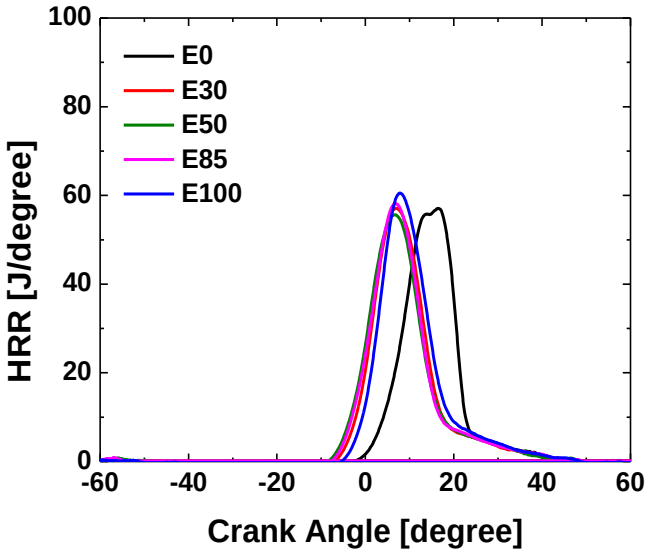

Figure A1.11: Heat release rate for MAP = 1.2 bar corresponding to the in-cylinder pressure data presented in **Figure A1.5**.

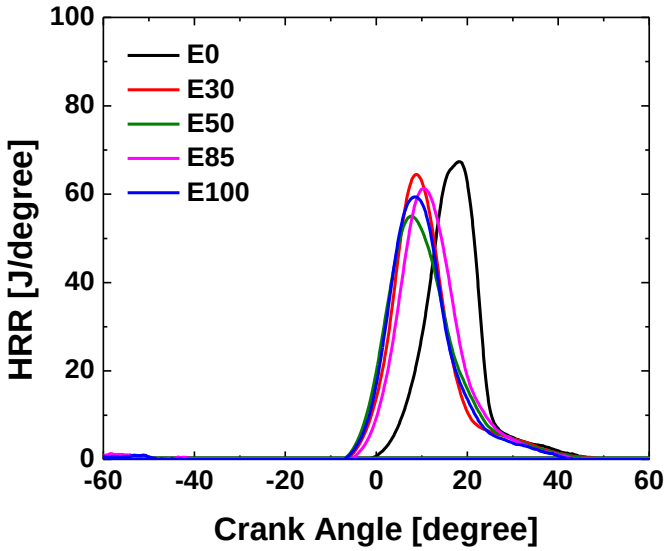

Figure A1.12: Heat release rate for MAP = 1.3 bar corresponding to the in-cylinder pressure data presented in **Figure A1.6**.

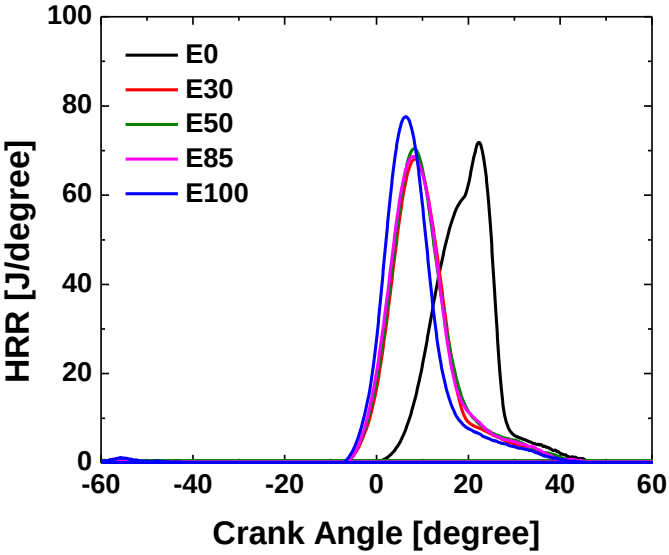

Figure A1.13: Heat release rate for MAP = 1.4 bar corresponding to the in-cylinder pressure data presented in **Figure A1.7**.

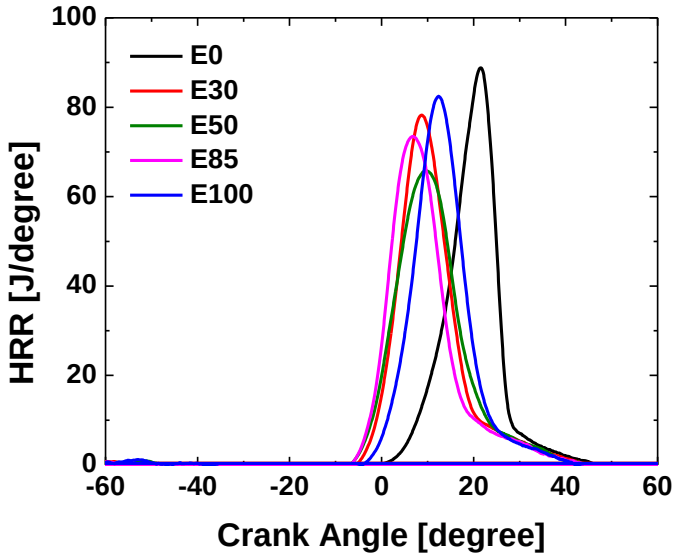

Figure A1.14: Heat release rate for MAP = 1.5 bar corresponding to the in-cylinder pressure data presented in **Figure A1.8**.

Methodology for determining error bars

The measurements made while running experiments could have uncertainties due to the:

1) Measurement apparatus used
2) Experimental variations (cycle-to-cycle variations or day-to-day variation)

For the steady state experiments performed in this study the measurements which are of interest and govern majority of the analysis are as follows:

Measured Parameter	Uncertainty	
	Measurement Apparatus	Experimental Variation
In-cylinder pressure	±0.5% (Kistler 6052C)	±4%
Fuel flow rate	±0.2% (Max Machinery P213-611-000 piston flow meter)	±2%

As the uncertainty due to experimental variation is 10 times that from the measurement apparatus, one standard deviation of the recorded combustion cycles is chosen as the measurement of uncertainty in this work (presented as error bars). This is a standard practice in experimental community when the measured data points follow a normal distribution, as is the case with our measurements. The **Figure A1.15** presents the histogram for peak in-cylinder pressure with a normal

distribution fit (normality = 82%). This implies the error bars (or one standard deviation) present values falling within 68% of the mean.

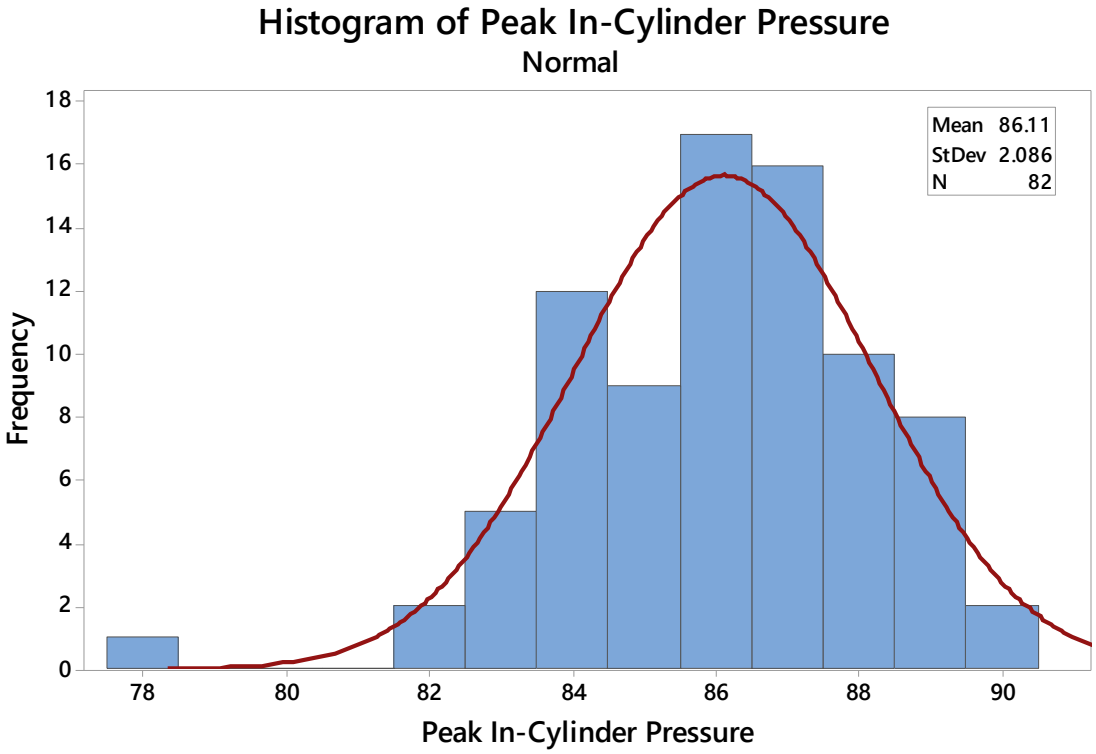

Figure A1.15: Frequency distribution (with normal fit) of peak in-cylinder pressure for 82 cycles recorded at MAP = 1.5 for E100 fuel

Appendix 2: Supplemental material for multi-cylinder engine study

Table A2.1. Fuel properties based on supplier specifications, unless stated otherwise.

Property	**Units**	**Reference grade gasoline (E0)**	**Anhydrous ethanol (E100)**
Reid Vapor Pressure	kPa	61.5*	15.85[a]
Lower Heating Value (gravimetric fuel basis)	MJ/ kg-fuel	43.6*	26.9[b]
Lower Heating Value (gravimetric stoichiometric fuel and air mixture basis)	MJ/ kg-stoich mixture	2.8	3.0
Stoichiometric Air/Fuel Ratio	Mass basis	14.6	9.0
Hydrogen/Carbon Ratio	Mole basis	1.9*	3.0
Oxygen	Mass fraction [%]	None	0.5
Research Octane Number	-	91.5*	~108[c]
Motoring Octane Number	-	83.4*	~91[c]
Octane Sensitivity (S)		8.1*	17
Heat of Vaporization (gravimetric fuel basis)	kJ/ kg-fuel	373[b]	840[b]
Heat of Vaporization (gravimetric fuel and air mixture basis)	kJ/ kg-stoich mixture	25.5	93.3
Initial Boiling Point	°C	32.1*	78[d]

*Gage Products (http://www.gageproducts.com)
[a]http://cta.ornl.gov/cta/
[b]SAE paper 2012-01-0403
[c]SAE paper 2012-01-1274
[d]https://pubchem.ncbi.nlm.nih.gov/

Multiple Fuel Injection Events- Equal Fuel Mass

Figures A2.1 – A2.6 compare the effects of multiple injection events with the single injection baseline data for E30 and E85 at a MAP of 1000 mbar.

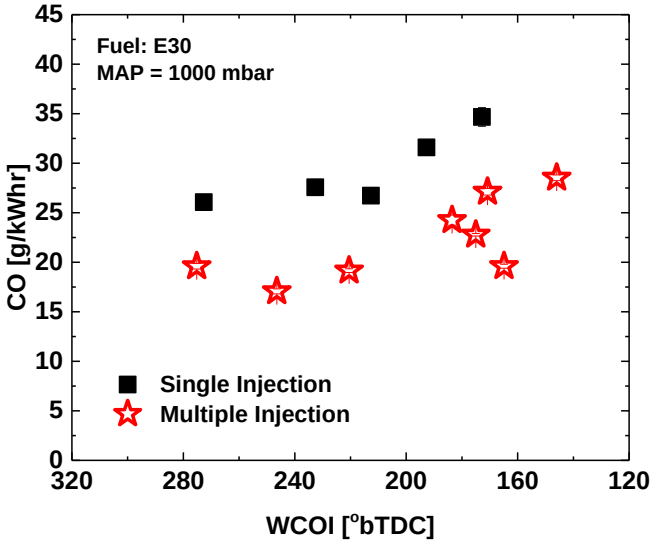

Figure A2.1. Comparison of CO emissions for single and multiple fuel injection events for E30 fuel and MAP = 1000 mbar.

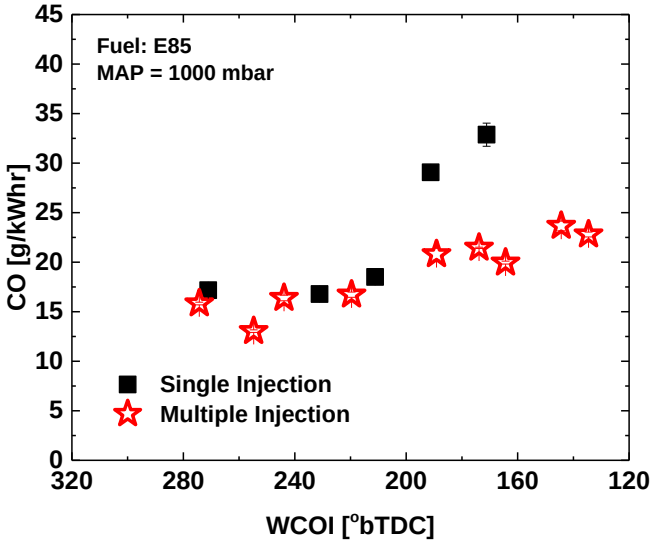

Figure A2.2. Comparison of CO emissions for single and multiple fuel injection events for E85 fuel and MAP = 1000 mbar.

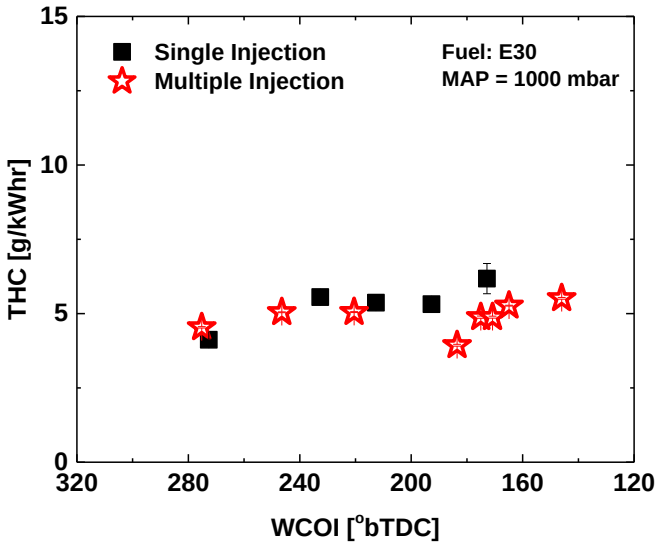

Figure A2.3. Comparison of THC emissions for single and multiple fuel injection events for E30 fuel and MAP = 1000 mbar.

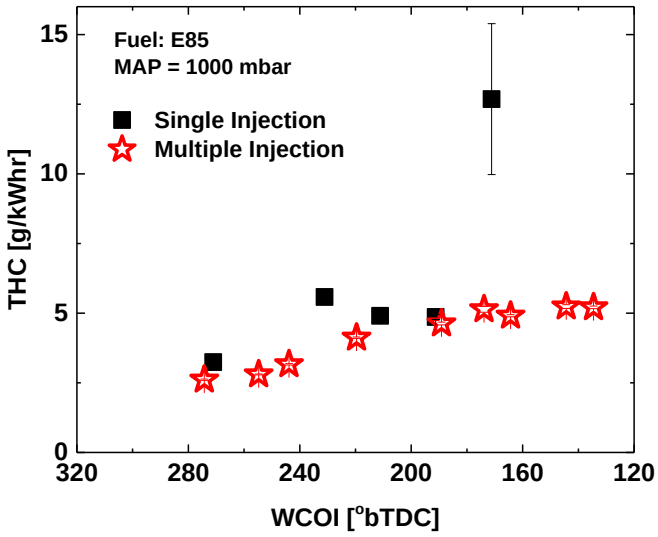

Figure A2.4. Comparison of THC emissions for single and multiple fuel injection events for E85 fuel and MAP = 1000 mbar.

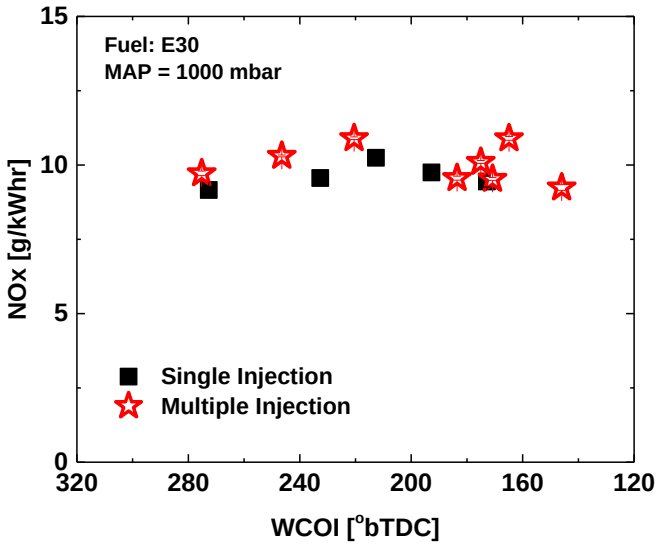

Figure A2.5. Comparison of NOx emissions for single and multiple fuel injection events for E30 fuel and MAP = 1000 mbar.

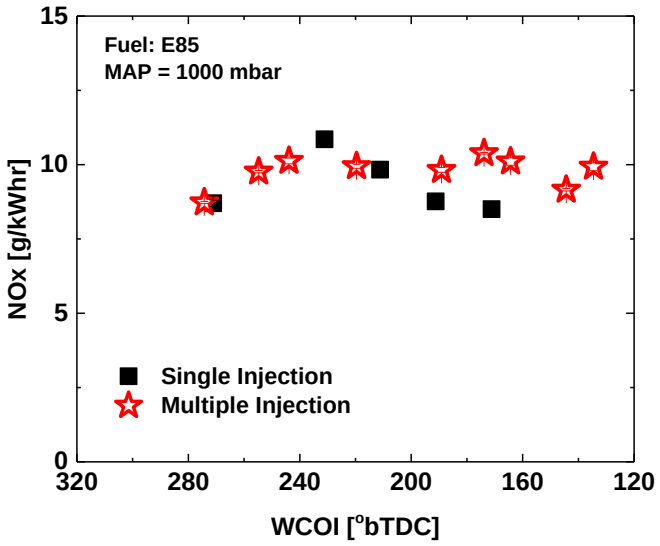

Figure A2.6. Comparison of NOx emissions for single and multiple fuel injection events for E85 fuel and MAP = 1000 mbar.

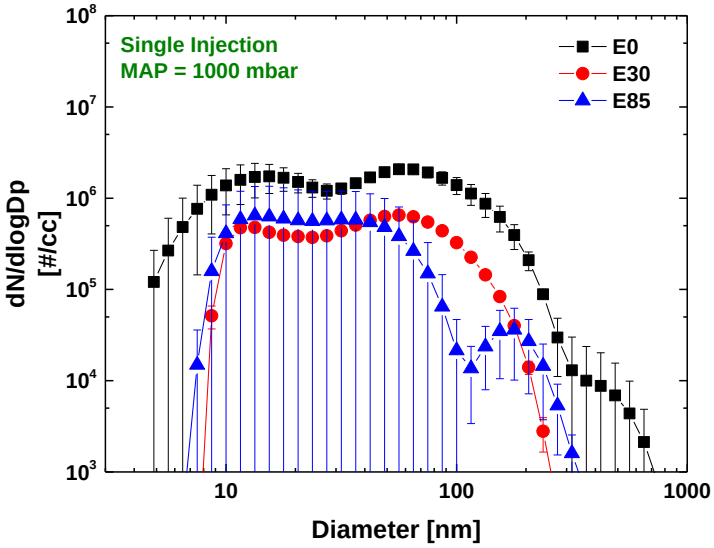

Figure A2.7. Comparison of PN size distributions for E0, E30 and E85 at MAP = 1000 mbar using the single injection strategy shown in **Figure 3.19.**

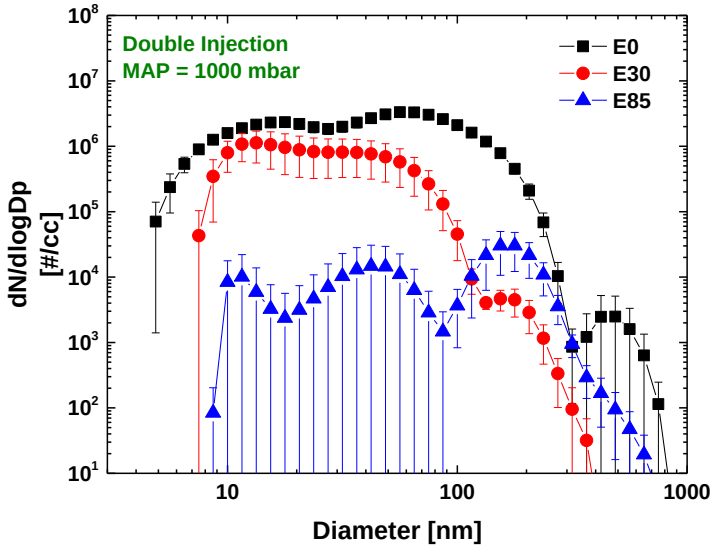

Figure A2.8. Comparison of PN size distributions for E0, E30 and E85 at MAP = 1000 mbar using the double injection strategy shown in **Figure 3.19.**

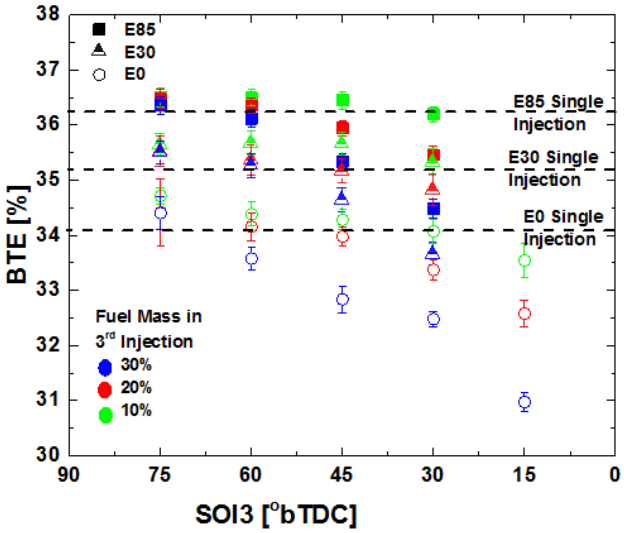

Figure A2.9. Effects of SOI3 timing and fuel mass on BTE for E0, E30 and E85 and MAP = 1000 mbar. The results for single injection are provided for comparison as the dashed lines (corresponds to **Figure 3.14**).

Appendix 3: Supplemental material for Ghana case-study

Table A3.1. Sources of statistical data used in the study.

Data	Source
Regional and district level agricultural food crop production (MT), cropped area (Ha) and crop production yield (MT/Ha) for the following food crops for the year 2012: maize, rice, millet, sorghum, cassava, yam, cocoyam, plantain, groundnut, cowpea and soybean	Statistics, Research and Info. Directorate (SRID), Ministry of Food and Agriculture, Ghana - February, 2013 []
Petroleum products imported, produced, exported and consumed from 2006-2015	National Energy Statistics 2006-2015, Ghana [119]
Total number of certified motor vehicles by city or district in Ghana from 2010-2013	Ghana Statistical Yearbook 2010-2013[120]
Number of industry establishments created in a district or city for all regions in Ghana from 2005-2014	Regional Spatial Business Report Ghana -November 2016 [126]
Distance between two locations in Ghana.	Google Maps (https://www.google.com/maps)

Table A3.2. Regional vehicle registration data, gasoline consumption and corresponding ethanol volume required to create E10 blend

Region	City/Town (Demand Centers)	% certified vehicles of national total	Gasoline consumption (ML)	Ethanol volume required to create E10 blend (ML)
Ashanti	Kumasi	18.7%	249.18	25.82
	Obuasi	2.1%	27.81	2.88
	Bekwai	0.8%	10.48	1.09
Brong Ahafo	Techiman	2.1%	28.32	2.93
	Sunyani	1.0%	13.85	1.44
Central	Winneba	6.7%	88.90	9.21
	Cape Coast	2.0%	26.25	2.73
	Agona	0.9%	11.27	1.17
	Dunkwa	0.5%	7.1	0.74
Eastern	Koforidua	2.6%	34.47	3.58
	Akim Oda	1.9%	24.75	2.57
	Nkawkaw	1.1%	15.25	1.59
Greater Accra	Accra	26.5%	352.51	36.5
	Tema	11.1%	147.22	15.3
	Weija	5.8%	77.30	8.01
Northern	Tamale	1.4%	18.97	1.97
Upper East	Bolgatanga	1.9%	24.67	2.56
Upper West	Wa	1.9%	25.25	2.62
Volta	Ho	2.0%	26.50	2.75
	Denu	1.4%	18.60	1.93
	Hohoe	0.6%	7.70	0.8
Western	Takoradi	5.6%	74.70	7.74
	Tarkwa	1.6%	21.42	2.22
		TOTAL	**1332.5**	**138**

Table A3.3. Total transportation costs for three candidate biorefinery locations to the regional ethanol demand locations.

Candidate biorefinery (ethanol capacity) → Demand city ↓	**Sunyani (100 ML-maize) [MGHC]**	**Techiman (100 ML-maize) [MGHC]**	**Koforidua (100 ML-maize) [MGHC]**	**Koforidua (50 ML-cassava) [MGHC]**	**Koforidua (50 ML-maize) [MGHC]**	**Sunyani (50 ML-maize) [GHC]**
Accra	235	238	170	117	125	197
Agona	5	5	7	5	5	4
Akim Oda	14	14	12	9	9	11
Bekwai	5	5	6	5	5	4
Bolgatanga	19	18	27	24	24	16
Cape Coast	17	17	15	12	12	14
Denu	16	16	11	9	9	14
Dunkwa	4	4	5	4	4	3
Ho	24	20	14	10	11	21
Hohoe	6	6	4	3	4	5
Koforidua	21	21	14	8	9	17
Kumasi	105	110	145	108	114	78
Nkawkaw	8	8	7	5	5	7
Obuasi	13	14	18	14	14	10
Sunyani	4	5	10	8	8	3
Takoradi	51	54	50	39	40	43
Tamale	12	11	18	15	16	10
Tarkwa	13	14	15	12	12	11
Techiman	10	9	20	15	16	7
Tema	102	103	70	48	51	86
Wa	16	16	26	22	23	14
Weija	52	53	38	26	28	44
Winneba	59	61	47	34	36	49

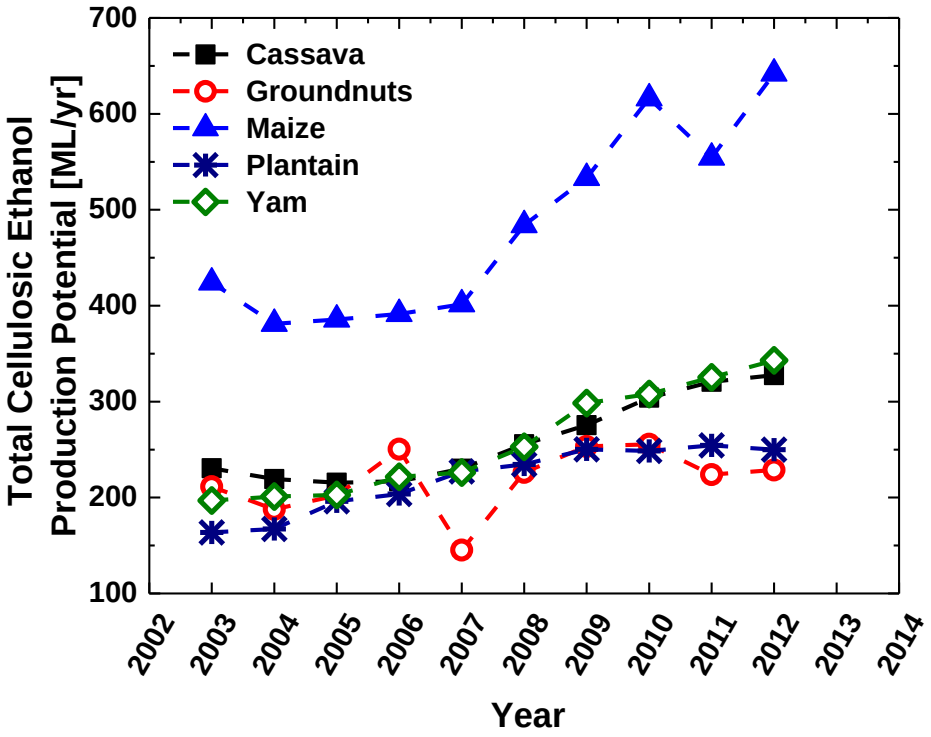

Figure A3.1. Total Cellulosic Ethanol Production Potential [ML/yr] from selected crops from 2003 to 2012**.** Crop residues from maize historically have the highest ethanol production potential with compound annual growth rate of 4.7%.